NUREG/IA-0522

International Agreement Report

RELAP5 and TRACE Constitutive Relations Comparison

Prepared by:
S. Shin*, J. Lee*, A. Shin**, and M. Cho**

*Korea Advanced Institute of Science and Technology (KAIST)
N7-1 4409 291 Daehak-ro. Yuseong-gu
Daejeon 34141 Republic of Korea

**Korea Institute of Nuclear Safety
62 Gwahak-ro, Yuseong-gu, Daejeon 34142, Republic of Korea

K. Tien, NRC Project Manager

Division of Systems Analysis
Office of Nuclear Regulatory Research
U.S. Nuclear Regulatory Commission
Washington, DC 20555-0001

Manuscript Completed: February 2020
Date Published: January 2021

Prepared as part of
The Agreement on Research Participation and Technical Exchange
Under the Thermal-Hydraulic Code Applications and Maintenance Program (CAMP)

Published by
U.S. Nuclear Regulatory Commission

AVAILABILITY OF REFERENCE MATERIALS IN NRC PUBLICATIONS

NRC Reference Material

As of November 1999, you may electronically access NUREG-series publications and other NRC records at NRC's Library at www.nrc.gov/reading-rm.html. Publicly released records include, to name a few, NUREG-series publications; *Federal Register* notices; applicant, licensee, and vendor documents and correspondence; NRC correspondence and internal memoranda; bulletins and information notices; inspection and investigative reports; licensee event reports; and Commission papers and their attachments.

NRC publications in the NUREG series, NRC regulations, and Title 10, "Energy," in the *Code of Federal Regulations* may also be purchased from one of these two sources.

1. **The Superintendent of Documents**
   U.S. Government Publishing Office
   Mail Stop IDCC
   Washington, DC 20402-0001
   Internet: bookstore.gpo.gov
   Telephone: (202) 512-1800
   Fax: (202) 512-2104

2. **The National Technical Information Service**
   5301 Shawnee Road
   Alexandria, VA 22312-0002
   www.ntis.gov
   1-800-553-6847 or, locally, (703) 605-6000

A single copy of each NRC draft report for comment is available free, to the extent of supply, upon written request as follows:

Address: **U.S. Nuclear Regulatory Commission**
Office of Administration
Multimedia, Graphics, and Storage &
Distribution Branch
Washington, DC 20555-0001
E-mail: distribution.resource@nrc.gov
Facsimile: (301) 415-2289

Some publications in the NUREG series that are posted at NRC's Web site address www.nrc.gov/reading-rm/doc-collections/nuregs are updated periodically and may differ from the last printed version. Although references to material found on a Web site bear the date the material was accessed, the material available on the date cited may subsequently be removed from the site.

Non-NRC Reference Material

Documents available from public and special technical libraries include all open literature items, such as books, journal articles, transactions, *Federal Register* notices, Federal and State legislation, and congressional reports. Such documents as theses, dissertations, foreign reports and translations, and non-NRC conference proceedings may be purchased from their sponsoring organization.

Copies of industry codes and standards used in a substantive manner in the NRC regulatory process are maintained at—

The NRC Technical Library
Two White Flint North
11545 Rockville Pike
Rockville, MD 20852-2738

These standards are available in the library for reference use by the public. Codes and standards are usually copyrighted and may be purchased from the originating organization or, if they are American National Standards, from—

American National Standards Institute
11 West 42nd Street
New York, NY 10036-8002
www.ansi.org
(212) 642-4900

Legally binding regulatory requirements are stated only in laws; NRC regulations; licenses, including technical specifications; or orders, not in NUREG-series publications. The views expressed in contractor prepared publications in this series are not necessarily those of the NRC.

The NUREG series comprises (1) technical and administrative reports and books prepared by the staff (NUREG–XXXX) or agency contractors (NUREG/CR–XXXX), (2) proceedings of conferences (NUREG/CP–XXXX), (3) reports resulting from international agreements (NUREG/IA–XXXX), (4) brochures (NUREG/BR–XXXX), and (5) compilations of legal decisions and orders of the Commission and Atomic and Safety Licensing Boards and of Directors' decisions under Section 2.206 of NRC's regulations (NUREG–0750).

DISCLAIMER: This report was prepared under an international cooperative agreement for the exchange of technical information. Neither the U.S. Government nor any agency thereof, nor any employee, makes any warranty, expressed or implied, or assumes any legal liability or responsibility for any third party's use, or the results of such use, of any information, apparatus, product or process disclosed in this publication, or represents that its use by such third party would not infringe privately owned rights.

NUREG/IA-0522

International Agreement Report

RELAP5 and TRACE Constitutive Relations Comparison

Prepared by:
S. Shin*, J. Lee*, A. Shin**, and M. Cho**

*Korea Advanced Institute of Science and Technology (KAIST)
N7-1 4409 291 Daehak-ro. Yuseong-gu
Daejeon 34141 Republic of Korea

**Korea Institute of Nuclear Safety
62 Gwahak-ro, Yuseong-gu, Daejeon 34142, Republic of Korea

K. Tien, NRC Project Manager

Division of Systems Analysis
Office of Nuclear Regulatory Research
U.S. Nuclear Regulatory Commission
Washington, DC 20555-0001

Manuscript Completed: February 2020
Date Published: January 2021

Prepared as part of
The Agreement on Research Participation and Technical Exchange
Under the Thermal-Hydraulic Code Applications and Maintenance Program (CAMP)

Published by
U.S. Nuclear Regulatory Commission

ABSTRACT

A system thermal hydraulic analysis code is generally used for nuclear power plant safety analysis, and it solves the fluid field equations to model two phase flow. System codes typically solve mass, momentum and energy equations of each phase numerically by approximating a one dimensional flow. However, the constitutive relation based on empiricism must be included for mathematical closure of the approximated governing equations.

The best available approach to evaluate the constitutive relation models is to compare the code results with the data from separate effect tests (SET). However, available experimental data cover only a small fraction of the thermal hydraulic conditions in SET. Thus, there is no available method to evaluate the constitutive relation models that include all regimes expected in applications of the system codes. This study proposes a new method for evaluating the constitutive relations by comparing between RELAP5 and TRACE to analyze the constitutive relation models of the two codes.

RELAP5 and TRACE are very different in the implemented constitutive relation models even though the field equations are almost identical. To compare the different constitutive relations of the two codes, models and correlations of each code are studied and compared. Then constitutive relation modules are extracted in a separate computational environment. The developed platform is based on MATLAB and REFPROP, and it is proven to reproduce the same values of RELAP5 MOD3.3 patch5 and TRACE 5.0 patch5, respectively.

In the wall heat transfer models, different heat transfer regimes are occasionally chosen in the two codes and they reveal substantial deviations. In the interfacial heat transfer models, while RELAP5 includes a void generation term, TRACE does not consider the term, which results in a difference in the calculation of interfacial heat transfer. In the wall friction models, almost all regimes show good agreement between TRACE and RELAP5 except for slug and transition flow regimes. In the interfacial friction models, the interfacial drag coefficient has a larger difference than the wall drag coefficient between TRACE and RELAP5.

This work was supported by the Nuclear Safety Research Program through the Korea Foundation Of Nuclear Safety(KoFONS), granted financial resource from the Nuclear Safety and Security Commission(NSSC), Republic of Korea. (No. 1903002)

TABLE OF CONTENTS

ABSTRACT .... **iii**

TABLE OF CONTENTS .... **v**

LIST OF FIGURES .... **vii**

LIST OF TABLES .... **xi**

EXECUTIVE SUMMARY .... **xiii**

ACKNOWLEDGMENTS .... **xv**

ABBREVIATIONS AND ACRONYMS .... **xvii**

1 INTRODUCTION **1**

2 METHOD **7**
- 2.1 Separate Computational Platform 7
  - 2.1.1 Verification of Separate Computational Platform 9
- 2.2 Comparison Method 11
  - 2.2.1 Selecting Thermal-hydraulic Conditions for Comparison 13

3 WALL HEAT TRANSFER MODELS **17**
- 3.1 Background 17
- 3.2 Description of Wall Heat Transfer Modules 18
  - 3.2.1 Selection Logic of Wall Heat Transfer Regime 18
  - 3.2.2 Critical Heat Flux Calculation Model 20
  - 3.2.3 Wall Heat Transfer Models & Correlations 21
- 3.3 Wall Heat Transfer Models and Correlations of TRACE 21
- 3.4 Wall Heat Transfer Models and Correlations of RELAP5 26
- 3.5 Comparison Results 28

4 INTERFACIAL HEAT TRANSFER MODELS **39**
- 4.1 Background 39
- 4.2 Description of Interfacial Heat Transfer Modules 41
- 4.3 Flow Regime Map 41
- 4.4 Interfacial Heat Transfer Models and Correlations of TRACE 44
- 4.5 Interfacial Heat Transfer Models and Correlations of RELAP5 49
- 4.6 Comparison Results 56

5 WALL FRICTION MODELS **61**
- 5.1 Background 61
- 5.2 Description of Wall Friction Modules 61
- 5.3 Wall Friction Models and Correlations of TRACE 61
- 5.4 Wall Friction Models and Correlations of RELAP5 64
- 5.5 Comparison Results 66

6 INTERFACIAL FRICTION MODELS **69**
- 6.1 Background 69

6.2 Description of Interfacial Friction Modules 69
6.3 Interfacial Friction Models and Correlations of TRACE 70
6.4 Interfacial Friction Models and Correlations of RELAP5 73
6.5 Comparison Results 80

7 SUMMARY AND CONCLUSIONS 83

8 REFERENCES 85

LIST OF FIGURES

Figure 1 LBLOCA Analysis Results of Different Codes and from Different Users [2]. (a) MARS-KS2.3 from KAERI (b) RELAP5/MOD3.3 from KINS (c) TRACE4.05 from PSI (d) CATHARE2.5 from CEA 2

Figure 2 Total Ranking of the Influence on the Cladding Temperature [2] 3

Figure 3 Similarity of Conservation Equations in System Codes (6-equation, 2-fluid Model) 4

Figure 4 Dissimilarity of Constitutive Relation Models in System Codes (6-equation, 2-fluid Model) 5

Figure 5 Flow Chart of Separate Computational Platform to Model the Constitutive Relations of TRACE 7

Figure 6 Flow Chart of Separate Computational Platform to Model the Constitutive Relations of RELAP5 8

Figure 7 Verification Process. (a) Verification Procedure Chart (b) Simplified Modeling Diagram in the Original Code 9

Figure 8 Verification Results of Separate Platforms 10

Figure 9 Flow Chart of Evaluation Methodologies 11

Figure 10 DBAs Based on F-V Initiating Events Importance of the Barakah NPP 14

Figure 11 Needed Variables to Determine Thermal-hydraulic Conditions. (a) Slip Ratio According to Void Fraction [14] (b) p-v Diagram [15] 15

Figure 12 Typical Pool Boiling Curve for Water under Atmospheric Pressure [17] and Simplified Bubble Shape in Regions of Heat Transfer [19] 17

Figure 13 Simplified Wall Heat Transfer Modules (a) RELAP5 (b) TRACE 18

Figure 14 Wall Heat Transfer Selection Logic Diagram of TRACE. 20

Figure 15 Wall Heat Transfer Selection Logic Diagram of RELAP5. 20

Figure 16 Comparison of Heat Transfer Models for Forced Convection [13] 22

Figure 17 Comparison of Pool Boiling Models [13] (a) at Low Pressure (b) at High Pressure 23

Figure 18 Schematic of Heat Transfer Paths in the Film Boiling Heat Transfer Regime. (a) for Inverted Annular Film Boiling (b) for Dispersed Flow Film Boiling 24

Figure 19 Pool Boiling Curve Calculated from a Separate Platform. (a) at 10 MPa (b) at 101.325 kPa (1 atm) 28

Figure 20 The Differences between TRACE and RELAP5 for the Case of (a) Selected Same HT Regime and (b) Different HT Regime 29

Figure 21 Calculated Wall Heat Flux in the Case of the Same Selected Wall HT Regime 30

Figure 22 Weighting Function with Wall Temperature in the Transition Boiling HT Regime 31

Figure 23 Percentages of the Selected Different HT Regimes between TRACE and RELAP5 31
Figure 24 Evaluated Temperature of the MFB in TRACE and RELAP5........32
Figure 25 Calculated Temperature of ONB at 0.1 MPa and 15.5 MPa in TRACE and RELAP5 33
Figure 26 Calculated (a) CHF and (b) Temperature of CHF in TRACE and RELAP5 34
Figure 27 Calculated Total HTC in the Nucleate Boiling HT Regime. (a) in TRACE (b) in RELAP5 34
Figure 28 Calculated Pool Boiling HTC in the Nucleate Boiling HT Regime. (a) TRACE (b) RELAP5 35
Figure 29 Exponent of dT_{wall} in the Pool Boiling Term of the Nucleate Boiling HT Regime Correlation........35
Figure 30 Calculated Wall Heat Flux in TRACE and RELAP5 with SUBO Experimental Data (a) Base (b) T1 (c) V1 36
Figure 31 Calculated Wall Heat Flux in TRACE and RELAP5 with Bennett's Heated Tube Experimental Data (a) 5379 (b) 5394........37
Figure 32 Two-phase Flow Schematic Diagram in a Vertical Heating Tube [58]. (a) Low Heat Flux (b) High Heat Flux 40
Figure 33 Two-phase Flow Schematic Diagram in a Horizontal Heating Tube (Low Heat Flux) [58] 41
Figure 34 Flow Regime Map for Interfacial Heat Transfer of (a) TRACE [13] and (b) RELAP5 in Vertical Flow (c) RELAP5 in Horizontal Flow [12] 42
Figure 35 Schematic of Stratified Flow in a Horizontal Pipe [13]........49
Figure 36 Interfacial Heat Transfer in the Bulk and near the Wall for Subcooled Boiling [12] 55
Figure 37 Calculated Liquid-interface Volumetric Heat Transfer of TRACE and RELAP5 (a) in a Bubbly/Slug Flow Regime (b) in an Annular Flow Regime 56
Figure 38 Calculated Liquid-interface Volumetric Heat Transfer of TRACE and RELAP5 without the Vapor Generation Term. (a) in a Bubbly/Slug flow Regime (b) in an Annular Flow Regime 57
Figure 39 Calculated Vapor-interface Volumetric Heat Transfer of TRACE and RELAP5 (a) in a Bubbly/Slug Flow Regime (b) in an Annular Flow Regime 57
Figure 40 Separated Variables Affecting Vapor-interface Heat Transfer in a Bubbly Flow Regime (a) Heat Transfer Coefficient (b) Interfacial Area (c) Diameter of Bubble 58
Figure 41 Bubble Diameter Calculated from Equation (4.63) in a Bubbly Flow Regime........59
Figure 42 Calculated Wall Friction when TRACE and RELAP5 Select the Same Flow Regimes 67
Figure 43 Calculated Wall Friction when TRACE and RELAP5 Select Different Flow Regimes 68
Figure 44 Calculated Wall Friction in the Slug Flow Regime according to the Mass Flux 68

Figure 45 Calculated Wall Friction when TRACE Selects Transition and RELAP5 Selects Annular Flow Regimes 68

Figure 46 Comparison of the Interfacial Coefficient for the Bubbly-Slug and Annular-Mist Flow Regimes [13] 70

Figure 47 Calculated Interfacial Friction of TRACE and RELAP5 in a Horizontal Flow 81

Figure 48 Calculated Interfacial Friction of TRACE and RELAP5 in a Vertical Flow 82

Figure 49 Interfacial Area of TRACE and RELAP5 in an Annular Flow Regime 82

LIST OF TABLES

Table 1 Verification Results of Separate Platforms....11
Table 2 Thermal-hydraulic Conditions of the Selected DBAs....14
Table 3 Defined Conditions for Comparison....15
Table 4 Wall Heat Transfer Regimes of (a) RELAP5 and (b) TRACE....18
Table 5 Experimental Conditions for SUBO....36
Table 6 Experimental Conditions for Bennett's Heated Tube Test....36
Table 7 Void Fraction on the Wall for Different Flow Regimes....66
Table 8 Drift Flux Correlation for a Vertical Bubbly Slug Flow Regime....74

EXECUTIVE SUMMARY

System thermal hydraulic analysis codes such as TRACE or RELAP5 are often used for nuclear power plant simulation to evaluate the safety of the system. In a system thermal hydraulic analysis code, the fluid field equations are used to a model two phase flow. System codes typically solve mass, momentum and energy equations for each phase. To solve field equations, constitutive relations are needed to close the governing equations, and these correlations are often dependent on the flow regime or heat transfer (HT) regime map. The major constitutive relation models in the codes are the wall heat transfer, wall and interfacial friction, interfacial heat and mass transfer. However, TRACE and RELAP5 are very different in the implemented thermal hydraulics models and correlations even though the governing field equations are almost identical. This report summarizes the differences in the obtained results from the two codes by first examining the models and correlations for modeling the two phase flow. To compare different constitutive models of the two codes, each constitutive relation module is extracted and constructed in a separate computational environment. The platforms contain various constitutive relations of TRACE and RELAP5: wall heat transfer, interfacial heat transfer, wall friction, and interfacial friction. This is followed by suggesting a new evaluation method for comparing constitutive relation models. Qualitative and quantitative comparisons of the constitutive relation models of TRACE and RELAP5 codes are conducted with the computational platforms.

The comparison results of the constitutive relation models of the two codes lead to the following conclusions.

- In the wall heat transfer models, different HT regimes are often selected and show substantial deviations. This is because the HT regime selection logics of TRACE and RELAP5 are different. TRACE includes models for determining the temperature of the ONB and MFB, but RELAP5 does not have this logic. In RELPA5, the temperature of ONB is set as a value of T_{sat} – 0.001 and heat fluxes calculated from the transition and film boiling HT regimes are used as the MFB condition. Whether the two codes select the same HT regime or select another HT regime, the difference in heat fluxes calculated from the two codes is the largest when TRACE selects the transition boiling HT regime.
- In the interfacial heat transfer, RELAP5 includes a void generation term for evaluating the liquid interfacial heat transfer, but TRACE does not consider this term. This causes the major differences between the two codes. In the vapor interfacial heat transfer, the order of the heat transfer calculated between the two codes is found to be significantly different in the bubbly flow regime, which is up to 1600 times for the vapor heat transfer coefficient and 40 times for the interfacial area.
- In the wall friction models, there is fairly good agreement in all flow regimes, but when the void fraction is from 0.8 to 0.9, where TRACE selects the transition flow regime, wall friction values from the two codes differ substantially.
- In the interfacial friction models, the calculated friction values are inconsistent between the two codes in all flow regimes and the largest difference is observed in the annular flow regime due to the difference in the calculated interfacial area of the two codes.

ACKNOWLEDGMENTS

This work was supported by the Nuclear Safety Research Program through the Korea Foundation Of Nuclear Safety(KoFONS), granted financial resource from the Nuclear Safety and Security Commission(NSSC), Republic of Korea. (No. 1903002)

ABBREVIATIONS AND ACRONYMS

a_i	interfacial area (1/m)
C	drag coefficient
C_p	specific heat at constant pressure (J/kg-K)
d	diameter (m)
e	specific internal energy (J/kg)
f	friction (Pa/m)
f	friction factor
g	gravitational constant (m/s^2)
G	mass flux (kg/m^2-sec)
h	heat transfer coefficient (W/m^2-K)
h	enthalpy (J/kg)
h_{fg}	latent heat (J/kg)
H	volumetric interfacial heat transfer coefficient (W/m^3)
j	superficial velocity
k	thermal conductivity (W/m-K)
L	heated length from entrance to point
q	heat transfer rate per unit volume (W/m^3)
q_w	heat flux (W/m^2)
P	pressure (Pa)
r	radius (m)
R	surface roughness
t	time (sec)
T	temperature (K)
v	velocity (m/s)
wf	weighting factor
x_e	equilibrium quality

Greek Symbols

α	void fraction
Γ	volumetric mass transfer rate (kg/m^3-sec)
δ	film thickness (m)
θ	flow direction (rad)
λ	friction factor
μ	viscosity (kg/m-sec)
ρ	density (kg/m^3)
σ	surface tension (J/m^2)

Subscripts

AM	annular-mist to mist flow regime transition boundary
bub	bubble, bubbly
BS	bubbly to slug flow regime transition boundary
BT	bubbly to transition flow regime transition boundary
cap	cap bubble
$crit$	critical
crit	criterion
d	direct heating
$drop$	droplet
e	equilibrium
FC	forced convection
$film$	film
i	interfacial
l	liquid phase
MFB	minimum film boiling
NB	nucleate boiling
ONB	onset of boiling
PB	pool boiling

r	relative
SA	slug to annular flow regime transition boundary
sat	saturation
$slug$	slug
sub	subcooled
Tb	Taylor bubble
TS	transition to slug flow regime transition boundary
$term$	terminal
v	vapor phase
w	wall

Superscripts

sat	saturation
$Wall$	wall
B	bulk fluid

1 INTRODUCTION

Thermal hydraulic system analysis codes, such as RELAP5, TRACE, COBRA-TF, CATHARE, and MARS-KS are commonly used for reactor simulation to analyze and evaluate the safety of a nuclear power plant because full-scale experiments are very challenging. The development projects of these thermal analysis codes were initiated in 1970s and 1980s, and the main applications were for nuclear safety analysis and nuclear system design. Nearly all current thermal-hydraulic analysis codes are based on the two-fluid model, which was determined after inherent flaws were found in the previous homogeneous equilibrium model approaches. Phases are dealt with by transferring part of the mass of each phase at the interface, and separate conservative equations of each phase are solved by averaging the space and time ensemble of the local governing equations of fluid with appropriate source terms, including the interfacial transfer for mass, momentum and energy.

Because of averaging the local flow processes, information is smeared and it has to be compensated for by additional modeling at the interface between phases or at the location near the walls. Hence, it was very challenging to develop codes with respect to a number of such problems [1]. The codes must be capable of covering a wide range of transients to simulate all types of two-phase flow regimes and associated heat transfers phenomena. Additionally, since the various flow regimes and heat transfer regimes are the most important phenomena for evaluating safety, modeling these regimes require a special effort. The model for these various regimes are the essence of the constitutive relations and is also important for mathematically closing the problem. In other words, to apply the two-fluid model to the system analysis codes, it is crucial to develop physical models to solve the system of equations.

The level of the complexity of the model must remain compatible with both the available scientific knowledge and experimental data and the required reliability of predictions for nuclear system safety. To validate all constitutive relation models, a very extensive experimental program was required and the two-fluid model can be applied due to this effort. Extensive work during the last four decades was devoted to the improvement and validation of these two-phase constitutive relation models; this work resulted in a system with the ability to predict the main phenomena of most accidental transients of nuclear power plants with reasonable accuracy.

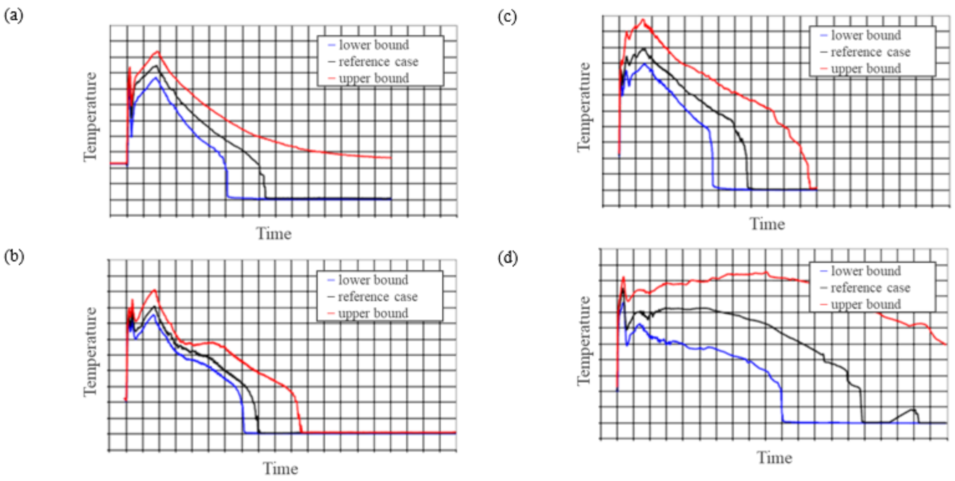

Figure 1 LBLOCA Analysis Results of Different Codes and from Different Users [2]. (a) MARS-KS2.3 from KAERI (b) RELAP5/MOD3.3 from KINS (c) TRACE4.05 from PSI (d) CATHARE2.5 from CEA

Utilizing the Best Estimate Methods – Uncertainty and Sensitivity Evaluation (BEMUSE) project, we confirmed once again the importance of constitutive relation models. Figure 1 shows the maximum cladding temperature simulated from different participants in the program and different codes [2, 3]. Different trends can be observed, and BEMUSE projects confirmed what causes such differences. From Figure 2, the variables affecting the peak cladding temperature were identified and scored. The most influential parameters were identified to be the fuel and cladding gap size, UO_2 conductivity and gap conductivity. This shows that user effects have a significant impact on the analysis. These user effects are followed by factors such as the film boiling heat transfer coefficient and the critical heat flux (CHF), which is related to the physical models, i.e., the constitutive relations. In other words, constitutive relation models have substantial influence on the analysis results.

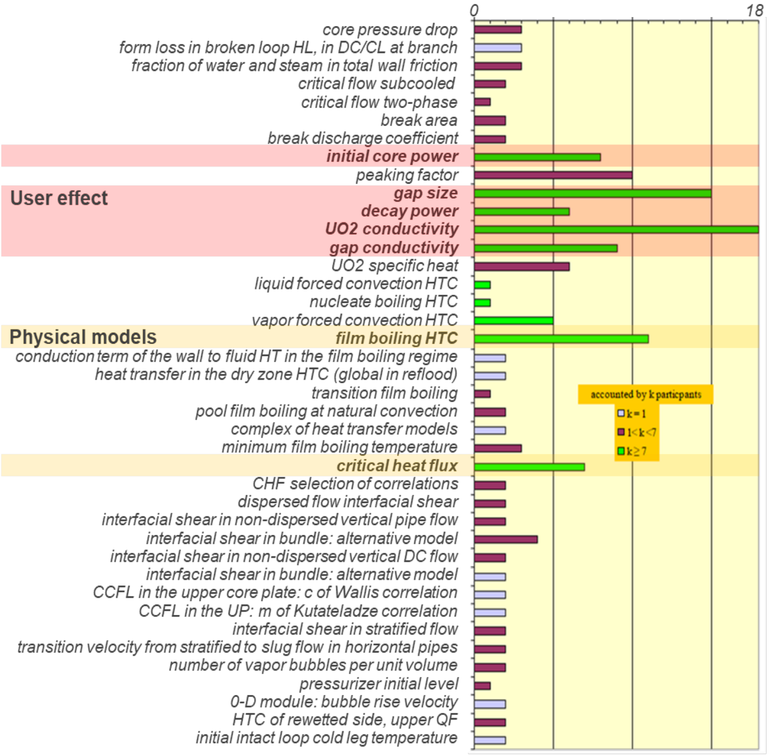

Figure 2 Total Ranking of the Influence on the Cladding Temperature [2]

The influence of the constitutive relation model can be identified by observing the governing equations of the system analysis codes. Figure 3 shows the similarity of the liquid and vapor conservation equations between RELAP5 and TRACE. The conservation equations of the two codes are almost identical. For the mass conservation equations, time and space dependent changes are calculated from the masses moving between the interfaces. For the momentum conservation equations, the two codes are the same except that only the RELAP5 code additionally considers momentum transfer due to virtual mass. The TRACE code does not use the virtual mass term for code stability. In the momentum equations of the two codes, the change of momentum consists of the momentum transfer due to frictional force (the sum of the wall and the interface), the mass transfer, and the body force. For the energy conservation equations, the equations are constructed with the same source terms except for the dissipation term. In the energy conservation equations of the two codes, the amount of energy change of each phase according to time and space is composed of the heat transfer at the wall surface and the interface and the heat transfer due to mass transfers.

- **mass conservation equations**
  - RELAP5

$$\frac{\partial\left[(1-\alpha)\rho_l\right]}{\partial t}+\frac{1}{A}\nabla\cdot\left[(1-\alpha)\rho_l v_l A\right]=-\Gamma \qquad \frac{\partial\left[\alpha\rho_g\right]}{\partial t}+\frac{1}{A}\nabla\cdot\left[\alpha\rho_g v_g A\right]=\Gamma$$

  - TRACE

$$\frac{\partial\left[(1-\alpha)\rho_l+\alpha\rho_g\right]}{\partial t}+\nabla\cdot\left[(1-\alpha)\rho_l v_l+\alpha\rho_g v_g\right]=0 \qquad \frac{\partial\left[\alpha\rho_g\right]}{\partial t}+\nabla\cdot\left[\alpha\rho_g v_g\right]=\Gamma$$

- **momentum conservation equations**
  - RELAP5

$$\frac{\partial v_l}{\partial t}+v_l\nabla\cdot v_l=-\frac{1}{\rho_l}\nabla P+\frac{\left[f_i-\Gamma\left(v_i-v_l\right)+f_{wl}\right]}{(1-\alpha)\rho_l}+B_x-C\alpha\frac{\rho_m}{\rho_l}\left[\frac{\partial\left(v_l-v_g\right)}{\partial t}+v_g\nabla\cdot v_l-v_l\nabla\cdot v_g\right]$$

$$\underbrace{\frac{\partial v_g}{\partial t}+v_g\nabla\cdot v_g=-\frac{1}{\rho_g}\nabla P}_{\substack{\text{Change rate}\\ \text{with time and space}}}+\underbrace{\frac{\left[f_{wg}-f_i-\Gamma\left(v_g-v_i\right)\right]}{\alpha\rho_g}}_{\substack{\text{momentum}\\ \text{transfer}\\ \text{by friction}} \quad \substack{\text{momentum}\\ \text{transfer}\\ \text{by mass transfer}}}+\underbrace{B_x}_{\substack{\text{body}\\ \text{force}}}\underbrace{-C(1-\alpha)\frac{\rho_m}{\rho_g}\left[\frac{\partial\left(v_g-v_l\right)}{\partial t}+v_l\nabla\cdot v_g-v_g\nabla\cdot v_l\right]}_{\text{force by virtual mass}}$$

  - TRACE

$$\frac{\partial v_l}{\partial t}+v_l\nabla\cdot v_l=-\frac{1}{\rho_l}\nabla P+\frac{\left[f_i-\Gamma\left(v_i-v_l\right)+f_{wl}\right]}{(1-\alpha)\rho_g}+\vec{g} \qquad \underbrace{\frac{\partial v_g}{\partial t}+v_g\nabla\cdot v_g=-\frac{1}{\rho_g}\nabla P}_{\substack{\text{Change rate}\\ \text{with time and space}}}+\underbrace{\frac{\left[f_{wg}-f_i-\Gamma\left(v_g-v_i\right)\right]}{\alpha\rho_g}}_{\substack{\text{momentum}\\ \text{transfer}\\ \text{by friction}} \quad \substack{\text{momentum}\\ \text{transfer}\\ \text{by mass transfer}}}+\underbrace{\vec{g}}_{\substack{\text{body}\\ \text{force}}}$$

- **energy conservation equations**
  - RELAP5

$$\frac{\partial\left[(1-\alpha)\rho_l e_l\right]}{\partial t}+\frac{1}{A}\nabla\cdot\left[(1-\alpha)\rho_l e_l v_l A\right]=-P\frac{\partial(1-\alpha)}{\partial t}-\frac{P}{A}\nabla\cdot\left[(1-\alpha)v_l A\right]+q_{wl}+q_{il}-\Gamma_{ig}h_l^{*}-\Gamma_w h_l^{'}+Diss_l$$

$$\underbrace{\frac{\partial\left[\alpha\rho_g e_g\right]}{\partial t}+\frac{1}{A}\nabla\cdot\left[\alpha\rho_g e_g v_g A\right]=-P\frac{\partial\alpha}{\partial t}-\frac{P}{A}\nabla\cdot\left[\alpha v_l A\right]}_{\substack{\text{Change rate}\\ \text{with time and space}}}\underbrace{+q_{wg}}_{\substack{\text{heat}\\ \text{transfer}\\ \text{in the wall}}}\underbrace{+q_{ig}}_{\substack{\text{heat}\\ \text{transfer in}\\ \text{interfacial}\\ \text{face}}}\underbrace{+\Gamma_{ig}h_g^{*}-\Gamma_w h_g^{'}}_{\substack{\text{energy}\\ \text{transfer}\\ \text{by mass}\\ \text{transfer}}}\underbrace{+Diss_g}_{\text{dissipation}}$$

  - TRACE

$$\frac{\partial\left[(1-\alpha)\rho_l e_l+\alpha\rho_g e_g\right]}{\partial t}+\nabla\cdot\left[(1-\alpha)\rho_l e_l v_l+\alpha\rho_g e_g v_g\right]=-P\nabla\cdot\left[(1-\alpha)v_g+\alpha v_g\right]+q_{wl}+q_{wsat}+q_{wg}+q_{dl}+q_{dg}$$

$$\underbrace{\frac{\partial\left[\alpha\rho_g e_g\right]}{\partial t}+\nabla\cdot\left[\alpha\rho_g e_g v_g\right]=-P\frac{\partial\alpha}{\partial t}-P\nabla\cdot\left(\alpha v_g\right)}_{\substack{\text{Change rate}\\ \text{with time and space}}}\underbrace{+q_{wg}\qquad+q_{dg}}_{\substack{\text{heat}\\ \text{transfer}\\ \text{in the wall}}}\underbrace{+q_{ig}}_{\substack{\text{heat}\\ \text{transfer in}\\ \text{interfacial}\\ \text{face}}}\underbrace{+\Gamma h_g^{'}}_{\substack{\text{energy}\\ \text{transfer}\\ \text{by mass}\\ \text{transfer}}}$$

Figure 3 Similarity of Conservation Equations in System Codes (6-equation, 2-fluid Model)

On the other hand, Figure 4 shows the dissimilarity of the constitutive relation model implemented in RELAP5 and TRACE. The conservation equations are constructed very similarly, while the two codes use significantly different constitutive relations. The reason why system analysis codes have different constitutive relation models was that different approaches were used to establish the constitutive models in each code: the fully empirical approach, the empirical approach with dimensional analysis, the phenomenological or mechanistic approach, and the semi empirical approach [1]. As a result, the safety analysis results differed depending on the implemented constitutive relation models. The different models of the constitutive relation models will be described in detail later, and only the importance of the constitutive relation models is briefly mentioned in this chapter.

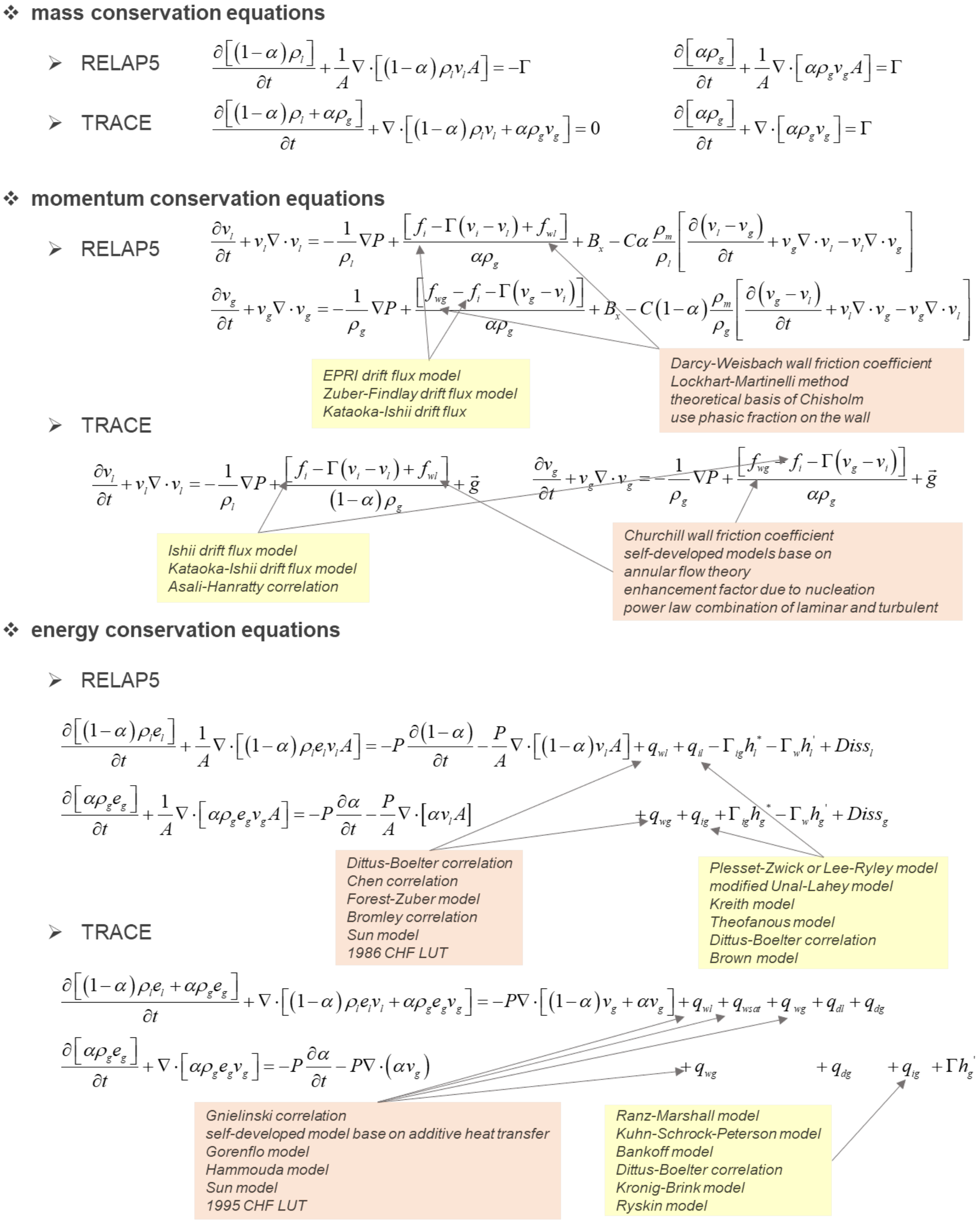

- **mass conservation equations**
  - RELAP5 $\frac{\partial\left[(1-\alpha)\rho_l\right]}{\partial t}+\frac{1}{A}\nabla\cdot\left[(1-\alpha)\rho_l v_l A\right]=-\Gamma$ $\quad\frac{\partial\left[\alpha\rho_g\right]}{\partial t}+\frac{1}{A}\nabla\cdot\left[\alpha\rho_g v_g A\right]=\Gamma$
  - TRACE $\frac{\partial\left[(1-\alpha)\rho_l+\alpha\rho_g\right]}{\partial t}+\nabla\cdot\left[(1-\alpha)\rho_l v_l+\alpha\rho_g v_g\right]=0$ $\quad\frac{\partial\left[\alpha\rho_g\right]}{\partial t}+\nabla\cdot\left[\alpha\rho_g v_g\right]=\Gamma$

- **momentum conservation equations**
  - RELAP5

$$\frac{\partial v_l}{\partial t}+v_l\nabla\cdot v_l=-\frac{1}{\rho_l}\nabla P+\frac{\left[f_i-\Gamma\left(v_i-v_l\right)+f_{wl}\right]}{\alpha\rho_g}+B_x-C\alpha\frac{\rho_m}{\rho_l}\left[\frac{\partial\left(v_l-v_g\right)}{\partial t}+v_g\nabla\cdot v_l-v_l\nabla\cdot v_g\right]$$

$$\frac{\partial v_g}{\partial t}+v_g\nabla\cdot v_g=-\frac{1}{\rho_g}\nabla P+\frac{\left[f_{wg}-f_i-\Gamma\left(v_g-v_i\right)\right]}{\alpha\rho_g}+B_x-C(1-\alpha)\frac{\rho_m}{\rho_g}\left[\frac{\partial\left(v_g-v_l\right)}{\partial t}+v_l\nabla\cdot v_g-v_g\nabla\cdot v_l\right]$$

EPRI drift flux model
Zuber-Findlay drift flux model
Kataoka-Ishii drift flux

Darcy-Weisbach wall friction coefficient
Lockhart-Martinelli method
theoretical basis of Chisholm
use phasic fraction on the wall

  - TRACE

$$\frac{\partial v_l}{\partial t}+v_l\nabla\cdot v_l=-\frac{1}{\rho_l}\nabla P+\frac{\left[f_i-\Gamma\left(v_i-v_l\right)+f_{wl}\right]}{(1-\alpha)\rho_g}+\vec{g} \qquad \frac{\partial v_g}{\partial t}+v_g\nabla\cdot v_g=-\frac{1}{\rho_g}\nabla P+\frac{\left[f_{wg}-f_i-\Gamma\left(v_g-v_i\right)\right]}{\alpha\rho_g}+\vec{g}$$

Ishii drift flux model
Kataoka-Ishii drift flux model
Asali-Hanratty correlation

Churchill wall friction coefficient
self-developed models base on
annular flow theory
enhancement factor due to nucleation
power law combination of laminar and turbulent

- **energy conservation equations**
  - RELAP5

$$\frac{\partial\left[(1-\alpha)\rho_l e_l\right]}{\partial t}+\frac{1}{A}\nabla\cdot\left[(1-\alpha)\rho_l e_l v_l A\right]=-P\frac{\partial(1-\alpha)}{\partial t}-\frac{P}{A}\nabla\cdot\left[(1-\alpha)v_l A\right]+q_{wl}+q_{il}-\Gamma_{ig}h_l^{*}-\Gamma_{w}h_l^{'}+Diss_l$$

$$\frac{\partial\left[\alpha\rho_g e_g\right]}{\partial t}+\frac{1}{A}\nabla\cdot\left[\alpha\rho_g e_g v_g A\right]=-P\frac{\partial\alpha}{\partial t}-\frac{P}{A}\nabla\cdot\left[\alpha v_l A\right]+q_{wg}+q_{ig}+\Gamma_{ig}h_g^{*}-\Gamma_{w}h_g^{'}+Diss_g$$

Dittus-Boelter correlation
Chen correlation
Forest-Zuber model
Bromley correlation
Sun model
1986 CHF LUT

Plesset-Zwick or Lee-Ryley model
modified Unal-Lahey model
Kreith model
Theofanous model
Dittus-Boelter correlation
Brown model

  - TRACE

$$\frac{\partial\left[(1-\alpha)\rho_l e_l+\alpha\rho_g e_g\right]}{\partial t}+\nabla\cdot\left[(1-\alpha)\rho_l e_l v_l+\alpha\rho_g e_g v_g\right]=-P\nabla\cdot\left[(1-\alpha)v_g+\alpha v_g\right]+q_{wl}+q_{wsat}+q_{wg}+q_{dl}+q_{dg}$$

$$\frac{\partial\left[\alpha\rho_g e_g\right]}{\partial t}+\nabla\cdot\left[\alpha\rho_g e_g v_g\right]=-P\frac{\partial\alpha}{\partial t}-P\nabla\cdot\left(\alpha v_g\right)+q_{wg}+q_{dg}+q_{ig}+\Gamma h_g^{'}$$

Gnielinski correlation
self-developed model base on additive heat transfer
Gorenflo model
Hammouda model
Sun model
1995 CHF LUT

Ranz-Marshall model
Kuhn-Schrock-Peterson model
Bankoff model
Dittus-Boelter correlation
Kronig-Brink model
Ryskin model

Figure 4 Dissimilarity of Constitutive Relation Models in System Codes (6-equation, 2-fluid Model)

Despite the importance of constitutive relation models, it is difficult to evaluate the constitutive relations in all possible thermal-hydraulic conditions [4, 5]. Some previous works have only summarized the constitutive relation models that are used in the several system codes [6-8]. Currently, the best available approach to evaluate the constitutive relation models is to compare the code results to the data from separate effect tests (SET). As mentioned above, after building the system analysis codes, it is necessary to confirm that the selected constitutive relation models are reasonable for modeling the actual phenomenon by comparing it with SET data, and if it is unsatisfactory, the constitutive relation models have to be modified, improved or developed. All these procedures are documented in the assessment manual of each code [9-11]. However, available experimental data covers only a limited fraction of the thermal hydraulic conditions in separate effect tests (SET). That is, there was no available method to evaluate the constitutive relation models including all regimes expected in applications of the system codes. Thus, this study presents an evaluation method for the constitutive relation models.

The method is to evaluate whether the built-in constitutive relation models in the system codes reasonably predict phenomena during the hypothetical accidents of nuclear power plants. Since the current system analysis codes simulate accidents with reasonable accuracy [1], the comparison between several system analysis codes can be regarded as a valid and thorough methodology. This comparison process, identifying the strengths or weaknesses of the selected constitutive relation models implemented in each system analysis code, will also be useful for the future development of the safety analysis codes.

In this document, we present a new evaluation method for the implemented constitutive relation models. Using this method, we conducted a comparative evaluation of the constitutive relation models implemented in the selected thermal-hydraulic system analysis codes. In order to proceed with the comparison, it was necessary to select two or more thermal-hydraulic system analysis codes. The two codes TRACE and RELAP5 were chosen for this study. The new evaluation method is discussed in the next chapter. Chapters 3 – 6 present wall heat transfer, interfacial heat transfer, wall friction, and interfacial friction models, respectively. Chapters 3 – 6 include a discussion of how the constitutive relation models are composed, which constitutive relation correlations were adopted, and why each developer chose these correlations. The last chapter summarizes and concludes the study.

2 METHOD

2.1 Separate Computational Platform

Firstly, constitutive relation models implemented in RELAP5 and TRACE are analyzed literately by referring to the code manuals and source codes of RELAP5 [12] and TRACE [13], respectively. Then, two separate computational platforms for RELAP5 and TRACE are developed on the basis of literature studies to separate constitutive relation models from governing equations. If the constitutive relation models are not separated, an analysis of constitutive relation models only is not possible because of the combined effect from numerical solutions of governing equations.

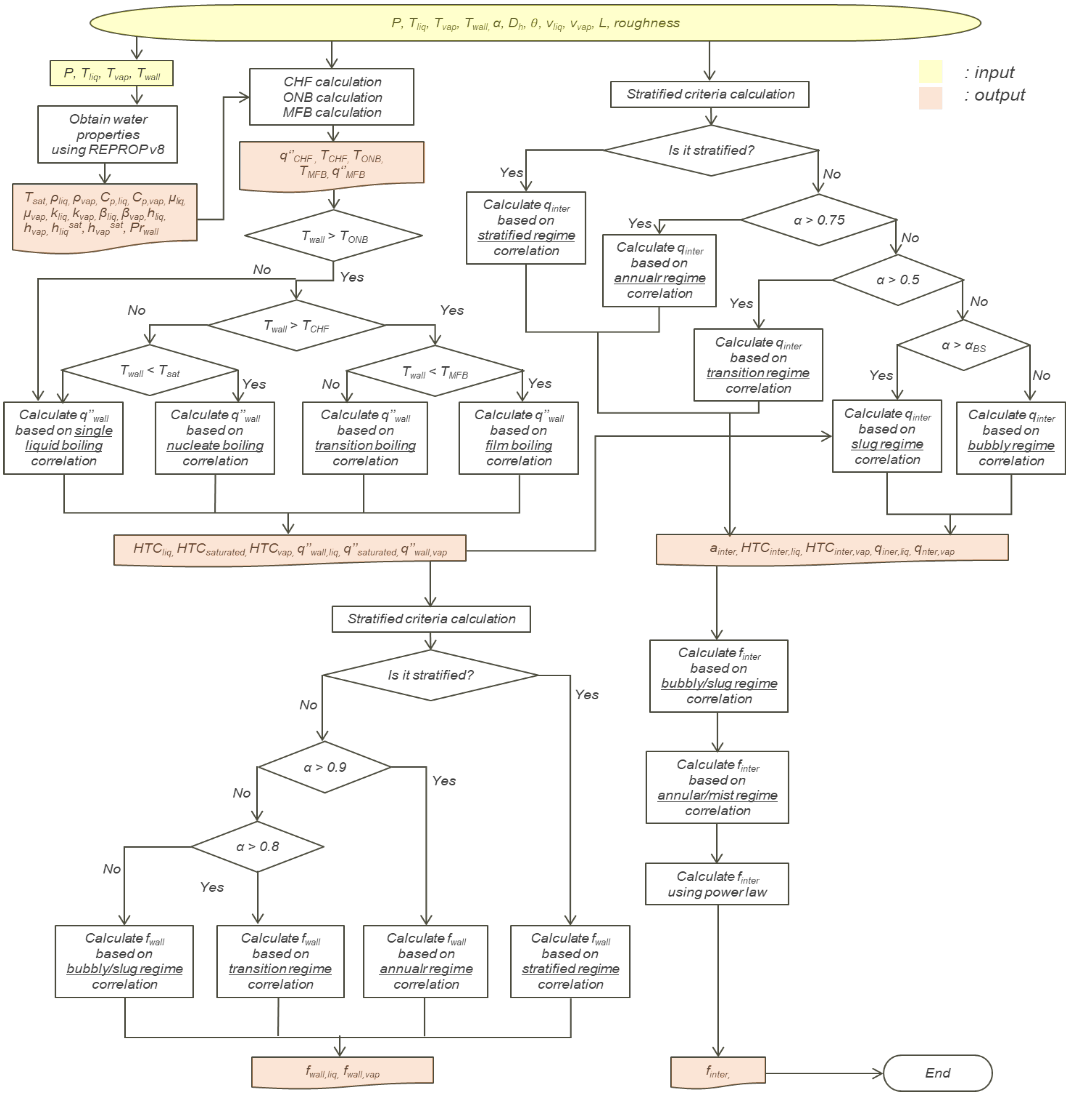
P, T_{liq}, T_{vap}, $T_{wall,}$ α, D_h, θ, v_{liq}, v_{vap}, L, roughness
: input
: output
P, T_{liq}, T_{vap}, T_{wall}
Obtain water properties using REPROP v8
$T_{sat,}$ $\rho_{liq,}$ $\rho_{vap,}$ $C_{p,liq,}$ $C_{p,vap,}$ $\mu_{liq,}$ $\mu_{vap,}$ $k_{liq,}$ $k_{vap,}$ $\beta_{liq,}$ $\beta_{vap,}$ $h_{liq,}$ $h_{vap,}$ h_{liq}^{sat}, h_{vap}^{sat}, Pr_{wall}
CHF calculation
ONB calculation
MFB calculation
q''_{CHF}, $T_{CHF,}$ $T_{ONB,}$ $T_{MFB,}$ q''_{MFB}
$T_{wall} > T_{ONB}$
No
Yes
$T_{wall} > T_{CHF}$
No
Yes
$T_{wall} < T_{sat}$
Yes
$T_{wall} < T_{MFB}$
No
Yes
Calculate q''_{wall} based on single liquid boiling correlation
Calculate q''_{wall} based on nucleate boiling correlation
Calculate q''_{wall} based on transition boiling correlation
Calculate q''_{wall} based on film boiling correlation
$HTC_{liq,}$ $HTC_{saturated,}$ $HTC_{vap,}$ $q''_{wall,liq,}$ $q''_{saturated,}$ $q''_{wall,vap}$
Stratified criteria calculation
Is it stratified?
Yes
No
Calculate q_{inter} based on stratified regime correlation
$\alpha > 0.75$
Yes
No
Calculate q_{inter} based on annualr regime correlation
$\alpha > 0.5$
Yes
No
Calculate q_{inter} based on transition regime correlation
$\alpha > \alpha_{BS}$
Yes
No
Calculate q_{inter} based on slug regime correlation
Calculate q_{inter} based on bubbly regime correlation
$a_{inter,}$ $HTC_{inter,liq,}$ $HTC_{inter,vap,}$ $q_{iner,liq,}$ $q_{nter,vap}$
Stratified criteria calculation
Is it stratified?
No
Yes
$\alpha > 0.9$
No
Yes
$\alpha > 0.8$
No
Yes
Calculate f_{wall} based on bubbly/slug regime correlation
Calculate f_{wall} based on transition regime correlation
Calculate f_{wall} based on annualr regime correlation
Calculate f_{wall} based on stratified regime correlation
$f_{wall,liq,}$ $f_{wall,vap}$
Calculate f_{inter} based on bubbly/slug regime correlation
Calculate f_{inter} based on annular/mist regime correlation
Calculate f_{inter} using power law
$f_{inter,}$
End

Figure 5 Flow Chart of Separate Computational Platform to Model the Constitutive Relations of TRACE

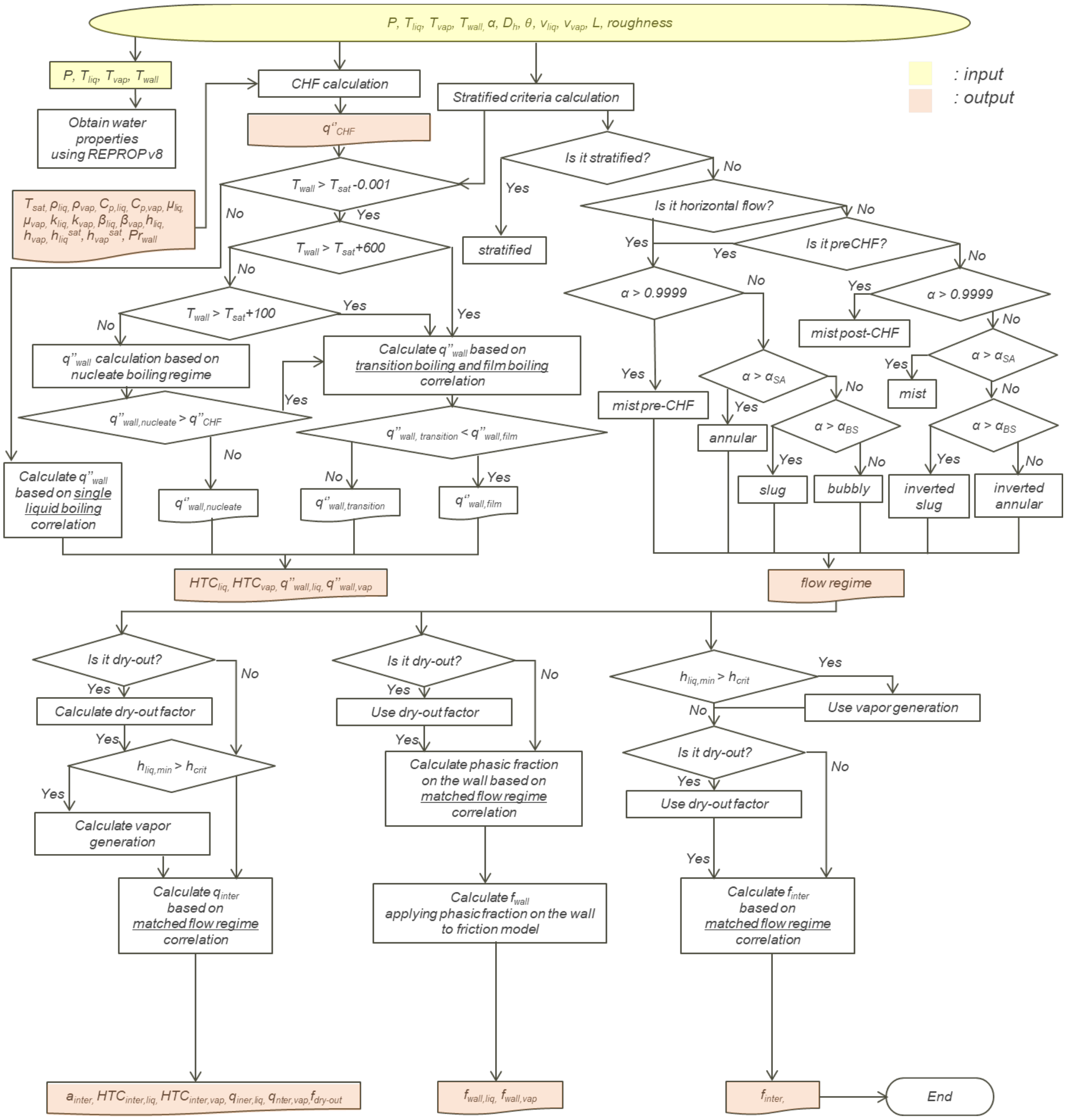
P, T_liq, T_vap, T_wall, α, D_h, θ, v_liq, v_vap, L, roughness
: input
: output
P, T_liq, T_vap, T_wall
Obtain water properties using REPROP v8
T_sat, ρ_liq, ρ_vap, C_p,liq, C_p,vap, μ_liq, μ_vap, k_liq, k_vap, β_liq, β_vap, h_liq, h_vap, h_liq^sat, h_vap^sat, Pr_wall
CHF calculation
q''_CHF
T_wall > T_sat-0.001
T_wall > T_sat+600
T_wall > T_sat+100
q''_wall calculation based on nucleate boiling regime
Calculate q''_wall based on transition boiling and film boiling correlation
q''_wall,nucleate > q''_CHF
q''_wall, transition < q''_wall,film
Calculate q''_wall based on single liquid boiling correlation
q''_wall,nucleate
q''_wall,transition
q''_wall,film
HTC_liq, HTC_vap, q''_wall,liq, q''_wall,vap
Stratified criteria calculation
Is it stratified?
stratified
Is it horizontal flow?
Is it preCHF?
α > 0.9999
α > 0.9999
mist post-CHF
mist pre-CHF
α > α_SA
α > α_SA
mist
α > α_BS
α > α_BS
annular
slug
bubbly
inverted slug
inverted annular
flow regime
Is it dry-out?
Calculate dry-out factor
h_liq,min > h_crit
Calculate vapor generation
Calculate q_inter based on matched flow regime correlation
Use dry-out factor
Calculate phasic fraction on the wall based on matched flow regime correlation
Calculate f_wall applying phasic fraction on the wall to friction model
Use vapor generation
Calculate f_inter based on matched flow regime correlation
a_inter, HTC_inter,liq, HTC_inter,vap, q_iner,liq, q_inter,vap, f_dry-out
f_wall,liq, f_wall,vap
f_inter,
End
Yes
No

Figure 6 Flow Chart of Separate Computational Platform to Model the Constitutive Relations of RELAP5

The separate computational platform for TRACE is developed to calculate the same wall heat transfer, interfacial heat transfer, wall friction, and interfacial friction calculated in the original code TRACE v 5.0 patch 5. This platform uses MATLAB for the working environment and REFPROP v.8 for the fluid properties. Figure 5 shows the flow chart of the separated computational platform to model the constitutive relations of TRACE. Eleven variables are required for input, which consist of thermal hydraulic conditions, geometry information, and material properties. The required thermal hydraulic conditions are the pressure, liquid and vapor temperatures, temperature at the wall, liquid and vapor velocities, and void fraction. The hydraulic diameter, flow direction, and pipe length have to be prescribed as geometry information, and the roughness is also needed for material properties. For the prescribed eleven variables, the CHF, heat flux on the wall, and wall heat transfer coefficient (HTC) are calculated in the wall heat transfer function, and then the interfacial area, HTC and volumetric heat transfer are also calculated in the interfacial heat transfer function. The wall friction and drag force in the interface are calculated in the wall and interfacial friction function, respectively. In a similar way as in TRACE, a separate computational platform is developed to model the constitutive relations of RELAP5 MOD3.3 patch5, which is shown in Figure 6. With the same 11 valuables as in the platform for TRACE, the CHF is calculated from the CHF calculation function and then the wall heat transfer is evaluated from the wall heat transfer function. Then, the flow regime is determined in the flow regime decision function, and from the selected flow regime, the interfacial heat transfer, wall friction, and interfacial friction are calculated from the interfacial heat transfer function, wall friction function and interfacial friction function, respectively.

2.1.1 Verification of Separate Computational Platform

To ensure that the developed platforms are calculating the same amount of heat transfer and friction as with the original codes, the results calculated from platforms are compared to the values from the original codes RELAP5 MOD3.3 patch5 and TRACE v 5.0 patch 5. The verification procedure is summarized in Figure 7. After simple modeling as shown in Figure 7(b), the thermal-hydraulic conditions and fluid properties from the original codes are given as the input of the platform, and then the amount of heat transfer and friction from the original codes are compared with the outputs from the platform as shown in Figure 7(a). For TRACE, one pipe, one fill as the flow boundary, one break as the pressure boundary, and one heat structure are used for the modeling. For RELAP5, one pipe, one tmdpvol with one single junction as the pressure boundary, one tmdpjun with one tmdpvol as the flow boundary, and heat structure components are used.

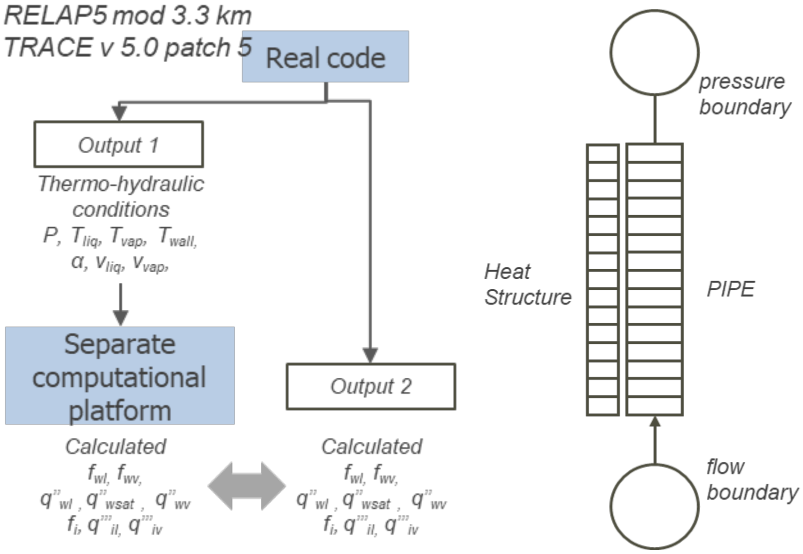
RELAP5 mod 3.3 km
TRACE v 5.0 patch 5
Real code
Output 1
Thermo-hydraulic conditions
$P, T_{liq}, T_{vap}, T_{wall}, \alpha, v_{liq}, v_{vap},$
Separate computational platform
Output 2
Calculated
$f_{wl}, f_{wv}, q''_{wl}, q''_{wsat}, q''_{wv}$
$f_i, q'''_{il}, q'''_{iv}$
Calculated
$f_{wl}, f_{wv}, q''_{wl}, q''_{wsat}, q''_{wv}$
$f_i, q'''_{il}, q'''_{iv}$
pressure boundary
Heat Structure
PIPE
flow boundary

Figure 7 Verification Process. (a) Verification Procedure Chart (b) Simplified Modeling Diagram in the Original Code

720 data items in total were obtained by varying the conditions of pressure or flow boundary and used for verification process. The degree matching the calculated heat transfer and friction from the platform with the original codes can be checked in Figure 8 and Table 1. The developed platforms have a slight difference from the original codes up to 7.14%. In the case of wall heat transfer, the maximum error is 6.98% for TRACE and 5.80% for RELAP5 in liquid –wall heat flux. For interfacial heat transfer case, the maximum error is 5.84% for TRACE and 4.54% for RELAP5 in vapor – interface heat flux. For wall friction and interfacial friction, the maximum error is 7.14% for TRACE in interfacial friction and 5.99% for RELAP5 in liquid – wall friction. These results seem to be reasonable since the separate platform uses different computational languages and also different property packages. Therefore, the developed platforms are considered to reproduce the results of the original codes quite well.

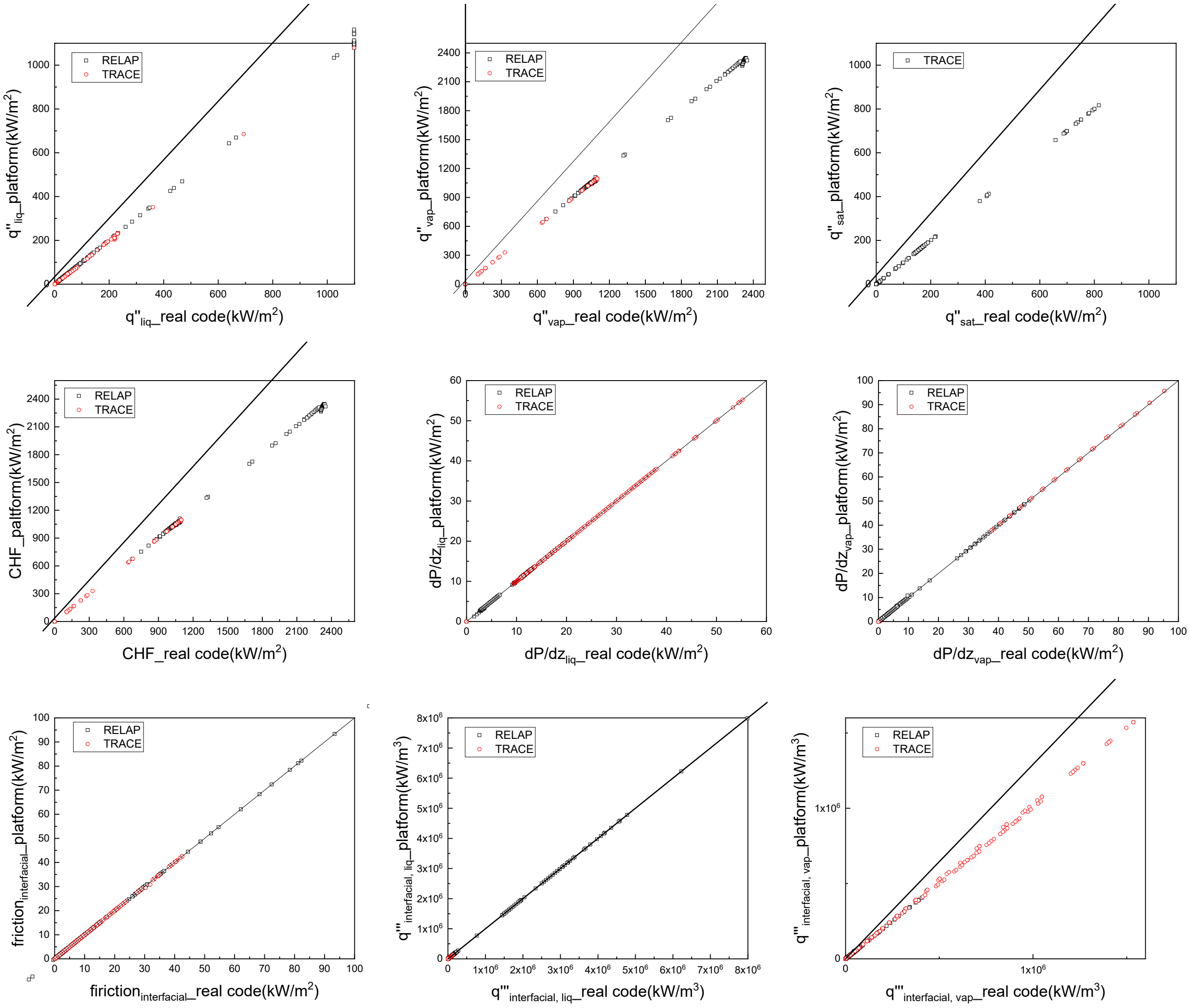

Figure 8 Verification Results of Separate Platforms

Table 1 Verification Results of Separate Platforms

variable	Code	Max error	variable	Code	Max error
q''_{liq}	RELAP5	5.80	q''_{vap}	RELAP5	2.40
	TRACE	6.98		TRACE	0.228
q''_{sat}	RELAP5	-	q''_{CHF}	RELAP5	2.01
	TRACE	6.35		TRACE	0.228
dP/dz_{liq}	RELAP5	5.99	dP/dz_{vap}	RELAP5	4.53
	TRACE	0.100		TRACE	0.466
$q'''_{i,liq}$	RELAP5	4.54	$q'''_{i,vap}$	RELAP5	2.65
	TRACE	5.84		TRACE	7.14

2.2 Comparison Method

In Figure 9, the entire comparison process is summarized. If several conditions (thermal-hydraulic conditions, geometry information, and material property) are given as input of the platform, two platforms calculate the heat transfer and friction, and then those output values are compared. Before proceeding to the comparison results of RELPA5 and TRACE, the compared thermal-hydraulic conditions must be defined and the compared variables have to be determined as well.

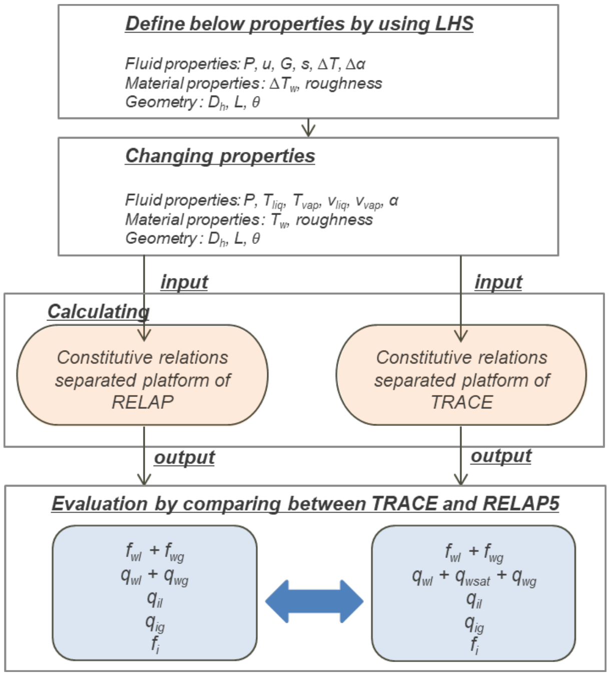

Define below properties by using LHS
Fluid properties: P, u, G, s, ΔT, $\Delta\alpha$
Material properties: ΔT_w, roughness
Geometry: D_h, L, θ
Changing properties
Fluid properties: P, T_{liq}, T_{vap}, v_{liq}, v_{vap}, α
Material properties: T_w, roughness
Geometry: D_h, L, θ
input
input
Calculating
Constitutive relations separated platform of RELAP
Constitutive relations separated platform of TRACE
output
output
Evaluation by comparing between TRACE and RELAP5
$f_{wl} + f_{wg}$
$q_{wl} + q_{wg}$
q_{il}
q_{ig}
f_i
$f_{wl} + f_{wg}$
$q_{wl} + q_{wsat} + q_{wg}$
q_{il}
q_{ig}
f_i

Figure 9 Flow Chart of Evaluation Methodologies

To determine the variables to compare, governing equations of TRACE and RELAP5 are first analyzed. Equations (2.1) – (2.12) describe the mass, momentum and energy conservation of

RELAP5 and TRACE. The mass conservation equations of TRACE are equation (2.1) for the total and (2.2) for the vapor phase, and (2.3) and (2.4) are those of RELAP5 for the liquid and vapor phases. The momentum conservation equations are shown in equations (2.5) – (2.8). It can be observed that the friction term of both the wall and the interface in equations (2.5) – (2.8) is applied in the same way, where f_i is the force per unit volume due to shear at the phase interface, and f_{wl} and f_{wv} are the wall shear force per unit volume acting on the liquid and vapor phases. For evaluation of the wall friction models, the total wall shear force per unit volume $f_{wl} + f_{wv}$ (kPa/m) is selected for comparison. In a similar manner, interfacial shear force f_i (kPa/m) is compared between the two codes. Equations (2.9) – (2.10) and (2.11) – (2.12) show energy conservation implemented in TRACE and RELAP5, respectively. It is confirmed that the interfacial heat transfer term is similarly applied, so the volumetric heat transfer between the interface and each phase q_{il}, q_{iv} (kW/m^3) are compared. In the case of the vapor – wall heat transfer, the same heat flux q_{wv} is applied, but in the liquid – wall heat transfer, TRACE distributes the liquid – wall heat flux to q_{wl} and q_{wsat}, where q_{wv} is heat flux to the vapor, q_{wl} represents the heat flux to the liquid except q_{wsat}, and q_{wsat} is the heat flux to the liquid which goes directly to boiling. For evaluation of the wall heat transfer models, the total heat flux on the wall $q_{wl} + q_{wsat} + q_{wv}$ of TRACE and $q_{wl} + q_{wv}$ of RELAP5 are compared, and the unit is kW/m^2.

$$\frac{\partial\left[(1-\alpha)\rho_l + \alpha\rho_g\right]}{\partial t} + \nabla\cdot\left[(1-\alpha)\rho_l v_l + \alpha\rho_g v_g\right] = 0 \tag{2.1}$$

$$\frac{\partial\left[\alpha\rho_v\right]}{\partial t} + \nabla\cdot\left[\alpha\rho_v v_v\right] = \Gamma \tag{2.2}$$

$$\frac{\partial\left[(1-\alpha)\rho_l\right]}{\partial t} + \frac{1}{A}\nabla\cdot\left[(1-\alpha)\rho_l v_l A\right] = -\Gamma \tag{2.3}$$

$$\frac{\partial\left[\alpha\rho_v\right]}{\partial t} + \frac{1}{A}\nabla\cdot\left[\alpha\rho_v v_v A\right] = \Gamma \tag{2.4}$$

$$\frac{\partial v_l}{\partial t} + v_l\nabla\cdot v_l = -\frac{1}{\rho_l}\nabla P + \frac{\left[f_i - \Gamma(v_i - v_l) + f_{wl}\right]}{(1-\alpha)\rho_v} + \vec{g} \tag{2.5}$$

$$\frac{\partial v_v}{\partial t} + v_v\nabla\cdot v_v = -\frac{1}{\rho_v}\nabla P + \frac{\left[f_{wv} - f_i - \Gamma(v_v - v_i)\right]}{\alpha\rho_v} + \vec{g} \tag{2.6}$$

$$\frac{\partial v_l}{\partial t} + v_l\nabla\cdot v_l = -\frac{1}{\rho_l}\nabla P + \frac{\left[f_i - \Gamma(v_i - v_l) + f_{wl}\right]}{(1-\alpha)\rho_l} + B_x - C\alpha\frac{\rho_m}{\rho_l}\left[\frac{\partial(v_l - v_v)}{\partial t} + v_v\nabla\cdot v_l - v_l\nabla\cdot v_v\right] \tag{2.7}$$

$$\frac{\partial v_v}{\partial t} + v_v\nabla\cdot v_v = -\frac{1}{\rho_v}\nabla P + \frac{\left[f_{wv} - f_i - \Gamma(v_v - v_i)\right]}{\alpha\rho_v} + B_x - C(1-\alpha)\frac{\rho_m}{\rho_v}\left[\frac{\partial(v_v - v_l)}{\partial t} + v_l\nabla\cdot v_v - v_v\nabla\cdot v_l\right] \tag{2.8}$$

$$\frac{\partial\left[(1-\alpha)\rho_l e_l + \alpha\rho_v e_v\right]}{\partial t} + \nabla\cdot\left[(1-\alpha)\rho_l e_l v_l + \alpha\rho_v e_v v_v\right] = -P\nabla\cdot\left[(1-\alpha)v_v + \alpha v_v\right] + q_{wl} + q_{wsat} + q_{wv} + q_{dl} + q_{dv} \tag{2.9}$$

$$\frac{\partial\left[\alpha\rho_v e_v\right]}{\partial t} + \nabla\cdot\left[\alpha\rho_v e_v v_v\right] = -P\frac{\partial\alpha}{\partial t} - P\nabla\cdot(\alpha v_v) + q_{wv} + q_{dv} + q_{iv} + \Gamma h_v' \tag{2.10}$$

$$\frac{\partial\left[(1-\alpha)\rho_l e_l\right]}{\partial t}+\frac{1}{A}\nabla\cdot\left[(1-\alpha)\rho_l e_l v_l A\right]=-P\frac{\partial(1-\alpha)}{\partial t}-\frac{P}{A}\nabla\cdot\left[(1-\alpha)v_l A\right]+q_{wl}+q_{il}-\Gamma_{iv}h_l^{*}-\Gamma_{w}h_l^{'}+Diss_l \quad (2.11)$$

$$\frac{\partial\left[\alpha\rho_v e_v\right]}{\partial t}+\frac{1}{A}\nabla\cdot\left[\alpha\rho_v e_v v_v A\right]=-P\frac{\partial\alpha}{\partial t}-\frac{P}{A}\nabla\cdot\left[\alpha v_l A\right]+q_{wv}+q_{iv}+\Gamma_{iv}h_v^{*}-\Gamma_{w}h_v^{'}+Diss_v \quad (2.12)$$

Finally, the total 5 variables to be compared are determined as the total wall heat transfer ($q_{wl}+q_{wsat}+q_{wv}$ or $q_{wl}+q_{wv}$), each phasic interfacial heat transfer (q_{il} , q_{iv}), the total wall friction ($f_{wl}+f_{wv}$), and the interfacial friction (f_i). It was necessary to determine how to compare these variables. There are many ways to compare two values, such as the absolute difference, relative difference, ratio and so on. Among them, the sum of least squares is adopted, which is reasonable when the amount of heat transfer or friction is compared. In other words, the R-squared value is utilized to evaluate the difference in the calculated heat transfer and friction between the two codes. This is useful because: (1) The R-squared value is not dependent on the magnitude of the variables to be compared. (2) The signs of two variables to be compared are not of concern. (3) The calculated heat transfer and friction depend on the heat transfer regime or flow regime. Since the R-squared value varies depending on which of the two values is true, the average of the calculated R-squared values is used as the representative value. Using this method, one representative value can be derived for each regime.

2.2.1 Selecting Thermal-hydraulic Conditions for Comparison

After determining the variables to compare, input variables have to be defined. The total number of variables to be determined as input is 11, and this includes three items of geometry information and one item of material properties. Among the geometry information, hydraulic diameter is set to a random value between 0.01 and 0.3 m and the flow direction is also set to an angle of 0 or 90 degrees. Roughness in the wall is selected to be zero, so seven variables of thermal-hydraulic conditions remain to be determined.

To determine the range of thermal-hydraulic conditions for evaluating the constitutive relation models, several accident scenarios are selected among design basis accidents (DBAs) of the Barakah nuclear power plant (NPP). DBAs are listed by Fussell-Vesely (FV) importance in Figure 10. FV importance measures the overall percent contribution of cut sets that contains a basic event of interest to the total risk, which is described in equation (2.13), where $F(i)$ is the risk from just those cut sets that contain event x_i and $F(x)$ is the total risk from all cut sets. The top three DBAs based on the FV importance are selected for this study: loss of offsite power (LOOP), steam generator tube rupture (SGTR) and small loss of coolant accident (SLOCA). Evaluation is performed in the range including the minimum and the maximum thermal-hydraulic conditions of the selected DBAs. Table 2 briefly outlines the maximum and minimum thermal-hydraulic conditions of the selected DBAs. LOOP is considered for 4 cases: LOOP by turbine trip, large steam line break with LOOP, total loss of reactor coolant flow with LOOP, and single reactor coolant pump rotor seizure, which are numbered from 1 to 4. SGTR includes 2 cases: SGTR with LOOP (case1) and SGTR without LOOP (case2). SLOCA considers a total of 9 cases with different break sizes and locations: break in pump discharge leg (0.5 ft^2, 0.35 ft^2, 0.1 ft^2, 0.05 ft^2), in DVI line (0.4 ft^2, 0.1 ft^2, 0.05 ft^2, 0.02 ft^2), and on the top of pressurizer (0.03 ft^2), which are also numbered from 1 to 9.

$$FV_{xi}=F(i)/F(x) \quad (2.13)$$

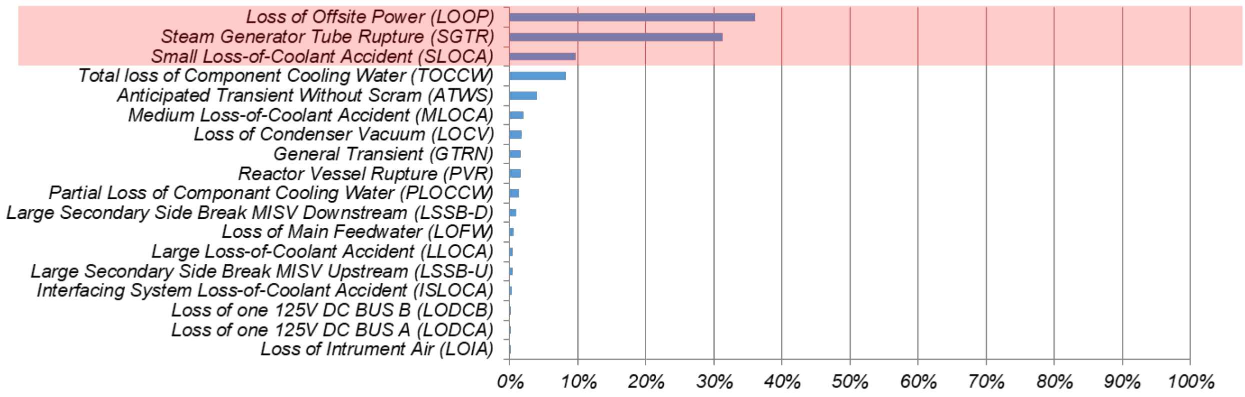

Figure 10 DBAs Based on F-V Initiating Events Importance of the Barakah NPP

Throughout all the DBAs, the maximum and the minimum pressure are 17.81 MPa and 1.38 MPa, so the range of pressure is set to from 1.38 to 17.81 MPa. In the same way, the internal energy, mass flux, and wall temperature is set to from 200 to 2700 kJ/kg, from 7 to 120% of the mass flux at the steady state, and from T_{sat} to T_{sat} + 350 K. There are still 3 variables to be determined. By Zuber-Findlay [14], the range of slip ratio is set as 1 to 3, which is estimated by assuming the distribution factor as 1.2 and this value can be seen in Figure 11(a). From the determined slip ratio and internal energy, the void fraction at equilibrium can be defined, so the void fraction is considered to have normal distribution with the equilibrium void fraction as the average value. By using internal energy and pressure, the temperature of one phase can be defined and the temperature of other phase is considered to have normal distribution with the saturated temperature for the given pressure as the average value to apply metastable by bubble generation or breakage as shown in Figure 11(b) [15]. The selected conditions for comparison are summarized in Table 3.

Table 2 Thermal-hydraulic Conditions of the Selected DBAs

		P (MPa)	$T - T_{sat}$ (ΔK)	G (%)	$T_w - T_{sat}$ (ΔK)
LOOP	case1	13.95 – **17.81**	- 60.0 – - 20.2	10 – 115	
	case2	10.76 – 15.87	- 95.0 – - 13.0	10 – 100	
	case3	9.56 – 16.12	**- 180.0** – - 8.0	10 – 100	
	case4	15.69 – 16.90	- 58.0 – -20.0	8 – 100	
SGTR	case1	10.34 – 16.55	- 42.0 – -15.0		
	case2	10.34 – 16.55	- 45.0 – - 6.0		
SLOCA	case1	**1.38** – 16.55	max: 122.81	**7** – 103	**1.28** – 212.68
	case2	3.45 – 16.55	max: 54.43	**7** – 106	2.35 – 159.44
	case3	3.52 – 16.55	max: 4.09	**7** – 112	7.86 – 166.87
	case4	3.65 – 16.55	max: 2.97	**7** – 114	18.89 – 207.97
	case5	**1.38** – 16.55	max: **194.74**	**7** – 106	2.43 – **346.98**
	case6	3.45 – 16.55	max: 85.88	**7** – **120**	12.63 – 226.41
	case7	3.52 – 16.55	max: 2.71	**7** – 113	29.02 – 213.52
	case8	8.27 – 16.55	max: 11.41	**7** - 114	30.22 – 216.87
	case9	7.58 – 16.55	max: 1.16	**7** - 114	30.33 – 220.94

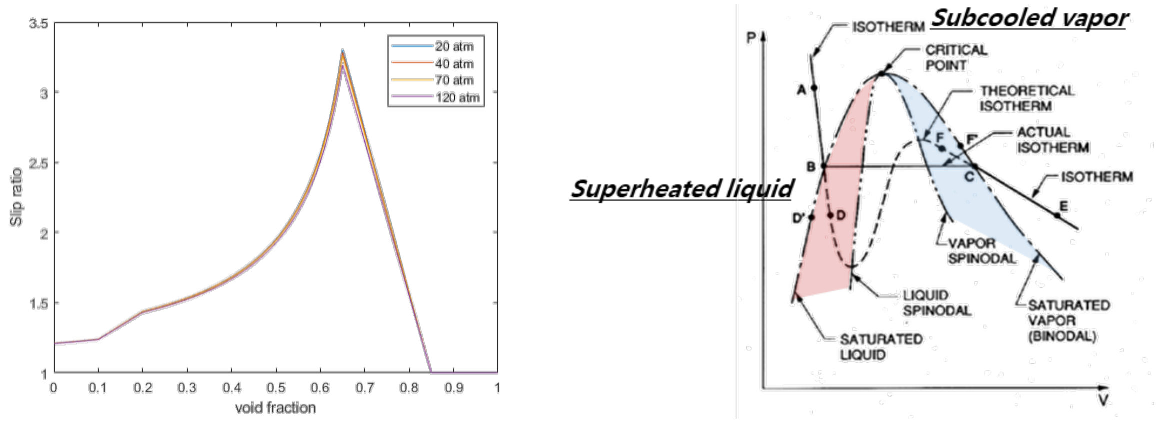

Figure 11 Needed Variables to Determine Thermal-hydraulic Conditions. (a) Slip Ratio According to Void Fraction [14] (b) p-v Diagram [15]

To sample seven thermal-hydraulic conditions, the Latin hypercube sampling method is used, which was suggested by McKay [16]. Latin hypercube sampling is a statistical method for generating a near-random sample of parameter values from a multidimensional distribution. A total of 900 data sets are generated in the horizontal direction and another total of 900 data sets are also generated in the vertical direction, in which the confidence coefficient is 0.999 and the fraction of the population between the smallest and the largest observations of the sample is 0.99.

Table 3 Defined Conditions for Comparison

Latin Hypercube Sampling (LHS) variables		
Thermal hydraulic conditions		
properties	range	distribution
P	1.35 – 17.8 MPa	uniform
u	200 – 2700 kJ/kg	uniform
G	7 – 120 %	uniform
ΔT_w	0 – 350 K	continuous linear
ΔT	mean = 0 SD = 0.5	normal
$\Delta\alpha$	mean = 0 SD = 0.05	normal
slip ratio	1 – 3	uniform
Geometry information		
D_h	0.01 – 0.3 m	uniform
θ	0 or π/2	
Material property		
roughness	0	

3 WALL HEAT TRANSFER MODELS

3.1 Background

The phenomena of heat transfer from the wall to the fluid is complex due to many possible configurations of liquid and vapor phases near the wall. Thus, when estimating the amount of heat transfer from the wall to the fluid, it is usually divided into four regimes based on the boiling curve, and then a different model is applied to each regime. These regimes are shown in Figure 12 [17]. The A-B region is a non-boiling region. There is only liquid near the wall, so it is called the single phase heat transfer regime. In this region, the process of heat transfer is not complicated, so there are many good correlations. An example is the Dittus-Boelter correlation [18]. After point B, nucleate boiling starts, so this point is called the onset of nucleate boiling (ONB). The B-C region is the nucleate boiling heat transfer regime, in which nucleate boiling occurs because the temperature of the wall exceeds the saturation temperature by a few degrees and it makes a small amount of nucleation as shown in Figure 12. These bubbles rise quickly and collapse. Thus, this slight agitation causes heat transfer to increase more rapidly. However, after point C, the nucleation rate becomes high enough to induce formation of vapor film at the wall. Point C is defined as the CHF, and based on this point, whether it is a pre-CHF or post-CHF regime can be distinguished. The C-D region is called the transition boiling heat transfer regime, which is an unstable region between the nucleate (B-C) and film (D-F) boiling heat transfer regimes. Point D is called the minimum film boiling (MFB) heat flux or Leidenfrost point. In D-E region, the wall is surrounded by continuous vapor film as shown in Figure 12, and this region is called the film boiling heat transfer regime.

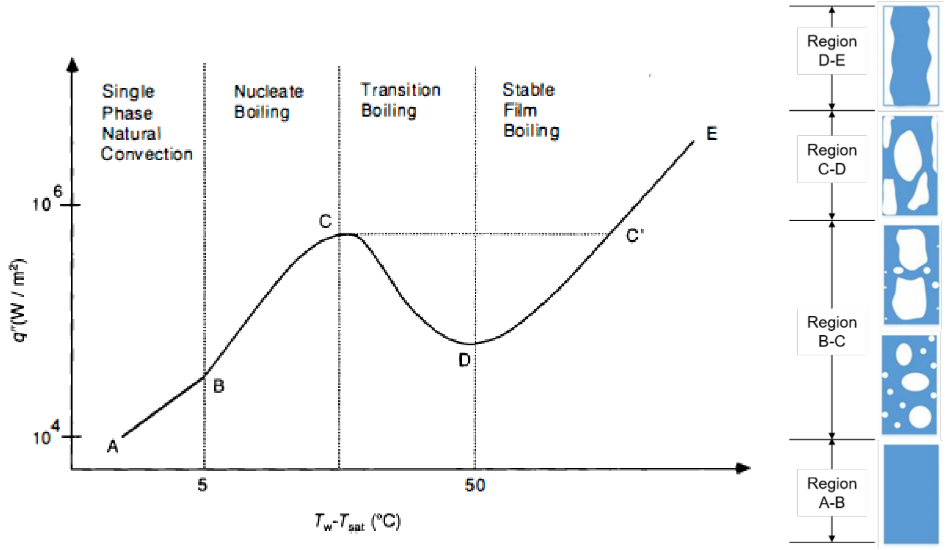

Figure 12 Typical Pool Boiling Curve for Water under Atmospheric Pressure [17] and Simplified Bubble Shape in Regions of Heat Transfer [19]

3.2 Description of Wall Heat Transfer Modules

As explained in chapter 2.2, information on the amount of energy transfer from a heat structure to a fluid volume is needed to solve the energy conservation equation in thermal-hydraulic system analysis codes. This amount is calculated in the wall heat transfer modules in RELAP5 and TRACE codes. The wall heat transfer module is configured as follows: Firstly, the wall heat transfer (HT) regime is determined based on the prescribed thermo-hydraulic conditions, as described in section 3.1. The amount of heat transfers from the wall to the fluid is evaluated by a correlation which matches the corresponding wall HT regime. Sometimes, if the CHF value is required to select the wall HT regime, the CHF is also calculated with the correlation. In other words, wall heat transfer modules of RELAP5 and TRACE have 3 components: (1) the wall HT regime selection logic, (2) the CHF calculation model, and (3) various heat transfer models and correlations. Figure 13 briefly shows the wall heat transfer modules of RELAP5 and TRACE.

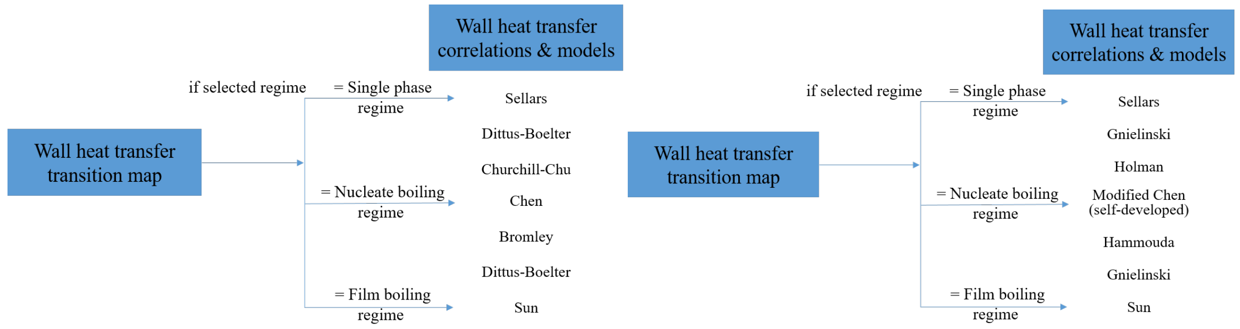
Wall heat transfer transition map
if selected regime
= Single phase regime
= Nucleate boiling regime
= Film boiling regime
Wall heat transfer correlations & models
Sellars
Dittus-Boelter
Churchill-Chu
Chen
Bromley
Dittus-Boelter
Sun
Wall heat transfer transition map
if selected regime
= Single phase regime
= Nucleate boiling regime
= Film boiling regime
Wall heat transfer correlations & models
Sellars
Gnielinski
Holman
Modified Chen (self-developed)
Hammouda
Gnielinski
Sun

Figure 13 Simplified Wall Heat Transfer Modules (a) RELAP5 (b) TRACE

3.2.1 Selection Logic of Wall Heat Transfer Regime

Both codes determine the wall HT regime with the wall HT regime selection logic based on the thermo-hydraulic conditions. Table 4 shows the HT regimes implemented in RELAP5 and TRACE. The HT regimes of both codes contain single phase, nucleate boiling, transition boiling, and film boiling HT regimes. In TRACE, the film boiling HT regime is divided into three (inverted annular, inverted slug, and dispersed flow film boiling HT regimes) according to the void fraction, but RELAP5 has only one film boiling HT regime.

Table 4 Wall Heat Transfer Regimes of (a) RELAP5 and (b) TRACE

regime number	Wall HT regime
2	single phase liquid HT
3	subcooled nucleate boiling HT
4	saturated nucleate boiling HT
5	subcooled transition boiling HT
6	saturated transition boiling HT
7	subcooled film boiling HT
8	saturated film boiling HT
9	single phase vapor HT
10	condensation HT

regime number	Wall HT regime
1	single phase liquid HT
2	nucleate boiling HT
3	transition boiling HT
4	inverted annular film boiling HT
5	dispersed flow film boiling HT
6	single phase vapor HT
7	condensation film HT
8	transition between film condensation HT and liquid phase HT

In TRACE, the wall HT regime is determined by the selection logic, which is shown in Figure 14. This figure briefly outlines the logic for the wall HT regimes but does not show the regimes that are not investigated in this study (condensation regime, super-critical regime, etc.). In this logic, the wall temperature is compared with the temperatures at ONB, CHF, MFB and the saturation temperature. TRACE has correlations to model temperature of ONB and MFB. To predict the temperature of ONB, Basu's correlation [20] is used as in equation (3.1). The MFB point is determined by the wall temperature calculated in equation (3.2). To model the temperature of MFB, TRACE applies Groeneveld's correlation [21] with the upper and lower limits due to quenching determined from the FLUCHT-SEASET low-pressure reflood test [22] and nine THTF high-pressure reflood tests [23, 24]. TRACE uses equation (3.4) as criteria for CHF, T_{CHF} is obtained from condition (3.5), in which the heat flux calculated by the model of nucleate regime is the same as CHF, using the Newton-Rapson method.

$$\Delta T_{ONB} = \frac{4\sigma T_{sat}}{D_c \rho_v h_{fg}} \tag{3.1}$$

$$T_{MFB} = \max\left(\min\left(800, T_{MFB,sat} - \frac{x \cdot 10^4}{(2.82 + 1.22P)} \right), 725 \right) \tag{3.2}$$

$$T_{MFB,sat} = 557.85 + 44.1P - 3.72P^2 \tag{3.3}$$

$$T_w = T_{CHF} \tag{3.4}$$

$$q''_{CHF} = q''_{nucleate}\left(T_{CHF}\right) \tag{3.5}$$

In a similar way, RELAP5 determines wall HT regime with the selection logic shown in Figure 15. However, in RELAP5, instead of temperature at ONB and MFB, temperature T_{sat} – 0.001 or condition (3.6) are applied respectively, because RELAP5 does not have correlations to model the temperature for ONB or MFB. Two heat flux values from film and transition boiling HT correlations are the criteria for choosing the transition or film HT regime. Similar to the method in TRACE, the condition (3.5) is used as the criteria for CHF. In Figure 14 and Figure 15, the criteria of CHF seems to be different because TRACE uses the wall temperature and RELAP5 uses the heat flux to determine the criteria for CHF, but T_{CHF} is obtained from condition (3.5) using the Newton-Rapson method, thus the logic for CHF is the same between TRACE and RELAP5. Although both codes have the same logic for CHF, the correlations used in the nucleate HT regime are different, which will be explained in the next chapter 3.3 and 3.4.

$$q''_{transition} = q''_{film} \tag{3.6}$$

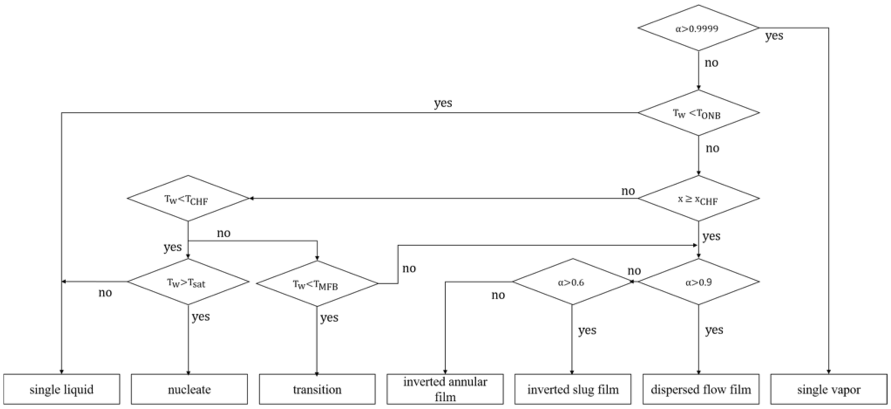
α>0.9999
yes
no
Tw <TONB
yes
no
Tw<TCHF
no
x ≥ xCHF
no
yes
yes
Tw>Tsat
no
Tw<TMFB
no
α>0.6
no
no
α>0.9
yes
yes
yes
yes
single liquid
nucleate
transition
inverted annular film
inverted slug film
dispersed flow film
single vapor

Figure 14 Wall Heat Transfer Selection Logic Diagram of TRACE

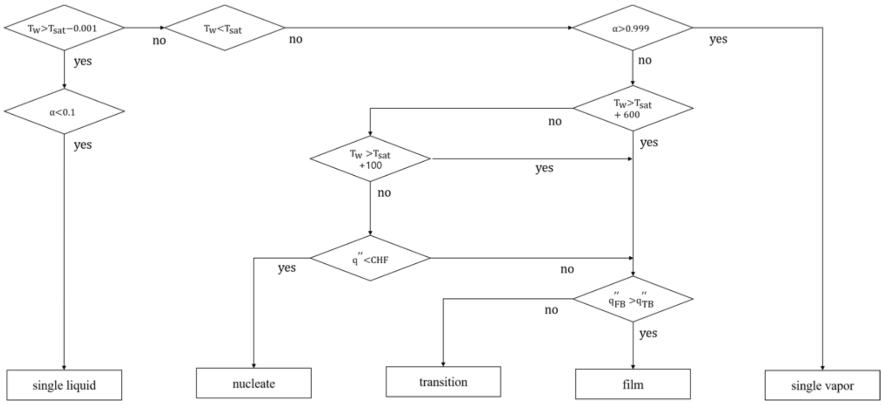
Tw>Tsat−0.001
no
Tw<Tsat
no
α>0.999
yes
yes
no
α<0.1
Tw>Tsat + 600
no
yes
yes
Tw >Tsat +100
yes
no
q″<CHF
yes
no
q″FB >q″TB
no
yes
single liquid
nucleate
transition
film
single vapor

Figure 15 Wall Heat Transfer Selection Logic Diagram of RELAP5

3.2.2 Critical Heat Flux Calculation Model

To select the wall HT regime, if RELAP5 or TRACE requires CHF information, the CHF prediction model is used. To evaluate CHF, RELAP5 and TRACE use the Groeneveld CHF look-up table as the default. However, the two codes use different versions of the table. TRACE uses the 1995 version and RELAP5 uses the 1986 version. Groeneveld et al. suggested that it is not good to model CHF for a wide range or thermal hydraulic conditions. They assumed CHF as a function of pressure, mass flux, and quality and geometry, and then constructed a CHF look-up table based on local conditions, i.e., $\mathrm{CHF} = f\left(P, G, x, \mathrm{geometry}\right)$. This table was developed first with the Atomic Energy of Canada Limited (AECL) and the University of Ottawa (UO), so it is called the 1986 AECL-UO Critical Heat Flux Lookup Table [25]. After that, Groeneveld et al. updated the lookup table and newly published it in 1996 with AECL and the Institute of Power and Physics (IPPE). The 1995 AECL-IPPE and 1986 AECL-UO Critical Heat Flux Lookup Tables were developed based on an 8 mm tube, so TRACE and RELAP5 have correction factors to adjust for the differences. TRACE has a correction factor k1 for the tube diameter, shown in equation (3.7). RELAP5 has correction factors k1, k4, k5, k7 for the tube diameter, heated length, axial power, and vertical flow, shown in equations (3.8) – (3.11), respectively. In equation (3.9), α_e is calculated from the equilibrium quality.

$$k_1 = \max\left(\sqrt{0.008/D_h}, 0.6\right) \tag{3.7}$$

$$k_1 = \begin{array}{ll} \left(0.008/D_h\right)^{0.3333} & \text{for } D_h < 0.016 \text{ m} \\ \left(0.008/0.016\right)^{0.3333} & \text{for } D_h > 0.016 \text{ m} \end{array} \tag{3.8}$$

$$k_4 = \exp\left(\min\left(D_h/L, 0.02\right) \times \exp\left(2\alpha_e\right)\right) \tag{3.9}$$

$$k_5 = \text{local heat flux} \Big/ \text{average heat flux from start of boiling to point} \tag{3.10}$$

$$k_7 = \begin{array}{lll} \left(1-\alpha\right) & \text{for } \alpha < 0.8 & \\ \left(1-\alpha\right)\dfrac{\left(0.8+0.2\,\rho_l/\rho_v\right)}{\left(\alpha+\left(1-\alpha\right)\rho_l/\rho_v\right)} & \text{for } \alpha > 0.8 & \text{for } -50 < G < 10 \text{ kg/m}^2\text{-sec} \\ & & \\ \text{interpolate} & & \begin{array}{l} \text{for } 10 < G < 100 \text{ kg/m}^2\text{-sec} \\ \text{for } -400 < G < -50 \text{ kg/m}^2\text{-sec} \end{array} \end{array} \tag{3.11}$$

3.2.3 Wall Heat Transfer Models & Correlations

After determining the wall HT regime, the heat transfer coefficient (HTC) or heat flux is calculated using heat transfer models and correlations matching the selected wall HT regime in the logic diagram. More details are given in sections 3.3 and 3.4.

3.3 Wall Heat Transfer Models and Correlations of TRACE

In the single phase HT regime, TRACE selects the largest Nusselt number among laminar, turbulent, and natural convection Nusselt numbers. TRACE utilizes Sellars [26] correlation (3.12) for a laminar flow and Gnielinski [27] correlation (3.13) for a turbulent flow. The friction factor in the Gnielinski correlation is evaluated using the smooth tube formula (3.14) of Filonenko [28], and property variation due to high wall temperature is corrected using the Hufschmidt and Burck [29] factor. Generally, the Dittus-Boelter correlation is used for a turbulent flow but the reason for using Gnielinski in TRACE is that the Dittus-Boelter [18] correlation over-predicts the HTC in the transition regime between the laminar and turbulent flows [13]. Figure 16 shows the over-prediction of the Dittus-Boelter correlation in the region between the laminar and turbulent flow regimes.

$$\mathrm{Nu}_{\mathrm{lam}} = 4.36 \tag{3.12}$$

$$\mathrm{Nu}_{\mathrm{turb}} = \frac{\left(f/2\right)\left(\mathrm{Re}-1000\right)\mathrm{Pr}}{1+12.7\left(f/2\right)^{0.5}\left(\mathrm{Pr}^{2/3}-1\right)} \times \left(\frac{\mathrm{Pr}_l}{\mathrm{Pr}_w}\right)^{0.11} \tag{3.13}$$

$$f = [1.58\ln\mathrm{Re} - 3.28]^{-2} \tag{3.14}$$

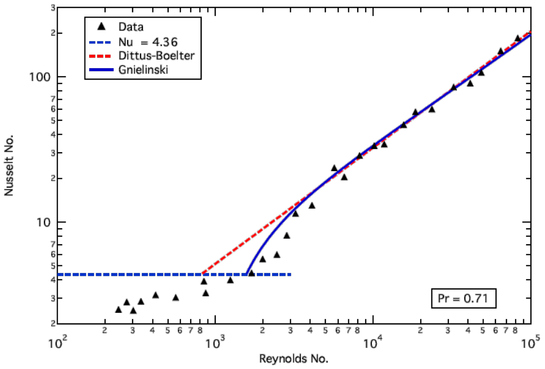

Figure 16 Comparison of Heat Transfer Models for Forced Convection [13]

In TRACE, a self-developed model is used for the nucleate boiling HT regime on the basis of additive contributions (3.15) in the Chen [30] correlation. Additive contributions were first suggested by Rohsenow [31] in 1952, and then Gambill [32] applied the additive concept with burnout data in 1963. After that, Chen [30] added the flow factor and the suppression factor because convective and boiling contributions could be superimposed in the saturated boiling regime without modifications. Using the flow factor, two-phase enhancement is accounted for and suppression of bubbles because convection is reflected in the suppression factor.

$$h_{\mathrm{NB}} = F \cdot h_{\mathrm{FC}} + S \cdot h_{\mathrm{PB}} \tag{3.15}$$

TRACE utilizes the newly suggested flow factor and suppression factor, and applies different models for the forced convection and pool boiling heat transfer terms. The forced convective heat transfer is predicted by a correlation used in the single phase HT regime, Gnielinski [27] correlation (3.13). Originally, in the Chen correlation, the flow factor is a function of the Martinelli parameter with flow quality, but the flow factor has oscillation when the flow quality is ill-defined. For this reason, TRACE uses Rezkallah and Sims [33] liquid-acceleration model (3.16) for the flow factor, where n is the exponent on the Reynolds number for the single-phase heat transfer model. That is, the two-phase enhancement effect can be considered by substituting the newly defined Reynolds number (3.17) to a single-phase heat transfer model. For the same reason, the suppression factor is not used in TRACE.

$$h_{2\phi} / h_l = (1-\alpha)^{-n} \tag{3.16}$$

$$\mathrm{Re}_{2\phi} = \frac{G_l \cdot D_h}{\mu_l} = \frac{(1-\alpha)\rho_l v_l D_h}{\mu_l} \tag{3.17}$$

The Gorenflo [34] model is adopted for the pool boiling heat transfer term in equation (3.15) in TRACE. The reason for changing the pool boiling model is the tendency to underestimate the heat flux in the Chen correlation. A more recent nucleate boiling correlation shows the dependency of the boiling heat flux on the wall superheat, where the exponent n is generally agreed to have a value between 3 and 4 [35]. Holman recommended the McAdams [36] correlation for low pressure and the Levy [37] correlation for high pressure [38]. From this recommendation, TRACE selects the Gorenflo correlation (3.18), which has a trend similar to the McAdams correlation at low pressure and the Levy correlation at high pressure. Figure 17 shows the comparison of correlations for selecting the pool boiling heat transfer model. The pool boiling model of Gorenflo has a reference point. For water, the reference point is expressed in equation (3.21). When the Gorenflo correlation is implemented in the code, a roughness factor is taken as unity, so equation (3.18) becomes (3.22), and it can be rearranged as equation (3.23).

$$h_{\mathrm{PB}} = h_0 \cdot F_P \cdot \left(q''/q''_0\right)^n \cdot \left(R/R_0\right)^{0.133} \tag{3.18}$$

$$F_P = 1.73\left(P/P_{crit}\right)^{0.27} + \left(6.1 + \frac{0.68}{1-\left(P/P_{crit}\right)}\right)\left(P/P_{crit}\right)^2 \tag{3.19}$$

$$n = 0.9 - 0.3\left(P/P_{crit}\right)^{0.15} \tag{3.20}$$

$$\begin{aligned} h_0 &= 5600 \ \left(\mathrm{W/m^2\text{-}K}\right) \\ q''_0 &= 20000 \ \left(\mathrm{W/m^2}\right) \end{aligned} \tag{3.21}$$

$$q''_{\mathrm{PB}} = h_{\mathrm{PB}}\left(T_w - T_{sat}\right) = h_0 F_p \left(q''_{\mathrm{PB}}/q''_0\right)^n \left(T_w - T_{sat}\right) \tag{3.22}$$

$$h_{\mathrm{PB}} = \left(\frac{5600F_P}{20000^n}\right)^{1/(1-n)} \left(\left(T_w - T_{sat}\right)^{n/(1-n)}\right) \tag{3.23}$$

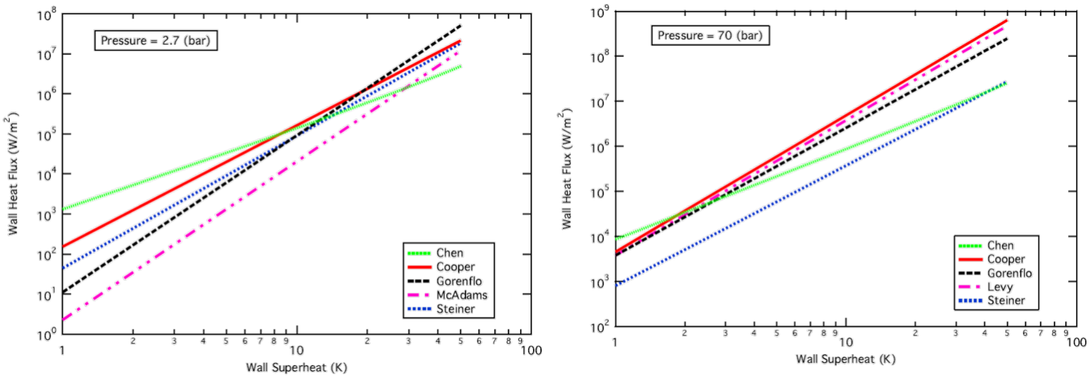

Figure 17 Comparison of Pool Boiling Models [13] (a) at Low Pressure (b) at High Pressure

The combination of heat flux, which is shown in (3.24), is used in TRACE instead of HTC. q''_{FC} is the product of $F \cdot h_{\mathrm{FC}}$ and $T_w - T_l$, but q''_{PB} is the product of h_{PB} and $T_w - T_{sat}$ with an interpolation function as in (3.25), since the heat flux value jumps at the point of ONB.

$$q''_{\mathrm{NB}} = q''_{\mathrm{FC}} + q''_{\mathrm{PB}} \tag{3.24}$$

$$q''_{\mathrm{PB}} = q''_{Gorenflo}\left(@T_w\right) - q''_{Gorenflo}\left(@T_{\mathrm{ONB}}\right) \tag{3.25}$$

In the transition boiling HT regime, TRACE uses the interpolation approach suggested by Bjornard-Griffith [39] as in equation (3.26), in which weighting function wf_{TB} is only a function of the wall temperature as shown in equation (3.27).

$$q''_l = wf_{TB}\, q''_{CHF} + \left(1 - wf_{TB}\right) q''_{MFB,l} \tag{3.26}$$

$$wf_{TB} = \left(\frac{T_w - T_{MFB}}{T_{CHF} - T_{MFB}} \right)^2 \tag{3.27}$$

As mentioned in chapter 3.2.1, TRACE divides the film boiling HT regime into 3 regimes: the inverted annular film boiling (IAFB), inverted slug film boiling (ISFB) and dispersed flow film boiling (DFFB) HT regimes. In each regime, wall heat transfer phenomena are simulated differently and the heat flux or the HTC is evaluated with different models. Figure 18 shows the heat transfer paths from wall to liquid or vapor in the IAFB and DFFB HT regimes. In the IAFB HT regime, vapor film is near the wall and the liquid core is inside the tube. In TRACE, it is assumed that wall heat is transferred to vapor by conduction and to the liquid core by radiation due to the high temperature of the wall resulting from film boiling. Furthermore, an additional term is included, which considers the heat transfer from the wall to vapor phase, from vapor to the saturated interface, and finally from the interface to the liquid phase. Ultimately, this additional term models heat transfers from the wall to the liquid.

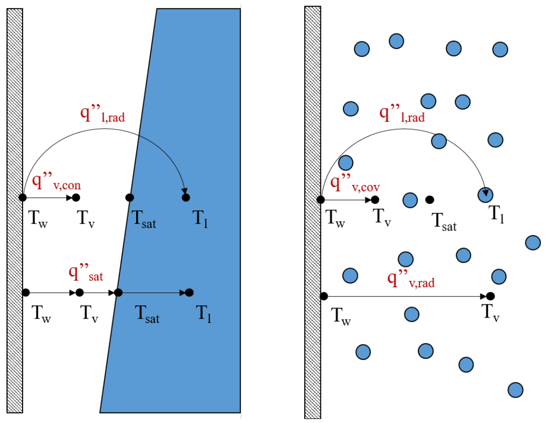

Figure 18 Schematic of Heat Transfer Paths in the Film Boiling Heat Transfer Regime. (a) for Inverted Annular Film Boiling (b) for Dispersed Flow Film Boiling

The conductive heat transfer in IAFB between the wall and vapor is simplified with laminar theory as in equation (3.28), since it can be assumed that the vapor-liquid interface is smooth and the vapor flow is laminar. In (3.28), δ is the film thickness, and it is calculated by the geometric relation (3.29). A factor of 2 is multiplied to the equation, because the wall-vapor HTC refers to the vapor temperature and this has been assumed to be an intermediate temperature between the wall and the saturated interface. From Fung's data [40] and Winfrith's data [41], the laminar theory is not satisfactory in large void fraction and pressure conditions, and also the thickness can be a function of a void fraction and pressure [13]. TRACE develops a simple empirical model (3.31) by referring to Cachard's suggestion [42] and using Fung's data while the abovementioned additional term is added to the model as in (3.32). In equation (3.31), the term in parentheses is the enhancement by waviness or oscillation of the liquid core. In IAFB, radiation from the wall to the liquid core occurs due to the evaluated temperature encountered in film boiling. A model for radiative heat transfer uses equation (3.33) suggested by Hammouda [43], where σ_{SB} is the Stefan-Boltzmann constant, ε_l is liquid emissivity set to 0.96 by Rohsenow [44], and ε_w is the wall emissivity set to 0.7 as recommended in the RELAP5 manual [12] for the zircaloy surface.

$$h_v = 2\frac{k_v}{\delta} \tag{3.28}$$

$$\delta = \frac{D_h}{2}\left(1-\sqrt{1-\alpha}\right) \tag{3.29}$$

$$\delta^* = \delta\left(\frac{\rho_v \cdot g \cdot (\rho_l - \rho_v)}{\mu_v^{\,2}}\right)^{1/3} \tag{3.30}$$

$$\mathrm{Nu}_w = 1 + \left(0.268\delta^{*0.77} - 0.34\right) \tag{3.31}$$

$$h_{l,\mathrm{cov}} = \frac{k_g}{\delta}\mathrm{Nu}_w \tag{3.32}$$

$$h_{l,rad} = \frac{\sigma_{SB}\left(T_w^{\,2} + T_{sat}^{\,2}\right)\left(T_w + T_{sat}\right)}{1\big/\varepsilon_l\sqrt{1-\alpha} + 1\big/\varepsilon_w - 1} \tag{3.33}$$

In the DFFB regime, there is a finely dispersed droplet mixture in which the continuous phase is superheated, as shown in Figure 18. The major phenomena of wall heat transfer are forced convective heat transfer from the wall to superheated vapor and thermal radiation. The forced convective heat transfer is estimated by a similar method as in the single phase HT regime with fluid properties of vapor phase. TRACE selects the largest Nusselt number from laminar, turbulent and natural convection correlations, which is the same as in the single phase HT model, but the modification term due to the property effect and the additional effect in the Gnielinski correlation is a little different from the liquid single phase correlation. The property effect of Sleicher [45] is adopted, and the entrance length effect of Mills [46] is added to the model. After selecting the largest Nusselt number, the self-developed two-phase enhancement factor is also multiplied as shown in equation (3.36). The model for radiation is implemented with the Sun [47] model (3.37) and (3.38), where σ_{SB} is Stefan-Boltzmann constant, and ε_l, ε_v, ε_w is the emissivity of liquid droplet, vapor and wall. These values are set to 90%, 90%, and 70% of the hydraulic diameter respectively following the recommendation of Sun. In the ISFB regime, the HTC or heat flux is determined by interpolating values in the IAFB regime and in the DFFB regime with respect to the void fraction.

$$\mathrm{Nu}_{\mathrm{turb}} = \frac{(f/2)(\mathrm{Re}-1000)\mathrm{Pr}}{1+12.7(f/2)^{0.5}\left(\mathrm{Pr}^{2/3}-1\right)} \times \left(\frac{T_w}{T_v}\right)^n \times \left(1 + \frac{2.4254}{\left(L/D_h\right)^{0.676}}\right) \tag{3.34}$$

$$n = -\left(\log_{10}\left(T_w/T_v\right)\right)^{1/4} + 0.3 \tag{3.35}$$

$$\mathrm{Nu}_{v,\mathrm{cov}} = \left(1 + 25\frac{(1-\alpha)\mathrm{Gr}_{2\phi}}{\mathrm{Re}_v^{\,2}}\right)^{1/2} \max\left(\mathrm{Nu}_{lam}, \mathrm{Nu}_{turb}, \mathrm{Nu}_{NC}\right) \tag{3.36}$$

$$h_{l,rad} = \frac{\sigma_{SB}\left(T_w^{\,2} + T_l^2\right)\left(T_w + T_l\right)}{R_2\left(1 + R_3/R_1 + R_3/R_2\right)} \tag{3.37}$$

$$h_{v,rad} = \frac{\sigma_{SB}\left(T_w^{\,2} + T_v^2\right)\left(T_w + T_v\right)}{R_1\left(1 + R_3/R_1 + R_3/R_2\right)} \tag{3.38}$$

$$R_1 = {(1-\varepsilon_v)}\big/{\varepsilon_v(1-\varepsilon_v\varepsilon_l)} \tag{3.39}$$

$$R_2 = {(1-\varepsilon_l)}\big/{\varepsilon_l(1-\varepsilon_v\varepsilon_l)} \tag{3.40}$$

$$R_3 = 1\big/{(1-\varepsilon_v\varepsilon_l)} + {(1-\varepsilon_w)}\big/{\varepsilon_w} \tag{3.41}$$

3.4 Wall Heat Transfer Models and Correlations of RELAP5

In RELAP5, the largest Nusselt number is selected for the single phase HT regime as in TRACE, and Sellars [26] correlation (3.12) is implemented for the laminar heat transfer model. Meanwhile, the Dittus-Boelter [18] correlation (3.42) is used to model the turbulent heat transfer. The Churchill-Chu [48] correlation and McAdams [35] correlation are used for the vertical and horizontal natural convective flows, respectively.

$$\mathrm{Nu}_{turb} = 0.023\,\mathrm{Re}^{0.8}\,\mathrm{Pr}^{0.4} \tag{3.42}$$

RELAP5 applies the Chen [30] model (3.15), which is widely used in the saturated nucleate boiling regime. The Chen model was developed for the saturated liquid condition, but RELAP5 assumes that the wall is fully wet with water and uses the Chen model in the subcooled HT regime with a slight modification. Chen selected the Dittus-Boelter correlation for the forced convection term in equation (3.15) and the Forster-Zuber [49] model (3.43) for the pool boiling model with a graphically obtained flow factor and suppression factor. Butterworth fitted this curve as shown in equations (3.44) – (3.47), which were reported by Bjornard and Griffith [39]. In the subcooled nucleate regime, RELAP5 modifies the Chen model with the modification suggested by Bjornard and Griffith: the flow factor is set to unity and the total mass flux is used in the Reynolds number if the regime is in the subcooled nucleate boiling. Moreover, according to Collier and Butterworth's suggestion [50], the $T_w - T_l$ value is used instead of $T_w - T_{sat}$ in the forced convection term. These modifications make discontinuity in the HTC value, so the flow factor for the subcooled liquid of 0-5K is linearly interpolated as shown in equation (3.48).

$$h_{\mathrm{PB}} = 0.00122\left(\frac{k_l^{\,0.79} c_{pl}^{\,0.45} \rho_l^{\,0.49}}{\sigma^{0.5} \mu_l^{\,0.29} h_{fg}^{\,0.24} \rho_v^{\,0.24}}\right)\Delta T_w^{\,0.24}\,\Delta P^{0.75} \tag{3.43}$$

$$S = \begin{matrix} \left(1+0.12\,\mathrm{Re}_{tp}^{\,-1.14}\right)^{-1} & \mathrm{Re}_{tp} < 32.5 \\ \left(1+0.42\,\mathrm{Re}_{tp}^{\,0.78}\right)^{-1} & 32.5 \le \mathrm{Re}_{tp} < 70 \\ 0.0797 & \mathrm{Re}_{tp} \ge 70 \end{matrix} \tag{3.44}$$

$$\mathrm{Re}_{tp} = \min\left(70, 10^{-4}\,\mathrm{Re}_l\,F^{1.25}\right) \tag{3.45}$$

$$F = \begin{matrix} 2.35\left(\chi_{tt}^{\,-1}+0.213\right)^{0.736} & 0.1 < \chi_{tt}^{\,-1} < 100 \\ 1 & \chi_{tt}^{\,-1} \le 0.1 \end{matrix} \tag{3.46}$$

$$\chi_{tt}^{\,-1} = \left(\frac{G_v}{G_l}\right)^{0.8}\left(\frac{\rho_l}{\rho_v}\right)^{0.5}\left(\frac{\mu_v}{\mu_l}\right)^{0.1} \tag{3.47}$$

$$F = \begin{cases} 1 & T_l < T_{sat} - 5 \\ F - 0.2\left(T_{sat} - T_l\right)\left(F - 1\right) & T_{sat} - 5 < T_l < T_{sat} \end{cases} \tag{3.48}$$

In the transition boiling HT regime, RELAP5 uses Chen's transition correlation [51] as in equation (3.49), in which the factor A_f is dependent on the void fraction and mass flux in addition to the wall temperature. While TRACE uses only the wall temperature in the weighting factor, RELAP5 uses three parameters as shown in equations (3.50) – (3.54).

$$q"_l = A_f q"_{CHF} \tag{3.49}$$

$$A_f = \exp\left(-\lambda\left(T_w - T_{sat}\right)^{0.5}\right) \tag{3.50}$$

$$\lambda = \max\left(C_1 - \frac{C_2 G}{10^5}, \frac{C_3 G}{10^5}\right) \tag{3.51}$$

$$C_1 = 2.4 C_2 \tag{3.52}$$

$$C_2 = \frac{0.05}{1 - \alpha^{40}} + 0.075\alpha \tag{3.53}$$

$$C_3 = 0.2 C_2 \tag{3.54}$$

The film boiling has different heat transfer mechanisms depending on the flow pattern as discussed in section 3.2. All film boiling HT regimes modeled in RELAP5 include the following heat transfer models: conductive heat transfers from the wall to vapor film, convective heat transfer from the wall to vapor and droplets, and radiative heat transfer from the heated wall to the liquid core, liquid droplets and vapor. To model the conductive wall heat transfer, the Bromley [52] model (3.55) is implemented. The exponent of thermal conductivity was set to 2 in the Bromley model, but RELAP5 uses 3, where h_{fg}' is corrected with the heat of vaporization, which additionally contains the energy absorbed by the vapor surrounding the tube. The parameter L is the tube diameter, which can be solved by the Berenson [53] model, but this model was developed for heat transfer above a flat plate, so RELAP5 replaces the parameter with the minimum critical wave length (3.56) based on the work by Breen [54]. In addition, RELAP5 added a void fraction factor Ma, which makes the HTC smoother in a broad void fraction range. The effect due to the liquid sub-cooling is fitted based on Sudo's work [55] as shown in equation (3.57). The convective heat transfer model uses the Dittus-Boelter correlation as in the single phase HT regime with vapor phase fluid properties. The radiation phenomenon is modeled with Sun's [47] model (3.37) – (3.38), which is the same as TRACE, but the assigned emissivity is defined differently and only the radiation to liquid phase is considered in RELAP5, i.e., no radiation from the wall to vapor phase. The emissivity of the vapor and wall are set to 0.02 and 0.7, respectively, and that of the liquid is evaluated from equation (3.58). In this equation, L_∞ is the mean path length, and a_l is the liquid absorption coefficient, respectively. The mean path length can be solved as 90% the hydraulic diameter [12], and the liquid absorption coefficient is calculated using the minimum diameter from equation (3.60).

$$h_{con} = 0.62\left[\frac{g\rho_v k_v^3\left(\rho_l - \rho_v\right)h_{fg}' c_{pv}}{L\left(T_w - T_{sat}\right)\mathrm{Pr}_v}\right]^{0.25}\mathrm{Ma} \tag{3.55}$$

$$L = (2\pi)^{0.25}\left(\frac{\sigma}{g(\rho_l - \rho_v)}\right)^{0.125} \tag{3.56}$$

$$h_{l,con} = h_{l,con}\left(1 + 0.025(T_{sat} - T_l)\right) \tag{3.57}$$

$$\varepsilon_l = \min\left(0.75, 1 - \exp(-a_l \cdot L_m)\right) \tag{3.58}$$

$$a_l = 1.11(1\text{-}\alpha)/d_{avg} \tag{3.59}$$

$$d_{avg} = \frac{7.5\sigma}{\rho_v (v_v - v_l)^2} \tag{3.60}$$

3.5 Comparison Results

Figure 19 shows that the boiling curve is calculated from separate platforms by setting no mass flux of liquid and vapor, which means pool boiling conditions. Figure 19(a) and (b) represent the cases of 10MPa and the ambient pressure for the system pressure, respectively, which confirms that the calculated heat flux has a larger difference in the lower pressure case than in the higher pressure case. More details will be explained later.

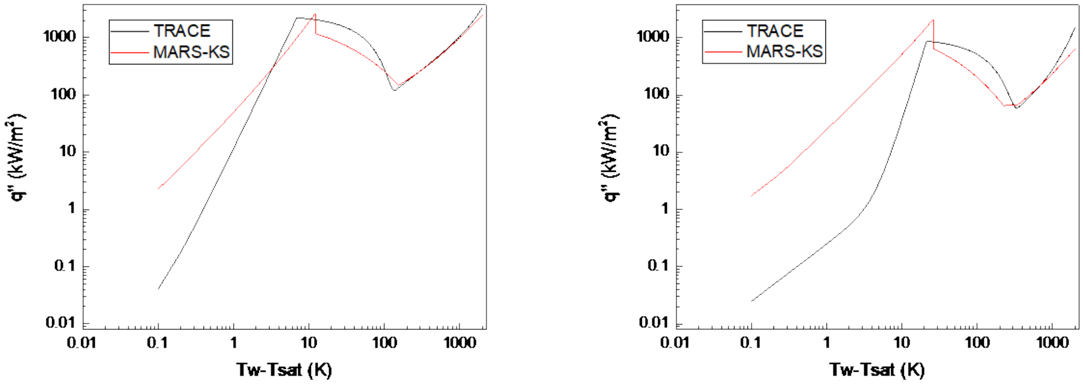

Figure 19 Pool Boiling Curve Calculated from a Separate Platform. (a) at 10 MPa (b) at 101.325 kPa (1 atm)

There are two major reasons why the two codes calculate the heat flux differently: (1) The two codes select different heat transfer regimes in the same thermal hydraulic conditions, which means the HT regime selection logic is the source of the difference. (2) The two codes use different heat transfer correlations in the same HT regime. The difference between the two codes is shown in Figure 20. Figure 20(a) shows when the two codes selected the same HT regime and Figure 20(b) shows when the two codes selected different HT regimes. In both cases, they have similar errors and standard deviations.

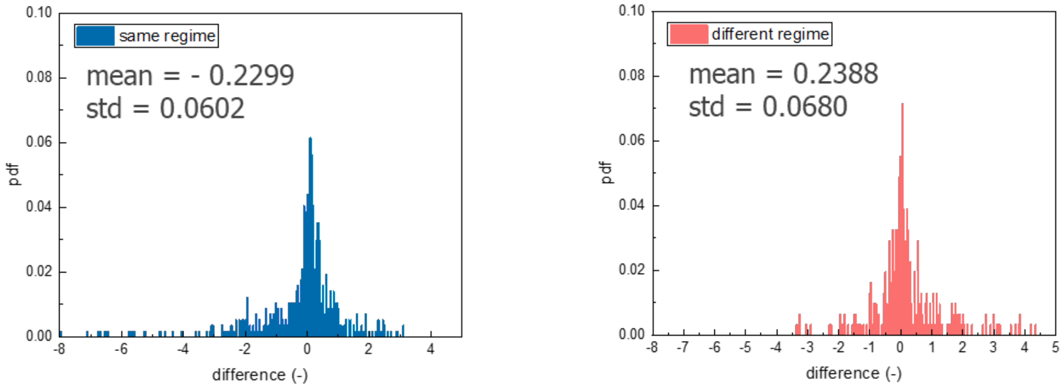

Figure 20 The Differences between TRACE and RELAP5 for the Case of (a) Selected Same HT Regime and (b) Different HT Regime

Figure 21 is the comparison of the calculated heat flux values when both codes chose identical HT regimes. In other words, the figures show the deviation of the wall heat transfer caused by having different heat transfer correlations in the two codes. When the two codes predict a nucleate boiling HT regime, the R-squared values are 0.7093 for a horizontal flow and 0.7178 for a vertical flow. When both codes select the transition boiling HT regime, the R-squared values are -0.4912 for a horizontal flow and – 0.4929 for a vertical flow. When both codes choose a film boiling HT regime, the R-squared values are -0.0277 for a horizontal flow and -0.0518 for a vertical flow. When both codes judge the TH conditions are in a single vapor convection HT regime, the R-squared values are 0.9234 for a horizontal flow and a vertical flow. The regime where the largest deviation exists is the transition boiling HT regime, which has a negative R-squared value.

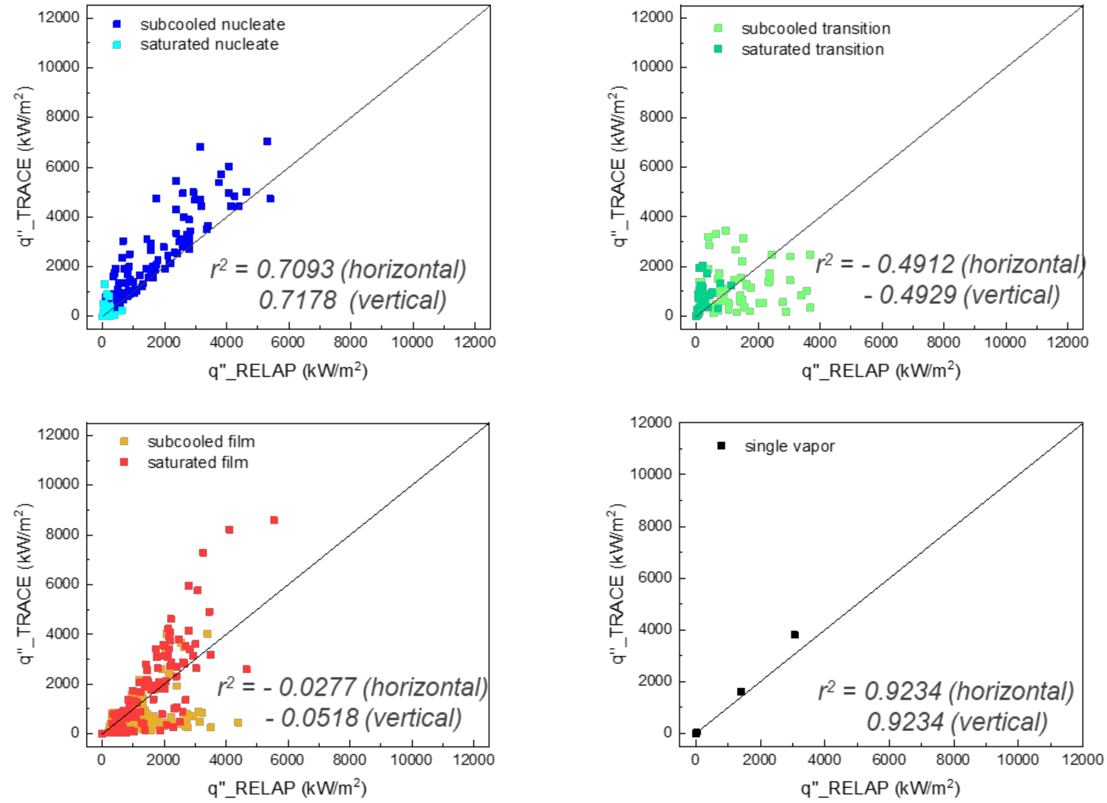

Figure 21 Calculated Wall Heat Flux in the Case of the Same Selected Wall HT Regime

As explained in the previous chapter, TRACE uses the interpolation approach suggested by Bjornard-Griffith [39] and RELAP5 uses Chen's transition correlation [51] to calculate the heat flux in the transition boiling HT regime, corresponding to equation (3.26) and (3.49), respectively. In the correlation of TRACE, weighting function wf_{TB} is only a function of the wall temperature, whereas in RELAP5 the factor A_f is dependent on the void fraction and mass flux in addition to the wall temperature. The calculated weight function is plotted with respect to the wall temperature as shown in Figure 22. The weighting function of TRACE changes linearly with the wall temperature between the CHF and MFB but the weighting function of RELAP5 is discontinuous. This causes major differences in the calculated heat flux in the transition boiling HT regime. The effect of the weighting function is also confirmed in the boiling curve as mentioned before in Figure 19.

In the pool boiling curve, the heat flux of TRACE varies linearly as transition boiling occurs just after CHF, but RELAP5 has a point where the wall heat flux decreases abruptly. The reason is that TRACE has a linear weighting function with respect to the wall temperature but this is not the case in RELAP5.

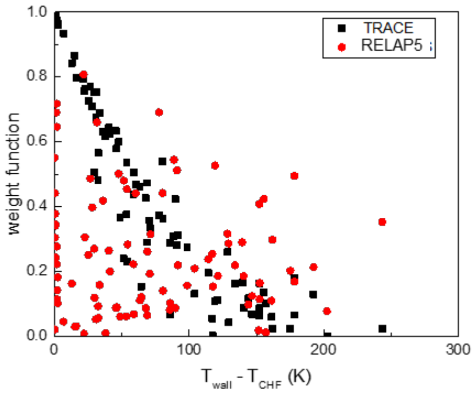

Figure 22 Weighting Function with Wall Temperature in the Transition Boiling HT Regime

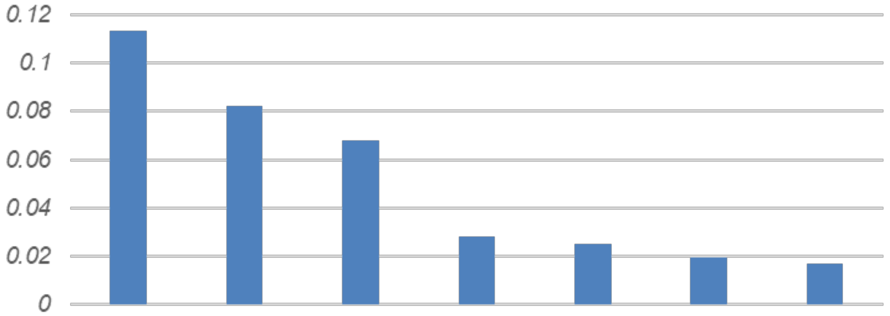

		saturated	subcooled	subcooled	saturated	subcooled	subcooled	saturated
	TRACE	transition	transition	single	nucleate	transition	film	transition
	RELAP5	film	film	nucleate	transition	nucleate	transition	nucleate
r^2	Horizontal	0.6881	-0.7131	0.9136	0.1453	-0.7219	-2.2205	0.8922
	vertical	0.6744	-0.7492	0.9136	0.37367	-0.3916	-3.0122	0.9033

Figure 23 Percentages of the Selected Different HT Regimes between TRACE and RELAP5

Next, heat flux values of the two codes are compared when TRACE and RELAP choose different HT regimes. It can be seen that there are significant differences between the selected wall HT regimes for the two codes. In a horizontal flow, 39.06% of the total 900 data set is differently selected, and in a vertical flow, 22.21% is chosen differently for RELAP5 and TRACE. Figure 23 shows how the two codes differently predict the heat transfer regime when the two codes chose different wall HT regimes. The fraction of the case in which TRACE predicts the transition boiling HT regime while RELAP5 chooses the film boiling HT regime is the highest among the cases. As presented in Figure 23, about 20% of all the data sets is included in this case. This is because the two codes have different logics to distinguish film boiling and transition boiling HT regimes. Referring to the chapter 3.2.1, the criteria of MFB can be checked.

In TRACE, the temperature of the MFB point is calculated by Groeneveld's correlation with upper and lower limits as shown in equation (3.2), while RELAP5 uses the conditions in (3.6), in which two heat flux values from the film and transition boiling HT correlations are the same. The wall temperature is shown in Figure 24 for when the TRACE and RELAP5 satisfy the conditions for the MFB point. In RELAP5, the Newton-Raphson method is used to obtain the wall temperature at which two heat fluxes coincide. While the MFB temperature of the TRACE appears in the minimum and maximum limits, RELAP5 has a wide range of temperature for the MFB point. This comparison confirms that the conditions to distinguish the transition and film boiling HT regimes are quite different between TRACE and RELAP5.

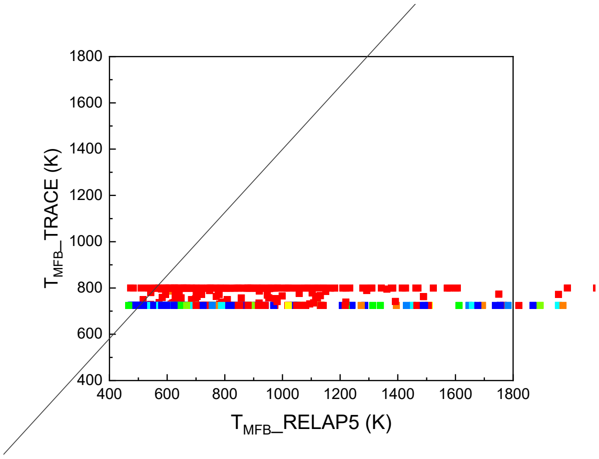

Figure 24 Evaluated Temperature of the MFB in TRACE and RELAP5

In Figure 23, the second most frequent case is when TRACE selects the single phase convection HT regime and RELAP5 choses the nucleate boiling HT regime. About 7% of the all the data sets are in this case. This is because the two codes use different ONB criteria. As described in chapter 3.2.1, TRACE uses the ONB temperature calculated from Basu's model but RELAP5 uses a value of Tsat - 0.001 instead of the ONB temperature. Figure 25 shows ONB temperatures of both codes in 15.5MPa and 0.1MPa, respectively. The influence of ONB on the HT regime can be confirmed again in the previously mentioned pool boiling curve, which is plotted in Figure 19. At 10 MPa, the slopes for the two codes are almost unchanged according to the heat flux until they approach the CHF because in high pressure both codes predict similar ONB temperatures. In contrast, at an ambient pressure, the slope before the CHF does not change in RELAP5 but TRACE has a point where the slope changes. While RELAP5 still predicts the nucleate boiling regime after $T_{wall} = T_{sat} - 0.001$ in ambient pressure, TRACE selects the single phase HT regime until the inflection point and considers the nucleate boiling regime after that point.

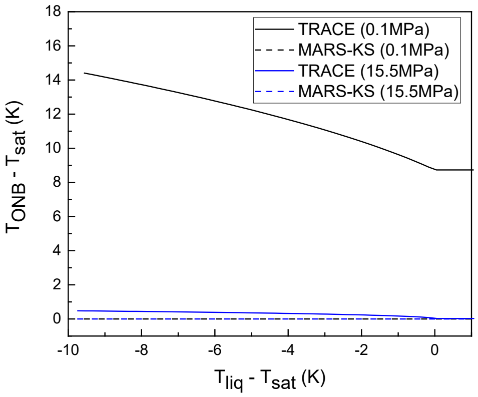

Figure 25 Calculated Temperature of ONB at 0.1 MPa and 15.5 MPa in TRACE and RELAP5

The third most frequent case is when TRACE and RELAP5 alternate between nucleate and transition boiling HT regimes. The case in which TRACE selects the film boiling HT regime while RELAP5 predicts the nucleate boiling HT regime is 5% of all the cases, and the opposite case in which TRACE selects the nucleate boiling HT regime while RELAP5 choses the film boiling HT is 3% of all the cases. To analyze the cause, the wall HT regime selection logic for the CHF is checked. As explained in chapter 3.2.1, TRACE and RELAP5 use the conditions in (3.5) as criteria for CHF. It is remarkable why TRACE and RELAP5 predict different CHF points even though the criterion of the CHF point is the same. There are two reasons: (1) both codes are referred to the CHF Lookup Table for the different versions (RELAP5: 1986, TRACE: 1995) and different k-effects are used. (2) Different HT correlations in the nucleate boiling HT regime are implemented in the two codes. To confirm which one has a more significant cause, the CHF values of both codes are calculated. Figure 26(a) represents the CHF values calculated by the two codes. When the void fraction becomes large, TRACE overestimates the CHF values slightly more than RELAP5 but the CHF values calculated by the two codes are close to identical. To compare the temperature of T_{CHF}, a platform of RELAP5 is added with a function to solve for the CHF temperature using the Newton-Rapson method with the conditions in (3.5) in the same way as that implemented in TRACE. The calculated temperature of the CHF is plotted in Figure 26(b). Unlike CHF values, the temperatures of the CHF of the two codes do not match when void fraction becomes small. The CHF values are similar for the two codes, but the CHF temperatures of the two codes are substantially different because the calculated heat flux values in the logic equation (3.5) are not the same. In short, the CHF point becomes different in the two codes even though the logic is the same due to the differences in the implemented correlation for the nucleate boiling HT regime.

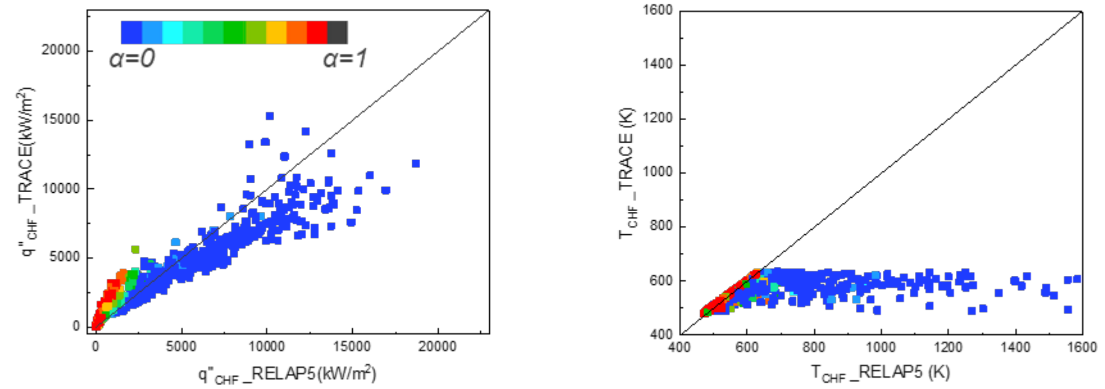

Figure 26 Calculated (a) CHF and (b) Temperature of CHF in TRACE and RELAP5

Figure 27 shows the calculated HTC of the nucleate boiling HT regime with respect to various wall temperatures and fluid liquid temperatures. The trends in the figure look similar but the magnitudes of the HTC are substantially different. For modeling nucleate heat transfer, correlations of TRACE and RELAP5 include forced convection and boiling heat transfer effects as shown in equation (3.15). The boiling HTC is a more significant term than the forced convection term as different heat flux values are calculated in the two codes. As shown in Figure 28, the pool boiling HTC of the two codes have largely different magnitudes in the total HTC as shown in Figure 27. TRACE uses the Gorenflo correlation as shown in equation (3.23) and RELAP5 uses the Forster-Zuber correlation as shown in equation (3.43) for the pool boiling model. According to the Forster-Zuber correlation, the exponent of dTwall is a constant as described in $\Delta T_w^{0.24} \Delta P^{0.75}$ but the exponent of dTwall in the Gorenflo correlation is a function of pressure as expressed in $\Delta T_w^{n/(1-n)}$. Figure 29 indicates the exponents of dT_{wall} applied in the pool boiling correlation using Claperyon relations. As a result, the exponents of TRACE are fairly larger than RELAP5 and moreover the lower pressure leads to a bigger deviation.

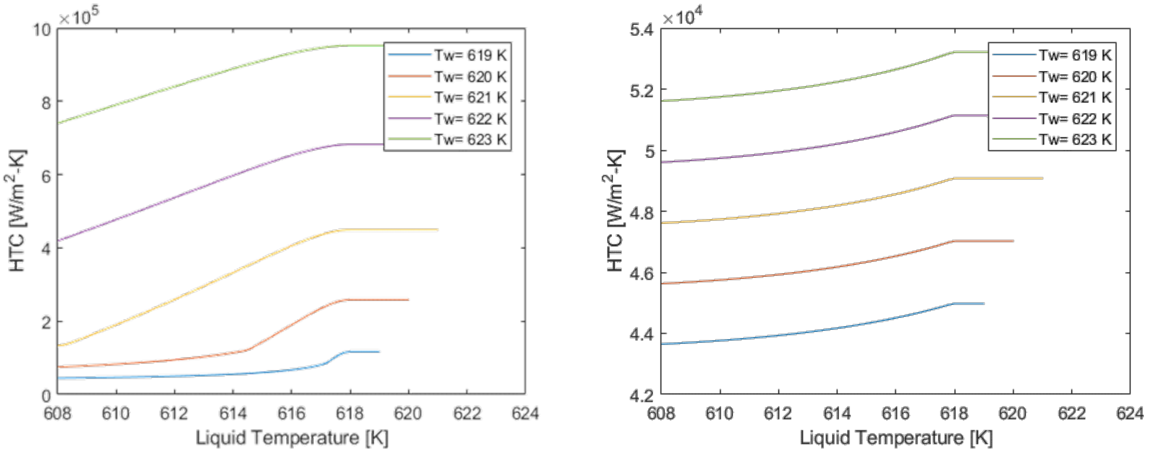

Figure 27 Calculated Total HTC in the Nucleate Boiling HT Regime. (a) in TRACE (b) in RELAP5

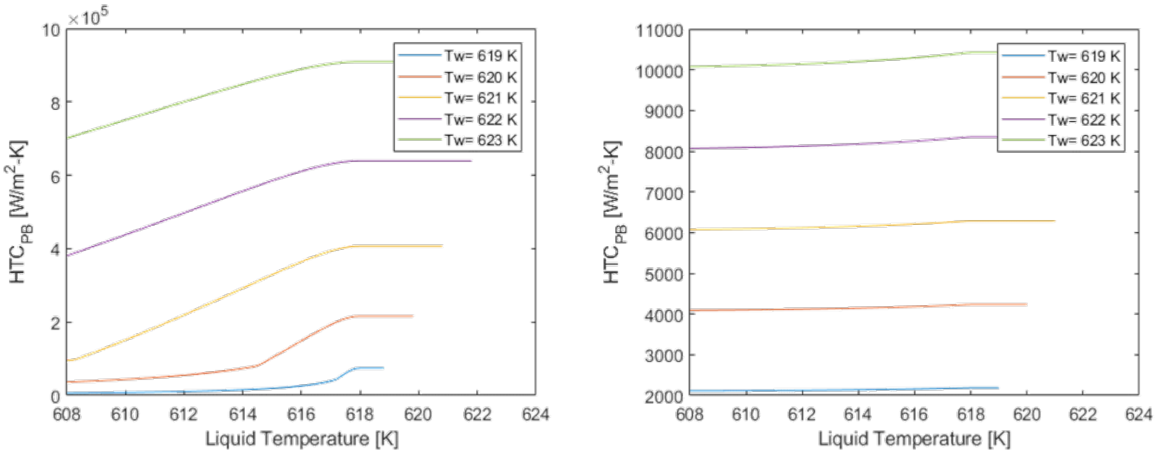

Figure 28 Calculated Pool Boiling HTC in the Nucleate Boiling HT Regime. (a) TRACE (b) RELAP5

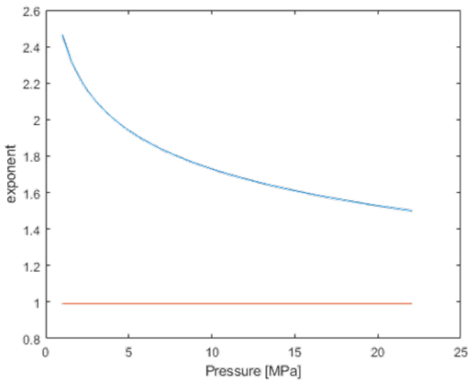

Figure 29 Exponent of dT_{wall} in the Pool Boiling Term of the Nucleate Boiling HT Regime Correlation

As a summary for selecting different wall HT regimes in the two codes, TRACE usually predicts higher ONB and MFB points and a lower CHF point than RELAP5 does, which means TRACE judges a single phase convection and transition boiling HT regimes to be broader than RELAP5 does.

To specifically assess which wall heat transfer model matches the actual phenomena well, a comparison with experimental data was conducted. SUBO [56] data obtained from KAERI and the heated tube test data by Bennett [57] were used. Experimental conditions are shown in Table 5 and Table 6. Figure 30 shows the calculated wall heat flux with the SUBO experimental data. Both codes select the nucleate boiling HT regime except for one point marked in Figure 30(a), in which TRACE predicts the transition boiling HT regime. Overall, TRACE shows a tendency to overestimate the heat flux more than the experimental data, and the larger sub-cooling, the more the overestimation of TRACE. Meanwhile, RELAP5 predicts the experimental data reasonably well.

Table 5 Experimental Conditions for SUBO

Case	P (MPa)	Heat flux (kW/m^2)	T_{in} (K)	G (kg/m^2-sec)
Base	1.6 ~ 1.92	473	375	1116
T1		470	363	1102
V1		472	375	2074

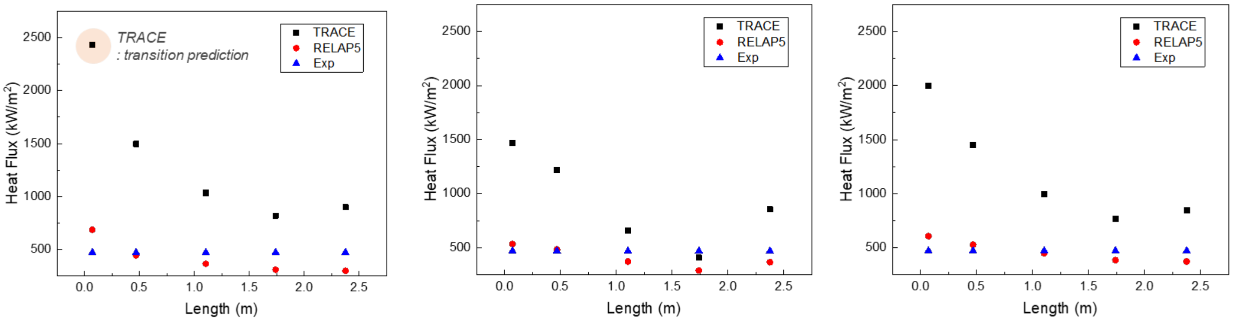

Figure 30 Calculated Wall Heat Flux in TRACE and RELAP5 with SUBO Experimental Data (a) Base (b) T1 (c) V1

Figure 31 shows the calculated wall heat flux with Bennett's heated tube experimental data. TRACE and RELAP5 select various wall HT regimes, so the wall HT regime is marked in the figure. Points marked with circles on the graph indicate the wall HT regime selected by TRACE, and points marked by a line below them indicate the wall HT regime predicted by RELAP5. Both codes predict the same film boiling HT regime. When RELAP5 selects the nucleate boiling HT regime, TRACE predicts the nucleate or transition boiling HT regime alternately. Excluding the film boiling HT regime in Figure 31(a), which denotes case 5379, TRACE has a tendency to overestimate heat flux more than the experimental data, while RELAP5 has a tendency to underestimate the experimental data. In case 5394 in Figure 31(b), RELAP5 still underestimates the heat flux, while TRACE tends to overestimate it in the transition boiling HT regime and underestimate it in the nucleate boiling HT regime. Overall, RELAP5 has a tendency to underestimate the data, whereas TRACE has a tendency to overestimate the data except for a few points similar to the previous SUBO experiment. In the film boiling HT regime, the two codes calculate a fairly similar heat flux and underestimate the experimental data.

Table 6 Experimental Conditions for Bennett's Heated Tube Test

Case	P (MPa)	Heat flux (kW/m^2)	dT_{sub} (K)	G (kg/m^2-sec)
5379	6.9	170.9	11.0	3798
5394		175.9	13.8	5181

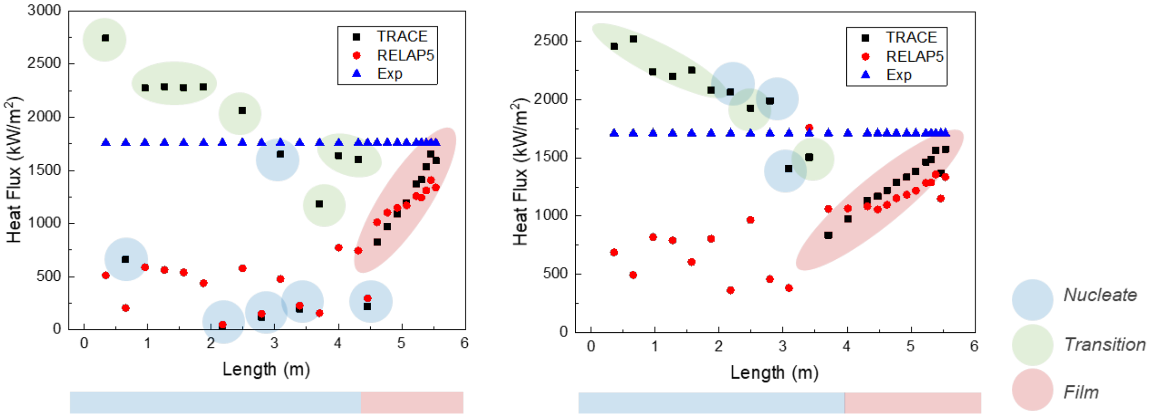

Figure 31 Calculated Wall Heat Flux in TRACE and RELAP5 with Bennett's Heated Tube Experimental Data (a) 5379 (b) 5394

4 INTERFACIAL HEAT TRANSFER MODELS

4.1 Background

Interfacial heat transfer occurs when the mass and energy are transferred through the phase interface. In thermal-hydraulic system analysis codes, accurate prediction of the interfacial transports of mass and energy are required, since they can significantly affect the overall heat transfer process during a nuclear power plant accident. To predict the amount of heat transfer at the interface, the interfacial area and the heat transfer coefficient (HTC) values are needed. The interfacial area per unit volume is the probability of the existing interfacial area at a local position, and from here on it will be referred to simply as the interfacial area. Meanwhile, the transport of energy via a phasic interface contributes to condensation or vaporization. If a liquid or vapor is superheated, it contributes to vaporization, and if a liquid or vapor is subcooled, it contributes to condensation. HTC can be obtained from condensation and vaporization correlations. The net rate of mass transfer can be determined by summing the amounts of vaporization and condensation with incoming and outgoing directions. Depending on thermal hydraulic conditions, the mixing of liquid and vapor has its unique form. That is, the shape of the interface is different. The interfacial shape can be modeled based on the flow regime and heat and mass transfer depends greatly on the flow regime. Eventually, in a way similar to the wall heat transfer models, different models are applied to divided flow regimes to estimate amount of heat transfers in the phase interface.

The difference in density between liquid and vapor is large, so that the vapor tends to float in the opposite direction to the gravity due to buoyancy. Therefore, the flow pattern changes depending on whether the flow direction is vertical or horizontal. In a vertical flow, gravity is equal or opposite to the direction of the flow, so the shape of the flow becomes axisymmetric. Vertical flow patterns are bubbly flow, slug flow, annular flow and drop flow. In the case of bubbly flow, the vapor phase is distributed in the form of small bubbles injected in a continuous liquid phase. In the slug flow, Taylor bubbles with a diameter almost equal to the tube diameter flow upward, and the liquid flows downward in the form of a thin film between the bubble and the tube wall. Annular flow refers to the flow of liquid in the form of liquid film along the tube wall, and the gas flowing along the center of the tube. The drop flow refers to a flow in which a liquid is carried in a gaseous flow in the state of a droplet, and is called another name such as dispersed flow or mist flow.

Figure 32 shows schematic diagrams of the two-phase flow pattern in a vertically oriented heated tube [58]. When the heat flux is lower than the CHF and the single phase liquid flows through the pipe as shown in Figure 32 (a), the temperature of the liquid gradually increases due to the convective heat transfer from the pipe wall, and if it reaches the boiling point, the generation of bubbles starts from the wall surface and a bubbly flow is formed. When the fluid continues to be heated, the amount of bubbles gradually increases, and by the coalescence of bubbles, slug bubbles are formed and flow transit to the slug flow. As the vapor amount continues to increase, the vapor velocity gradually increases, and the liquid of the slug flow becomes more discontinuous in the center and gradually forms an annular flow. In the annular flow, continuous evaporation occurs at the interface between the liquid film and the vapor. At this time, due to the continuous evaporation of the liquid film, the velocity of the vapor increases, and the liquid droplets flow from the liquid film into the gaseous phase of the tube to form an annular-mist flow. Finally, the liquid film on the wall completely evaporates, and the flow is in the form of droplets flowing with the vapor. These droplets evaporate and the flow ultimately becomes a single phase vapor flow.

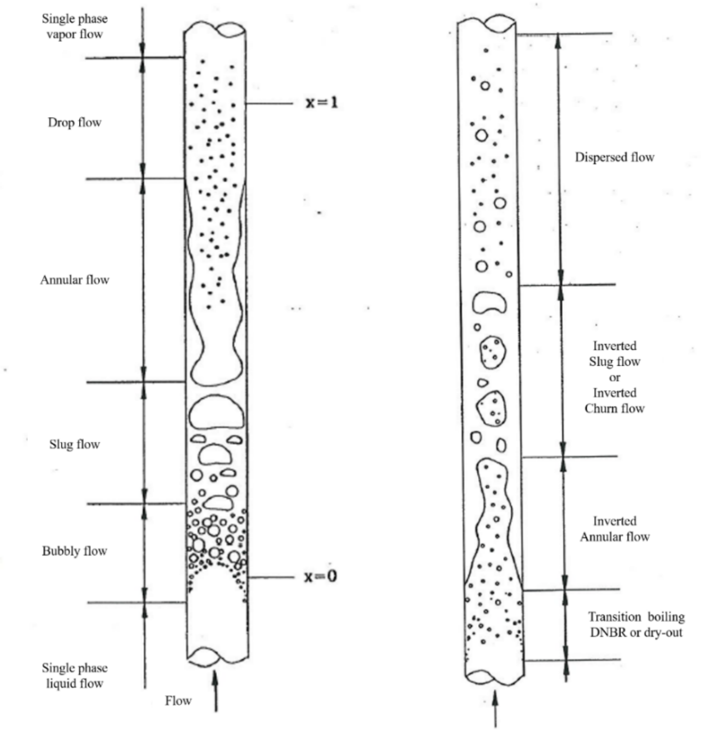
Single phase vapor flow
Drop flow
x=1
Annular flow
Slug flow
Bubbly flow
x=0
Single phase liquid flow
Flow
Dispersed flow
Inverted Slug flow or Inverted Churn flow
Inverted Annular flow
Transition boiling DNBR or dry-out

Figure 32 Two-phase Flow Schematic Diagram in a Vertical Heating Tube [58]. (a) Low Heat Flux (b) High Heat Flux

Under a larger heat flux than in CHF conditions, as it is shown in Figure 32 (b), the subcooled liquid starts to have nucleate boiling at the bottom of the tube, and vapor film at the wall is formed through the departure from the nucleate boiling point to dry-out and transition boiling. This flow is called an inverted annular flow in the sense that the positions of the vapor and the liquid are exchanged, which is similar to the shape of the annular flow. The liquid in the center of the tube is divided into small liquid droplets and a large liquid body due to instability. The instability is caused by the relative velocity of the liquid and the vapor film. This flow pattern is called inverted slug flow or inverted churn flow. The large liquid body is again divided into small droplets and the flow changes into a dispersed flow, which is called an inverted bubbly flow.

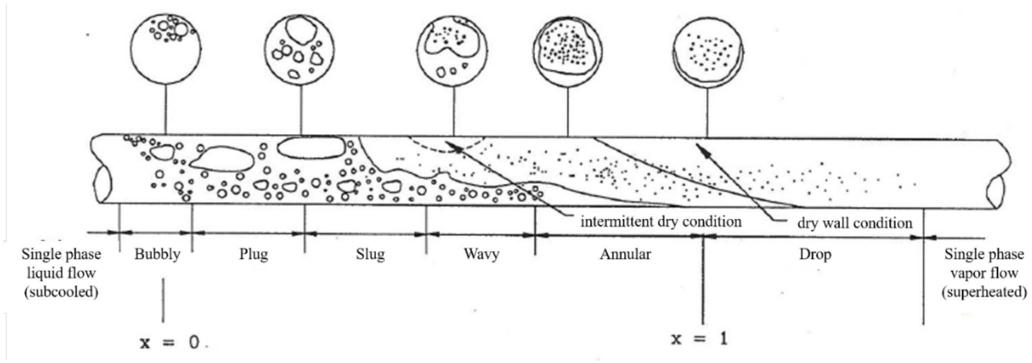
intermittent dry condition
dry wall condition
Single phase liquid flow (subcooled)
Bubbly
Plug
Slug
Wavy
Annular
Drop
Single phase vapor flow (superheated)
x = 0
x = 1

Figure 33 Two-phase Flow Schematic Diagram in a Horizontal Heating Tube (Low Heat Flux) [58]

In the horizontal flow, the gravity acts in the radial direction, so the flow has an asymmetrical shape with respect to the central axis, and the relatively denser liquid phase tends to flow downward. Horizontal flow patterns are bubbly flow, plug flow, stratified flow, wavy flow, slug flow, and annular flow. The bubbly flow is a form in which small bubbles are dispersed in a continuous liquid phase like a bubbly flow in the vertical direction. The plug flow is similar to the slug flow in the vertical flow. The stratified flow occurs when vapor and liquid flow through a horizontal tube at a slow rate, and it has a smooth interface between the two fluids. In the wavy flow, surface waves are generated in the stratified flow when the relative velocity between two fluids increases as the vapor velocity increases. The slug flow is similar to the plug flow, but its characteristics are different in that it is generated by vapor at a high speed. In the annular flow, a high velocity vapor flows through the center of the tube, while a relatively slow liquid flows along the wall. Figure 33 shows schematic diagrams in the form of a two-phase flow pattern in a horizontally oriented heated tube.

4.2 Description of Interfacial Heat Transfer Modules

The information on the amount of mass and energy transfer between phases is needed to solve the mass, momentum, and energy equations in the thermal-hydraulic system analysis codes. This amount is calculated in interfacial heat transfer modules in TRACE and RELAP5 codes. Since the shape of the interface and the mechanism of heat transfer depend on the flow regime, both codes determine the flow regime first in the interfacial heat transfer modules. Then, the interfacial area per unit volume and the interfacial HTC for phases is evaluated by the model which matches the flow regime. The volumetric heat transfer coefficient is defined as the interfacial heat transfer coefficient times the interfacial area per unit volume, as shown in equation (4.1). Here, subscript i is interfacial and p is phase p.

$$H_{ip} = h_{ip} a_i \tag{3.61}$$

4.3 Flow Regime Map

Both codes determine the flow regime with a flow regime map based on the thermal hydraulic conditions. Figure 34 shows the flow regime map implemented in TRACE and RELAP5. In TRACE, the post-CHF regime is not mentioned in this study because TRACE only uses correlations for the pre-CHF regime if the reflood option is turned off. To take into account the flow shape, such as the flow regime described in section 4.1, TRACE includes four principal flow regimes, but three bubbly flow regimes (dispersed bubble, slug, and Taylor cap bubble) are collectively referred to as the bubbly-slug regime. An annular-mist regime is also contained in TRACE flow regimes. The flow regime map of TRACE for interfacial heat transfer is that of TRAC-PF1/MOD2, as depicted in Figure 34(a) [13]. Traditionally, a flow regime map has been constructed with superficial velocities, but here the void fraction is used instead in TRACE. Based on the void fraction and mass flux, flow regime can be determined for both vertical and horizontal flows. The upper limit of the void fraction for the dispersed bubbly flow regime is 0.3, and the Choe-Weisman mass flux criterion [59] is applied for the maximum void fraction of the dispersed bubbly flow regime as shown in (4.2). The lower limit of the void fraction for the annular-mist flow regime is 0.75, and the transition regime between the bubbly-slug and annular-mist flow regime is approximated by interpolation between the values of other adjacent regimes.

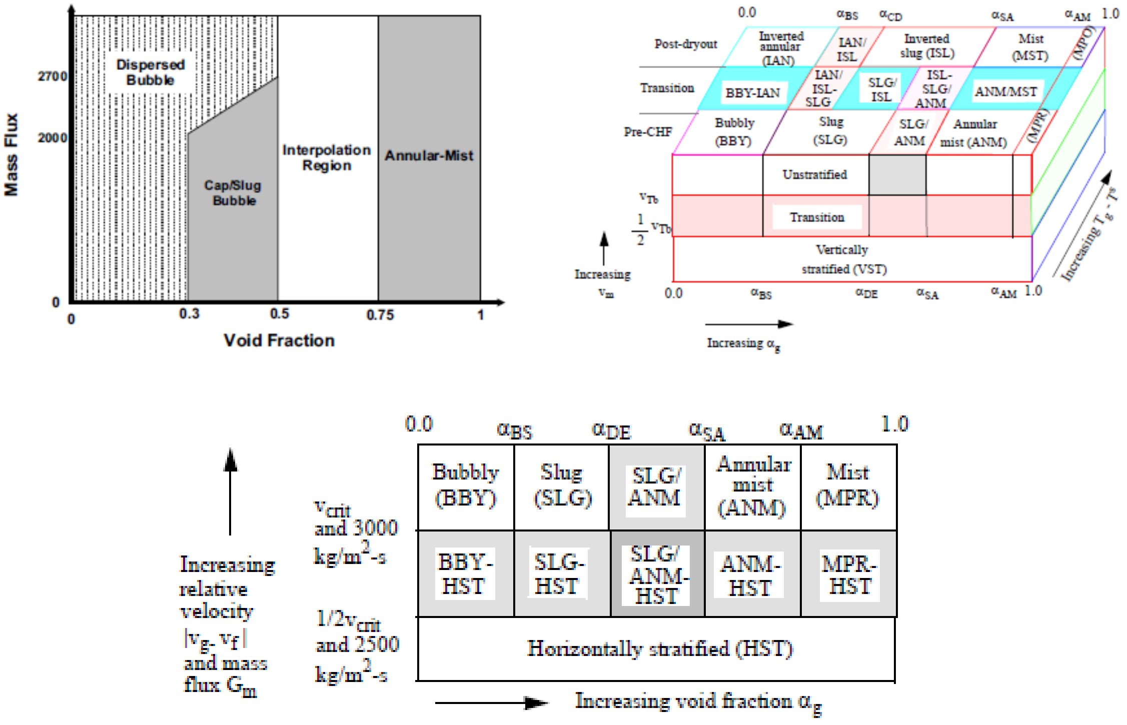

Mass Flux
2700
2000
0
Dispersed Bubble
Cap/Slug Bubble
Interpolation Region
Annular-Mist
0
0.3
0.5
0.75
1
Void Fraction
0.0
α_{BS}
α_{CD}
α_{SA}
α_{AM}
1.0
Post-dryout
Inverted annular (IAN)
IAN/ ISL
Inverted slug (ISL)
Mist (MST)
(MPO)
Transition
BBY-IAN
IAN/ ISL-SLG
SLG/ ISL
ISL-SLG/ ANM
ANM/MST
Pre-CHF
Bubbly (BBY)
Slug (SLG)
SLG/ ANM
Annular mist (ANM)
(MPR)
Unstratified
Transition
Vertically stratified (VST)
v_{Tb}
$\frac{1}{2}v_{Tb}$
Increasing v_m
0.0
α_{BS}
α_{DE}
α_{SA}
α_{AM}
1.0
Increasing α_g
Increasing $T_g - T^s$
0.0
α_{BS}
α_{DE}
α_{SA}
α_{AM}
1.0
Bubbly (BBY)
Slug (SLG)
SLG/ ANM
Annular mist (ANM)
Mist (MPR)
v_{crit} and 3000 kg/m^2-s
BBY-HST
SLG-HST
SLG/ ANM-HST
ANM-HST
MPR-HST
$1/2v_{crit}$ and 2500 kg/m^2-s
Horizontally stratified (HST)
Increasing relative velocity $|v_g - v_f|$ and mass flux G_m
Increasing void fraction α_g

Figure 34 Flow Regime Map for Interfacial Heat Transfer of (a) TRACE [13] and (b) RELAP5 in Vertical Flow (c) RELAP5 in Horizontal Flow [12]

$$\alpha_{BS} = \begin{cases} 0.3 & G \le 2000 \\ 0.3 + 0.2\left(\dfrac{G-2000}{2700-2000}\right) & 2000 < G < 2700 \\ 0.5 & G \ge 2700 \end{cases} \qquad (3.62)$$

RELAP5 contains flow regime maps for vertical and horizontal flows, respectively, as shown in Figure 34(b) and Figure 34(c) [12]. In a similar way, a flow regime map of RELAP5 is determined by the void fraction and mass flux. Meanwhile, the temperature is used to distinguish pre-CHF and post-CHF regimes in the vertical flow regime. The included flow regimes are bubbly, slug, annular-mist, and pre-CHF mist regimes for pre-CHF conditions and inverted annular, inverted slug, mist, post-CHF mist regimes for post-CHF conditions. Based on Taitel, Bornea, and Dukler (TBD) [60], the upper limit of the void fraction for a bubbly flow regime is expressed as equation (4.3) for horizontal and (4.4) for vertical flows. In the vertical flow, the effect of a small tube diameter is considered, because the rise velocity of a Taylor bubble is limited by the pipe diameter.

$$\alpha_{BS} = \begin{cases} 0.25 & G \le 2000 \\ 0.25 + 0.25\left(\dfrac{G-2000}{3000-2000}\right) & 2000 < G < 3000 \\ 0.5 & G \ge 3000 \end{cases} \tag{3.63}$$

$$\alpha_{BS} = \begin{cases} \alpha_{BS}^{\ *} & G \le 2000 \\ \alpha_{BS}^{\ *} + \left(0.5-\alpha_{BS}^{\ *}\right)\left(\dfrac{G-2000}{3000-2000}\right) & 2000 < G < 3000 \\ 0.5 & G \ge 3000 \end{cases} \tag{3.64}$$

$$\alpha_{BS}^{\ *} = 0.25\min\left[1,\left(0.045D^*\right)^8\right] \tag{3.65}$$

$$D^* = D_h\left(\frac{g\left(\rho_l-\rho_v\right)}{\sigma}\right)^{1/2} \tag{3.66}$$

The upper bound of the void fraction for the slug flow regime is 0.8 and it is suggested by the Barnea model [61] for the horizontal flow. For the vertical flow, the void fraction is derived from the transition condition from a churn flow to an annular flow of the TBD [60] and Mishima-Ishii [62]. The criteria, which is shown in equations (4.7) and (4.8), are suggested by Taitel and Mishimam and these criteria are simplified as in equations (4.9) – (4.11). The criteria $\alpha_{\text{crit}}^{\ f}$ and $\alpha_{\text{crit}}^{\ e}$ are derived from criteria (4.10) and (4.11), respectively. Here, $\alpha_{AM}^{\ \min}$ is the minimum void fraction at which an annular flow can exist, and $\alpha_{BS}^{\ \max}$ is the maximum void fraction at which a bubbly-slug flow can exist, and they are set to 0.8 and 0.9, respectively. The void fraction at the transition point from an annular-mist regime to a pre-CHF mist regime is a value of 0.9999. The post-CHF regime also uses the same conditions as those in the pre-CHF regime. The inverted annular, inverted slug, mist, post-CHF mist regimes correspond to the bubbly, slug, annular-mist and pre-CHF mist regime in pre-CHF conditions.

$$j_v^{\ *} = \frac{\alpha v_v}{\left(\dfrac{gD_h\left(\rho_l-\rho_v\right)}{\rho_v}\right)^{1/2}} \ge j_{v,\text{crit}}^{\ *} \tag{3.67}$$

$$\text{Ku}_v = \frac{\alpha v_v}{\left(\dfrac{gD_h\left(\rho_l-\rho_v\right)}{\rho_v^{\ 2}}\right)^{1/4}} \ge \text{Ku}_{v,\text{crit}} \tag{3.68}$$

$$\alpha_{SA} = \max\left[\alpha_{AM}^{\ \min}, \min\left(\alpha_{\text{crit}}^{\ f}, \alpha_{\text{crit}}^{\ e}, \alpha_{BS}^{\ \max}\right)\right] \tag{3.69}$$

$$\alpha_{\text{crit}}^{\ f} = \frac{1}{v_v}\left(\frac{gD_h(\rho_l - \rho_v)}{\rho_v}\right)^{1/2} \tag{3.70}$$

$$\alpha_{\text{crit}}^{\ e} = \frac{3.2}{v_v}\left(\frac{g\sigma(\rho_l - \rho_v)}{\rho_v}\right)^{1/4} \tag{3.71}$$

4.4 Interfacial Heat Transfer Models and Correlations of TRACE

In a bubbly flow regime, TRACE derives the interfacial area from the shape of a droplet with a Sauter-mean diameter as shown in equation (4.12). The diameter of a bubble is approximated as in (4.13) for a distorted bubble and is a function of the Laplace number, and it has a lower limit of 10^{-4} and an upper limit of 90% of the hydraulic diameter. The heat transfer between the liquid and bubble interface is modeled using the Ranz-Marshall [63] correlation (4.15) as recommended by Warrier [64]. In (4.15), the Reynolds number of the bubble, which is defined as (4.16), is a function of the bubble relative velocity, and the relative velocity has a terminal velocity (4.18) as the limiting value, since liquid and vapor velocities in the relative velocity are velocity values of a bubble with an average size in the distorted particle regime. This terminal velocity is based on Wallis' formula [65] while applying the Richardson-Zaki [66] correction. The vapor-interface HTC is seldom important in the bubbly flow regime, so it is considered simply as a constant value of 10^3, which is the same as that in TRAC-PF1/MOD2.

$$a_i = \frac{\text{interfacial area}}{\text{unit volume}} = \frac{\text{interfacial area}}{V_{drop}/\alpha_{drop}} = \frac{\pi d_{drop}^{\ 2}}{\pi d_{drop}^{\ 3}/6}\alpha_{drop} = \frac{6\alpha_{bub}}{d_{bub}} \tag{3.72}$$

$$d_{bub} = 2La = 2\left(\frac{\sigma}{g(\rho_l - \rho_v)}\right)^{0.5} \tag{3.73}$$

$$h_{il} = \frac{k_l}{d_{bub}}\mathrm{Nu}_{bub} \tag{3.74}$$

$$\mathrm{Nu}_{bub} = 2 + 0.6\,\mathrm{Re}_{bub}^{\ 0.5}\,\mathrm{Pr}_l^{1/3} \tag{3.75}$$

$$\mathrm{Re}_{bub} = \frac{\rho_l v_{r,bub} d_{bub}}{\mu_l} \tag{3.76}$$

$$v_{r,bub} = \min\left(\left|v_v - v_l\right|, v_{term}\right) \tag{3.77}$$

$$v_{term} = \sqrt{2}\left(\frac{\sigma g(\rho_l - \rho_v)}{\rho_l^{\ 2}}\right)^{1/4} \tag{3.78}$$

In the cap-slug regime, it is assumed that the vapor phase consists of small dispersed bubbles and large slug or cap bubbles in TRACE. The bubble diameter is much larger than that of the bubbly flow regime, so both the interfacial area and the HTC are much smaller, but for the code completeness, the large bubble component is calculated and added to that of the bubbly flow regime with some modifications in the interfacial area calculation. Ishii-Mishima [67] recommended the interfacial area as a function of the average void fraction within the liquid slug, which is equation (4.19). To evaluate the interfacial area of large slug or cap bubbles, formula (4.20) of Ishii-Mishima [67] is utilized, where the coefficients C^* and d^* depend on whether or not the flow regime is a slug or cap bubble. The assumption is similar to Kataoka-Ishii [68], which states that slug bubbles cannot be sustained for channels with a larger diameter than the diameter derived in equation (4.23). The interfacial HTC for large bubbles is evaluated by the same Ranz-Marshall correlation as the bubbly flow regime, but here, the Reynolds number of a bubble is defined in equation (4.25). The limiting value (4.27) of the relative velocity also depends on whether or not the flow regime is in a slug flow or a cap bubble flow, and is defined by the formula of Wallis [65]. Finally, the interfacial heat transfer in the cap-slug flow regime is solved by adding contributions from small and large bubbles, as shown in equation (4.28). The vapor-interface HTC still uses a constant value of 10^3 in the cap-slug flow regime.

$$a_{i,bub} = \frac{6\alpha_{BS}}{d_{bub}}\left(\frac{1-\alpha}{1-\alpha_{BS}}\right) \tag{3.79}$$

$$a_{i,slug/cap} = \frac{C^*}{d^*}\left(\frac{\alpha-\alpha_{BS}}{1-\alpha_{BS}}\right) \tag{3.80}$$

$$C^* = \begin{cases} 4.5 & D_h < D_{h,crit} \\ 16 & D_h \geq D_{h,crit} \end{cases} \tag{3.81}$$

$$d^* = \begin{cases} D_h & D_h < D_{h,crit} \\ D_{h,crit} & D_h \geq D_{h,crit} \end{cases} \tag{3.82}$$

$$D_{h,crit} = 50La = 50\left(\frac{\sigma}{g\left(\rho_l-\rho_v\right)}\right)^{0.5} \tag{3.83}$$

$$h_{il} = \frac{k_l}{d^*}\mathrm{Nu}_{bub} \tag{3.84}$$

$$\mathrm{Re}_{slug/cap} = \frac{\rho_l v_{r,slug/cap} d^*}{\mu_l} \tag{3.85}$$

$$v_{r,slug/cap} = \min\left(\left|v_v - v_l\right|, v_{term}\right) \tag{3.86}$$

$$v_{term} = \begin{cases} \dfrac{1}{\sqrt{2}}\left(\dfrac{g\left(\rho_l-\rho_v\right)d^*}{\rho_l}\right) & d^* < 0.125D_h \\ \dfrac{1.13}{\sqrt{2}}\left(\dfrac{g\left(\rho_l-\rho_v\right)d^*}{\rho_l}\right)\exp\left(-d^*/D_h\right) & 0.125D_h \leq d^* < 0.6D_h \\ \dfrac{0.496}{\sqrt{2}}\left(\dfrac{g\left(\rho_l-\rho_v\right)d^*}{\rho_l}\right)\dfrac{1}{\sqrt{d^*/D_h}} & d^* \geq 0.6D_h \end{cases} \tag{3.87}$$

$$h_{il}a_i = \left(h_{il}a_i\right)_{bub} + \left(h_{il}a_i\right)_{slug/cap} \tag{3.88}$$

When subcooled boiling occurs in bubbly flow and cap-slug flow regimes, the model for the liquid-interface heat transfer has to account for the near-wall condensation, so this effect is considered in the model of Lahey-Moody [69], which is shown in equation (4.29). For a smooth transition between subcooled boiling and a single phase flow, a simple void fraction ramp is applied as a weighting factor shown in (4.30). The subcooled boiling model engages when the pool boiling HTC is larger than zero and the liquid temperature is smaller than the wall temperature, in which the pool boiling HTC is calculated in wall heat transfer modules as described in section 3.

$$(h_{li}a_i)_{sub} = 0.075 h_{fg} \frac{\rho_l \rho_v}{(\rho_l - \rho_v)} \max(0.0001, \alpha) \tag{3.89}$$

$$wf_{sub} = \max\left[0, \min\left[1, 10(0.2-\alpha)\right]\right] \tag{3.90}$$

In the annular-mist regime, the interfacial area or HTC is separately calculated for annular film and entrained droplets, and then combined. To model annular film, the most important consideration is the film thickness, which is the characteristic length for heat transfer. The film thickness is computed using the formula for tube geometry shown in equation (4.31). The interfacial area is similarly calculated by geometry and given by equation (4.32), but the surface is not fully wetted by liquid film, so the interfacial area is modified by multiplication of the fraction of the wetted surface. The wetted parameter is given by (4.33), which is solved by thin film approximation. The liquid interface heat transfer is estimated by considering both laminar and turbulent regimes using power-law weighting as shown in equation (4.34). To model condensation phenomena, the correlation of Kuhn [70] and the modified correlation of Gnielinski [27] are used for laminar and turbulent conditions, respectively. In the same way as with the wall heat transfer modules, wall-liquid and interface-liquid heat transfer must be distributed from the correlation of Kuhn. In TRACE, heat transfer resistances for both is assumed to be the same, so equation (4.35) can be obtained by dividing the resistance in half by the correlation of Kuhn. For turbulent, the single phase forced convection heat transfer correlation of Gnielinski, which is referred to in section 3.3, was adopted and multiplied by 0.7 to use as an interfacial heat transfer correlation. The vapor-interface heat transfer for annular film is a secondary consideration, so correlations implemented in TRAC-PF1/MOD2 are utilized. The maximum Nusselt number of the Dittus-Boelter correlation for turbulent convection and a constant value of 4 for a laminar flow is applied. Here, the diameter of the annular core is approximated by geometry and is used instead of the hydraulic diameter, which is shown in equation (4.36).

$$\delta = \frac{D_h}{2}\left(1-\sqrt{\alpha}\right) \tag{3.91}$$

$$a_i = \frac{4}{D_h}\sqrt{\alpha} \tag{3.92}$$

$$f_{wet} = \frac{(1-\alpha)D_h}{4\left(25\times10^{-6}\right)} \tag{3.93}$$

$$h_{il,film} = \frac{k_l}{\delta}\left(\mathrm{Nu}_{il,lam}{}^2 + \mathrm{Nu}_{il,turb}{}^2\right)^{1/2} \tag{3.94}$$

$$\mathrm{Nu}_{il,lam} = 2\left(1+1.83\times10^{-4}\,\mathrm{Re}_l\right) \tag{3.95}$$

$$D_c = D_h\sqrt{\alpha} \tag{3.96}$$

For an entrained droplet, the characteristic length is the droplet diameter. From the definition of the Sauter mean diameter, the interfacial area is calculated and shown in equation (4.37), where α_d is the fraction of the annular core occupied by the droplet and d_d is the droplet's Sauter mean diameter. To determine the mass fraction of liquid flowing as entrained droplets, the Ishii-Mishima [71] correlation (4.39) is applied, but in a large Reynolds number flow, the entrainment fraction is over-predicted, so the Reynolds number is limited to 6400. In the Ishii-Mishima correlation (4.39), subscript ∞ indicates the value for a fully developed flow. A non-dimensional gas flux (4.40) is applied to the enhancement factor (4.41) by defining the effective Weber number for entrainment as shown in (4.42). To remedy the over-estimated tendency of Ishii-Mishima, TRACE added the Steen-Wallis entrainment correlation for a large pipe. Paleev and Filippovich [72] and Wallis suggest the modified formula to better represent the property dependence upon liquid viscosity as shown in equation (4.43). The final equation implemented in TRACE is equation (4.45), where the critical gas velocity π_{crit} is 1.83 x 10^{-4}. For the droplet Sauter mean diameter in the interfacial area equation (4.37), correlation (4.46) is selected, which is proposed by Kataoka, Ishii, and Mishima [73]. To consider the droplet diameter as the Sauter mean diameter, an expression for the droplet size distribution is applied, which is developed by Kataoka [73]. To model liquid interfacial heat transfers, parameters, such as the exposure time of the droplet and the internal circulation within the droplet, are important. As both of these are highly uncertain, the asymptotic value (4.47) is applied, which is given by Kronig and Brink [74]. The vapor-interface heat transfer is modeled by the Ryskin [75] correlation (4.49) to consider both condensation and evaporation with the Nusselt number (4.50) and Peclet number (4.51), in which the maximum dimensionless circulation velocity at the surface of the drop is included and it is shown in (4.52). The droplet relative velocity in equations (4.51) and (4.53) is calculated from the force balance of gravity and the interfacial drag. The droplet drag coefficient is assumed to be 0.44, as shown in equation (4.56). Finally, equations (4.57) and (4.58) are implemented in TRACE in the annular-mist regime.

$$a_{i,drop} = \frac{6\alpha_{drop}}{d_{drop}} \tag{3.97}$$

$$\alpha_{drop} = E_\infty \frac{j_l}{j_v} \tag{3.98}$$

$$E_\infty = \tanh\left(7.25\times10^{-7}\left(j_v^*\right)^{2.5}\left(D^*\right)^{1.25}\mathrm{Re}_l^{0.25}\right) \tag{3.99}$$

$$j_g^* = \frac{j_v}{\left[\sigma g\left(\rho_l-\rho_v\right)\Big/\rho_v^2\left(\frac{\rho_l-\rho_v}{\rho_v}\right)^{2/3}\right]^{0.25}} \tag{3.100}$$

$$E_\infty = \tanh\left(7.25\times10^{-7}\,\mathrm{We}_v^{1.25}\,\mathrm{Re}_l^{0.25}\right) \tag{3.101}$$

$$\mathrm{We}_v = \frac{\rho_v j_v^2 D_h}{\sigma}\left(\frac{\rho_l-\rho_v}{\rho_v}\right)^{1/3} \tag{3.102}$$

$$E_\infty = 0.015 + 0.44\log_{10}\left(2.77\times10^7\pi_2^2\right) \tag{3.103}$$

$$\pi_2 = \frac{j_v \mu_v}{\sigma} \sqrt{\frac{\rho_v}{\rho_l}} \tag{3.104}$$

$$E_\infty = 0.015 + 0.44 \log_{10} \left(0.9245 \left(\pi_2 / \pi_{crit} \right)^2 \right) \tag{3.105}$$

$$d_{drop} = 0.00796 \left(\frac{\sigma}{\rho_v {j_v}^2} \right) {\mathrm{Re}_v}^{2/3} \left(\frac{\mu_v}{\mu_l} \right)^{2/3} \left(\frac{\rho_v}{\rho_l} \right)^{-1/3} \tag{3.106}$$

$$\mathrm{Nu}_{il,drop} = 2\pi^2 \tag{3.107}$$

$$h_{il,drop} = \frac{k_l}{d_d} \mathrm{Nu}_{il,drop} \tag{3.108}$$

$$\mathrm{Nu}_{iv,drop} = 2 + \sqrt{v^*_{\max} \mathrm{Pe}} \tag{3.109}$$

$$\mathrm{Nu}_{iv,drop} = \frac{h_{iv,drop} d_d}{k_v} \tag{3.110}$$

$$\mathrm{Pe} = \frac{\rho_g C_{p,v} d_d v_r}{k_v} \tag{3.111}$$

$$v^*_{\max} = \frac{1.5}{1 + \dfrac{2.8(1+2\lambda)(2+3\kappa)}{(2+3\lambda)\sqrt{\mathrm{Re}_d}}} \tag{3.112}$$

$$\mathrm{Re}_{drop} = \frac{\rho_v v_r d_{drop}}{\mu_v} \tag{3.113}$$

$$\lambda = \sqrt{\frac{\rho_l \mu_l}{\rho_v \mu_v}} \tag{3.114}$$

$$\kappa = \mu_l / \mu_v \tag{3.115}$$

$$v_r = 2.462 \sqrt{\frac{g(\rho_l - \rho_v)}{\rho_v} \frac{d_{drop}}{2}} \tag{3.116}$$

$$h_{il} a_i = \left(h_{il} a_i \right)_{film} + \left(h_{il} a_i \right)_{drop} \tag{3.117}$$

$$h_{iv} a_i = \left(h_{iv} a_i \right)_{film} + \left(h_{iv} a_i \right)_{drop} \tag{3.118}$$

In the stratified flow regime, the interfacial area is calculated by geometry as depicted in Figure 35. In equation (4.59), S_i is the width of the stratified two-phase interface. In Figure 35, h_l is the height of the liquid layer and it is important for modeling liquid-interface heat transfers. To calculate this length, a curve-fit to geometrical formula (4.59) is utilized. The liquid interfacial heat transfer is evaluated by the same models as used for the liquid film in an annular flow (4.34), but the Reynolds number is calculated by equation (4.59) with the liquid phasic hydraulic diameter (4.60) suggested by Agrawal [76].

$$a_i = \frac{S_i}{A} \tag{3.119}$$

$$h_l = \begin{cases} \left(1-7.612668\alpha\right)D_h & \alpha < 0.001 \\ \left(1-0.70269591\alpha^{2/3} - 0.034146667\alpha - 0.161023911\alpha^2\right)D_h & 0.001 \le \alpha \le 0.5 \\ \left(1-0.70269591\left(1-\alpha\right)^{2/3} - 0.034146667\left(1-\alpha\right) - 0.161023911\left(1-\alpha\right)^2\right)D_h & 0.5 < \alpha \le 0.999 \\ 7.612668\left(1-\alpha\right)D_h & \alpha > 0.999 \end{cases} \tag{3.120}$$

$$\mathrm{Re}_l = \frac{\rho_l v_l D_l}{\mu_l} \tag{3.121}$$

$$D_l = \frac{4A_l}{S_l} \tag{3.122}$$

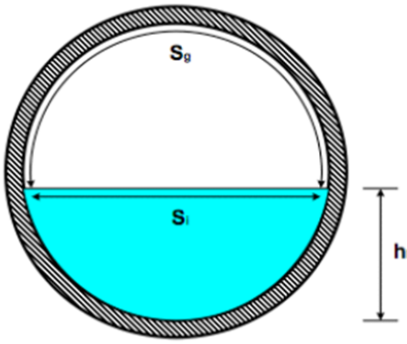

Figure 35 Schematic of Stratified Flow in a Horizontal Pipe [13]

4.5 Interfacial Heat Transfer Models and Correlations of RELAP5

In all the flow regimes, RELAP5 calculates subcooled or superheated heat transfer regimes based on the temperature of the liquid or vapor. If the temperature of the liquid is smaller than the saturation temperature (T_{sat}), the subcooled liquid interfacial heat transfer correlation is used. If the temperature of the liquid is larger than T_{sat} + 1, the superheated liquid interfacial heat transfer correlation is used. When the temperature of the liquid falls in between T_{sat} and T_{sat} +1, the liquid interfacial heat transfer is evaluated by cubic spline interpolation of the subcooled and the superheated heat transfer correlations. The case of vapor is also calculated in the same way.

In the bubbly flow regime, the interfacial area is solved from equations (4.12) and (4.13) as in TRACE, but with the upper limit of the bubble diameter as shown in (4.63). For the subcooled and the superheated vapor, the interfacial HTC is a constant value similar to TRACE, but, in RELAP5, the constant value is 10^4 not 10^3. This value is based on an empirical correlation suggested by Brucker [77]. To consider the enhancement tendency by the superheated vapor, an additional factor is further multiplied, as shown in equation (4.64).

For the subcooled liquid, the Unal-Lahey [78] correlation (4.66) is implemented with modifications, where ϕ is Unal's velocity dependency coefficient, and C is Unal's pressure dependent coefficient. Unal indicates that this correlation has discontinuity, so RELAP5 assumes that a dry area under a bubble disappears at 1.1272 MPa and modifies coefficient C to remove the discontinuity. This assumption was approved by Unal. RELAP5 also considered subcooled boiling as in TRACE using a factor f_s, which is the term from the subcooled boiling model of Lahey [79]. The smoothing factor between the Unal and Lahey model is also used in the factor f_s, which is suggested by Theofanous [80]. The final equation for the subcooled liquid interfacial heat transfers is described in (4.67) – (4.70).

For the superheated liquid, the largest HTC is applied among the Plesset-Zwick [81] correlation and modified Lee-Ryley [82] correlation. An additional term is multiplied by this value to represent the enhanced nucleation effect by using a curve fit to approximate Forster-Zuber's results. Plesset-Zwick derived the growth rate of a bubble radius and the result is shown in equation (4.71). The thermal diffusivity is replaced by its definition and according to a suggestion by Collier [50]. The interfacial HTC can be derived by substituting the growth rate of a bubble radius with the equation of mass transfer as the bubble grows, and it is shown in equation (4.72). The Plesset-Zwick correlation is for the pool boiling, so it is appropriate to use the relative velocity rather than the absolute bubble velocity. To account for the increase in the Nusselt number from the Plesset-Zwick correlation, RELAP5 utilizes the second correlation deduced by Lee-Ryley. The original form has the Prandtl number, but it is omitted in RELAP5, because the Prandtl number is close to one under the typical operating conditions of a nuclear power plant. Equation (4.73) shows the implemented form and, here, the Reynolds number of a bubble is the same as equation (4.16) in TRACE. An additional form, which is used for the contribution from the wall nucleation, is shown in (4.74). Here, pool boiling CHF is utilized as the upper limit, and this CHF is suggested by Zuber. The final term for superheated liquid is shown in equation (4.77). However, at zero void fraction, the interfacial HTC for liquid is set to zero.

$$d_{bubm} = \left(\frac{2.96\sigma^{0.6} D_h^{0.48} \mu_l^{0.08}}{\rho_l^{0.68} \left[(1-\alpha) v_l \right]^{1.12}} \right) \tag{3.123}$$

$$h_{iv} = 10^4 \left(1 + \eta \left(100 + 25\eta \right) \right) \tag{3.124}$$

$$\eta = \left| \max\left(-2, T_{sat} - T_v \right) \right| \tag{3.125}$$

$$h_{il} = \frac{C\phi h_{fg} d}{2\left(\frac{1}{\rho_v} - \frac{1}{\rho_l} \right)} \tag{3.126}$$

$$h_{il} = \frac{f_5 h_{fg} d}{2\left(\frac{1}{\rho_v} - \frac{1}{\rho_l} \right)} \tag{3.127}$$

$$f_5 = \begin{cases} 6 \times 0.075 & \alpha \geq 0.25 \\ 6 \times \left[1.8\phi C \exp\left(-45\alpha \right) + 0.075 \right] & \alpha < 0.25 \end{cases} \tag{3.128}$$

$$C = \begin{cases} 65 - 5.69 \times 10 \left(P - 0.1 \right) & P \leq 1.1272 \text{ MPa} \\ 2.5 \times 10^9 / \left(P \times 10^{-6} \right)^{1.1418} & P > 1.1272 \text{ MPa} \end{cases} \tag{3.129}$$

$$\phi = \begin{cases} 1 & |v_l| \le 0.61 \\ \left(\left(1/61\right)\times|v_l|\right)^{0.47} & |v_l| > 0.61 \end{cases} \tag{3.130}$$

$$\dot{r}_{bub} = \frac{6k_l \rho_l C_{p,l}}{\pi r_{bub}}\left(\frac{T_l - T_{sat}}{h_{fg}\rho_g}\right)^2 \tag{3.131}$$

$$\mathrm{Nu}_{\mathrm{Plesset}} = \frac{12\rho_l C_{p,l}\left(T_l - T_{sat}\right)}{\pi \rho_v h_{fg}} \tag{3.132}$$

$$\mathrm{Nu}_{\mathrm{Lee}} = 2 + 0.74\,\mathrm{Re}_{bub}{}^{0.5} \tag{3.133}$$

$$q''_{wall} = 0.0744P^{0.79}\left(T_l - T_{sat}\right)^2 \tag{3.134}$$

$$q''_{\mathrm{Zuber}} = \min\left(4\times10^6, 2.18 + 4P^{0.34}\right) \tag{3.135}$$

$$q''_{wall} = \min\left(q''_{wall}, q''_{\mathrm{Zuber}}\right) \tag{3.136}$$

$$h_{il} = \frac{k_l}{d_{bub}}\max\left(\mathrm{Nu}_{\mathrm{Plesset}}, \mathrm{Nu}_{\mathrm{Lee}}\right) + \frac{q''_{wall}}{\left(T_l - T_{sat}\right)} \tag{3.137}$$

In the subcooled liquid, an upper limit has been placed in all the flow regimes. This limit is an umbrella-shaped function in order to force the coefficient to have small values comparable to the void fraction value. This is shown in equation (4.78). This limit is required to prevent a code failure due to water property errors caused by high condensation rates. A similar umbrella-shaped limit has been used in the COBRA [83] and TRAC-BF [84].

$$h_{il} = \min\left[h_{il}, 17539\max\left(4.724, 472.4\alpha\left(1-\alpha\right)\min\left(0, \min\left(1, \frac{\alpha - 10^{-10}}{0.1 - 10^{-10}}\right)\right)\right)\right] \tag{3.138}$$

To solve heat transfer coefficient in the slug flow regime, similar to TRACE, the sum of small dispersed bubbles and large Taylor bubbles are considered as shown in (4.28). The interfacial area is also based on Ishii-Mishima [67] as in TRACE, and it can be shown in equations (4.19) and (4.20), but the coefficients C^* and d^* are set to 4.5 and the hydraulic diameter described in equation (4.79), respectively. First of all, the interfacial heat transfer for dispersed bubbles is calculated from correlations mentioned above in the bubbly flow regime. For a Taylor bubble, both subcooled and superheated liquid interfacial heat transfers are calculated from the maximum Nusselt number between Dittus-Boelter [18] and equation (4.81), where the film thickness is the same as in TRACE as shown in equation (4.31). In the subcooled boiling regime, a limiting function (4.78) is also applied to prevent code failure. For the subcooled vapor, it is still based on an empirical correlation of Brucker [77] and the enhancement factor is the same as the bubbly flow regime, which is shown in (4.64), but for the vapor, a roughness factor of 2 is multiplied by the interfacial area as shown in (4.83). For the superheated vapor, the Lee-Ryley [82] correlation (4.83) is implemented. The Lee-Ryley correlation is developed on the basis of a spherical form, so it does not match the Taylor bubble and it was modified as shown in equation (4.84).

$$D_{Tb} = 0.88D_{\text{pipe}} \tag{3.139}$$

$$\mathrm{Nu}_{D-B} = 0.023\,\mathrm{Re}_{film}{}^{0.8}\,\mathrm{Pr}_{film}{}^{0.4} \tag{3.140}$$

$$\mathrm{Nu} = 4\left(1+0.022\,\mathrm{Re}_{film}{}^{0.46}\right) \tag{3.141}$$

$$h_{il} = \frac{k_l}{\delta}\max\left(\mathrm{Nu}_{D-B}, \mathrm{Nu}_{\text{equation}(4.80)}\right) \tag{3.142}$$

$$a_{iv,Tb} = \frac{4.5}{D_h}\left(\frac{\alpha-\alpha_{BS}}{1-\alpha_{BS}}\right)\times 2 \tag{3.143}$$

$$h_{iv} = \frac{k_v}{D_h}\left(2.2+0.82\,\mathrm{Re}_v{}^{0.5}\right) \tag{3.144}$$

$$\mathrm{Re}_v = \frac{\rho_v\left|v_l - v_v\right|D_h}{\mu_v} \tag{3.145}$$

In the annular-mist flow, the interfacial area is separately calculated for annular film and entrained droplets and then combined, which is the same as with TRACE as shown in equations (4.57) and (4.58). For annular film, the interfacial area is calculated as in (4.86) based on an assumption of simple geometry as suggested by Ishii-Mishima [67], and it can be derived to (4.87), where $\alpha_{l,drop}$ and $\alpha_{l,film}$ is liquid fraction in the core and in the annular film, respectively. The liquid fraction of the annular film is defined as equation (4.88). Here, C_e and the velocity ratio parameter λ is dependent on the flow direction and defined as equations (4.89) – (4.91). In RELAP5, an additional coefficient C_{ann} is also multiplied by the interfacial area (4.87) and it becomes (4.92) to assure that the interfacial area approaches zero when the liquid fraction of the annular film approaches zero.

For both subcooled and superheated liquids, correlation (4.82) is utilized. In the same way in the slug flow regime, the maximum Nusselt number is applied among Dittus-Boelter and equation (4.81), but the film thickness is calculated from equation (4.94). As with other flow regimes, the limiting function (4.78) is also utilized to prevent failure of the code. In a similar way as in the slug flow regime, the roughness factor is multiplied by the vapor-interfacial heat transfer to increase the surface area for mass transfer, so the interfacial area in vapor becomes (4.95). To estimate the subcooled vapor interfacial heat transfer, an empirical correlation of Brucker [77] and the enhancement factor are applied in the same way as in the bubbly and slug flow regimes, which is shown in (4.64). For the superheated vapor, the interfacial heat transfer is represented by a correlation (4.96) based on the Dittus-Boelter [18] relation, and the smoothing factor f_{10} is multiplied, which greatly decreases as the velocity ratio parameter approaches zero.

For the entrained droplets, the interfacial area is determined by the Sauter-mean diameter, which is similar to the bubbly flow regime of TRACE. By replacing the Sauter-mean diameter with the mean droplet diameter and normalizing to the total volume, equation (4.12) becomes equation (4.99) with a Weber number of 1.5 and a constant diameter D' of 0.0025 m. For subcooled and superheated liquids, heat transfer is based on a paper by Brown [85]. Brown developed the correlation by solving a classical transient-heat conduction problem and forming the internal energy balance, and this correlation is shown in equation (4.104). The multiplication factor of the superheated liquid is shown in (4.105). For the subcooled vapor, the empirical correlation of Brucker and the enhancement factor are applied as in equation (4.64) and for the superheated vapor, the correlation of Lee-Ryley [82] is used in the bubbly regime and it is shown in (4.106).

$$a_{i,film} = \frac{4}{D_h}\left(\frac{\alpha}{1-\alpha_{l,drop}}\right) \tag{3.146}$$

$$a_{i,film} = \frac{4}{D_h}\left(1-\alpha_{l,film}\right) \tag{3.147}$$

$$\alpha_{l,film} = \left(1-\alpha\right)\exp\left(-C_e \times 10^{-5}\lambda^{6}\right)\max\left[0,\left(1-10^{-4}\,\mathrm{Re}_l^{\,0.25}\right)\right] \tag{3.148}$$

$$C_e = \begin{cases} 4 & \text{horizontal} \\ 7.5 & \text{vertical} \end{cases} \tag{3.149}$$

$$\lambda = \frac{\alpha v_v}{v_{crit}} \tag{3.150}$$

$$v_{crit} = \begin{cases} 0.5\left[\dfrac{\left(\rho_l-\rho_v\right)g\alpha A}{\rho_v D_h \sin\theta}\right]\left(1-\cos\theta\right) & \text{horizontal} \\ 3.2\left[\dfrac{\sigma g\left(\rho_l-\rho_v\right)}{\rho_v^{\,2}}\right]^{1/4} & \text{vertical} \end{cases} \tag{3.151}$$

$$a_{i,film} = \frac{4C_{ann}}{D_h}\left(1-\alpha_{l,film}\right) \tag{3.152}$$

$$C_{ann} = \left(30\alpha_{l,film}\right)^{1/8} \tag{3.153}$$

$$\delta = \frac{D_h}{4}\left(1-\alpha\right) \tag{3.154}$$

$$a_{iv,film} = \frac{4\times 2.5C_{ann}}{D_h}\left(1-\alpha_{l,film}\right) \tag{3.155}$$

$$h_{iv,film} = \frac{k_v}{D_h}0.023\,\mathrm{Re}_v^{\,0.8}\,f_{10} \tag{3.156}$$

$$f_{10} = \min\left[1+\left|\lambda\right|^{2}+0.05\left|\lambda\right|,6\right] \tag{3.157}$$

$$\mathrm{Re}_v = \frac{\alpha\rho_v\left(v_v-v_l\right)D_h}{\mu_v} \tag{3.158}$$

$$a_{i,drop} = \frac{3.6\alpha_{l,drop}}{d_{drop}}\left(1-\alpha_{l,film}\right) \tag{3.159}$$

$$\alpha_{l,drop} = \frac{\left(1-\alpha\right)-\alpha_{l,film}}{1-\alpha_{l,film}} \tag{3.160}$$

$$d_{drop} = \frac{\mathrm{We}\,\sigma}{\rho_v \hat{v}_{fg}^{\,2}} \tag{3.161}$$

$$\hat{v}_{fg}^{\;2} = \max\left[v_{fg}^{**2}, \frac{\mathrm{We}\sigma}{\rho_v \min\left(D'\alpha_{l,drop}^{\;1/3}, D_h\right)} \right] \tag{3.162}$$

$$v_{fg}^{**} = \left(v_v - v_l\right)\times\left(1-\exp\left(-C_e\times10^{-5}\lambda^6\right)\max\left[0,\left(1-10^{-4}\,\mathrm{Re}_l^{0.25}\right)\right]\right) \tag{3.163}$$

$$\mathrm{Nu}_{l,drop} = \left[2+7\min\left(1+\frac{C_{p,l}\max\left(0,T_{sat}-T_l\right)}{h_{fg}}\right),8 \right] \tag{3.164}$$

$$h_{l,drop} = \frac{k_l}{d_{drop}}\mathrm{Nu}_{l,drop}\left(1+0.25\left(\max\left(0,T_l-T_{sat}\right)\right)^2\right) \tag{3.165}$$

$$\mathrm{Nu}_{v,drop} = 2+0.5\,\mathrm{Re}_{drop}^{\;0.5} \tag{3.166}$$

$$\mathrm{Re}_{drop} = \frac{\mathrm{We}\sigma\left(1-\alpha_{l,drop}\right)^{2.5}}{\mu_v \hat{v}_{fg}} \tag{3.167}$$

In the pre-CHF mist flow regime, the same correlations are utilized as for the dispersed droplet in the annular-mist regime, but the liquid fraction of droplets and the modified relative velocity is replaced with the total liquid fraction in a cell and the relative velocity shown in (4.108) and (4.109).

$$\alpha_{l,drop} = 1-\alpha \tag{3.168}$$

$$v_{fg}^{**} = \left(v_v - v_l\right) \tag{3.169}$$

In RELAP5, the interfacial heat transfer consists of two parts, that is, the interfacial heat transfer in the bulk and the interface heat transfer in the thermal boundary layer near the wall as shown in equation (4.110), in which subscript p denotes the liquid or vapor phase. Figure 36 shows the interfacial heat transfer for subcooled boiling. The bulk interfacial heat transfer is evaluated through the above-described interfacial heat transfer coefficients and interfacial areas as shown in equation (4.111). The wall vapor generation or condensation process contributes to the interfacial heat transfer near the wall. In the boiling process, the vapor interfacial heat transfer in the boundary layer near the wall becomes zero. From the interface energy exchange equations, the vapor generation is defined as equation (4.112), where h denotes enthalpy not the heat transfer coefficient, and it can be derived from interfacial heat transfer equations (4.113) and (4.114) with equation (4.110). From Podowski's subcooled boiling model [86], the interfacial heat transfer fraction f_i in wall heat flux can be determined as equation (4.116) and then, the vapor generation becomes equation (4.115). Here, the wall heat flux is applied as a value calculated from the wall heat transfer modules described in chapter 3. Conditions necessary for the net voids to exist are calculated from the critical enthalpy h_{crit} shown in equation (4.115), which is from the Saha-Zuber method [87]. In the Saha-Zuber correlation (4.119), the Peclet number (4.121) is used to decide whether the heat flux should be related to the Nusselt number (4.122) in a low flow or the Stanton number (4.123) in a high flow. When the liquid flows through the heated wall in the axial direction, the enthalpy can be close enough to the saturation enthalpy, so the critical enthalpy is necessary to determine whether the conditions satisfy non-zero net void generation or zero.

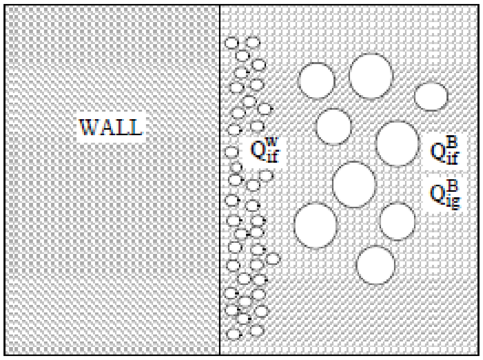

Figure 36 Interfacial Heat Transfer in the Bulk and near the Wall for Subcooled Boiling [12]

$$q_{ip}=q_{ip}^{Bulk}+q_{ip}^{Wall} \tag{3.170}$$

$$q_{ip}{}^{Bulk}=a_{ip}h_{ip}\left(T_{sat}-T_{p}\right) \tag{3.171}$$

$$\Gamma_{w}=\frac{-q_{il}^{Wall}}{h_{fg}} \tag{3.172}$$

$$q_{il}=a_{il}h_{il}\left(T_{sat}-T_{l}\right)-\Gamma_{w}\left(h_{g}{}^{sat}-h_{l}\right) \tag{3.173}$$

$$q_{iv}=a_{iv}h_{iv}(T_{sat}\text{-}T_{v}) \tag{3.174}$$

$$\Gamma_{w}=\begin{cases}\dfrac{q''_{wl}\;f_{i}A_{\text{pipe}}}{V_{\text{pipe}}\left[\max\left(h_{fg},10^{4}\right)\right]} & h_{\min}>h_{crit}\\ 0 & h_{\min}\le h_{crit}\end{cases} \tag{3.175}$$

$$f_{i}=\frac{f_{sub}+\dfrac{1.0782\left(P^{5}-f_{sub}\right)}{1.105+\exp\left(\dfrac{P/6894.757-140.75}{28.0}\right)}}{1+\dfrac{\rho_{l}\left(h_{l}^{sat}-h_{\min}\right)}{\rho_{v}h_{fg}}\left(\dfrac{1}{0.97+38\exp\left(-\dfrac{P/6894.757+60}{42.0}\right)}\right)} \tag{3.176}$$

$$f_{sub}=\frac{h_{\min}-h_{crit}}{h_{l}^{sat}-h_{crit}} \tag{3.177}$$

$$P^{5}=\min\left(1,0.0022+0.11262f_{sub}-0.59224f_{sub}{}^{2}+8.68227f_{sub}{}^{3}-11.29044f_{sub}{}^{4}+4.253448f_{sub}{}^{5}\right) \tag{3.178}$$

$$h_{crit} = \begin{cases} h_l^{sat} - \dfrac{\mathrm{St}C_{p,l}}{\left(0.0055 - 0.0009\left(\dfrac{1.0782}{1.015 + \exp\left(\dfrac{P/6894.757 - 140.75}{28.0}\right)}\right)\right)} & \mathrm{Pe} > 70000 \\ h_l^{sat} - \dfrac{\mathrm{Nu}C_{p,l}}{455} & \mathrm{Pe} \le 70000 \end{cases} \tag{3.179}$$

$$h_{\min} = \min\left(h_l, h_l^{sat}\right) \tag{3.180}$$

$$\mathrm{Pe} = \frac{GD_hC_{p,l}}{k_l} \tag{3.181}$$

$$\mathrm{Nu} = \frac{q''_{wl}D_h}{k_l} \tag{3.182}$$

$$\mathrm{St} = \frac{\mathrm{Nu}}{\mathrm{Pe}} \tag{3.183}$$

4.6 Comparison Results

Figure 37 shows the calculated volumetric heat transfer between the liquid phase and the interface from TRACE and RELAP5. When both codes select the bubbly regime or the slug flow regime, R-square is 0.6680 for a horizontal flow and 0.6744 for a vertical flow. When both codes determine an annular flow regime, R-square is 0.4478 for a horizontal flow and 0.3955 for a vertical flow.

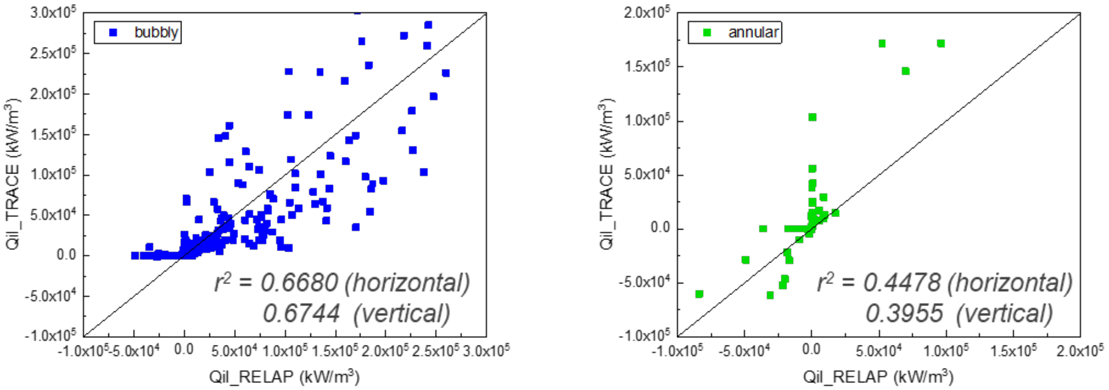

Figure 37 Calculated Liquid-interface Volumetric Heat Transfer of TRACE and RELAP5 (a) in a Bubbly/Slug Flow Regime (b) in an Annular Flow Regime

When RELAP5 predicts a negative heat transfer (from liquid to interface), the heat transfer of TRACE is estimated to be smaller by orders of magnitude. This trend is the same in all flow regimes. This is because RELAP5 includes the vapor generation term near the wall due to subcooled boiling in the interfacial heat transfer as shown in equation (4.110). In contrast, TRACE does not include the vapor generation term. To check the effect of the vapor generation term of RELAP5, the interfacial heat transfer between RELAP5 and TRACE without the vapor generation term is plotted in Figure 38. The figure shows that the vapor generation term has a significant effect on the interfacial heat transfer.

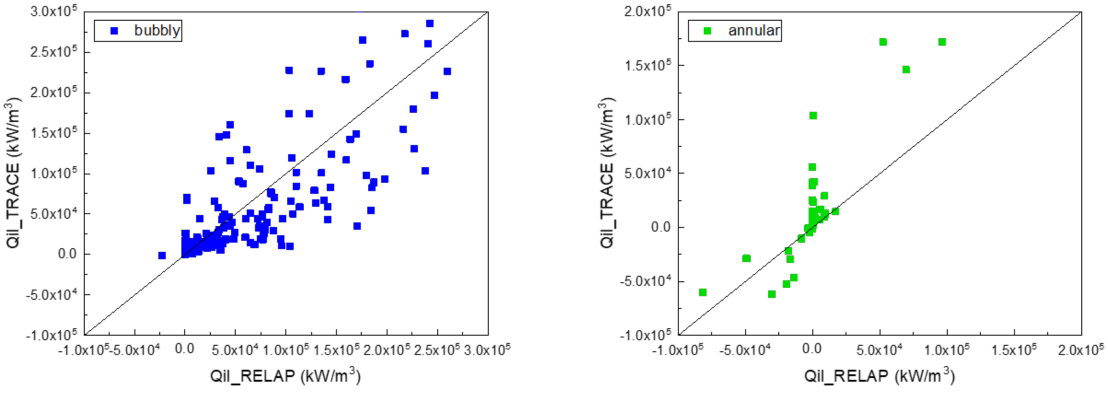

Figure 38 **Calculated Liquid-interface Volumetric Heat Transfer of TRACE and RELAP5 without the Vapor Generation Term. (a) in a Bubbly/Slug flow Regime (b) in an Annular Flow Regime**

Figure 39 shows the prediction of the volumetric heat transfer between the vapor phase and the interface from TRACE and RELAP5. There are large deviations in all flow regimes as shown in Figure 39, but the differences in the bubbly flow regime are substantial. It seems that the interfacial heat transfer of TRACE has a zero value, which is different from RELAP5, but the calculated interfacial heat transfer of RELAP5 is considerably larger than TRACE.

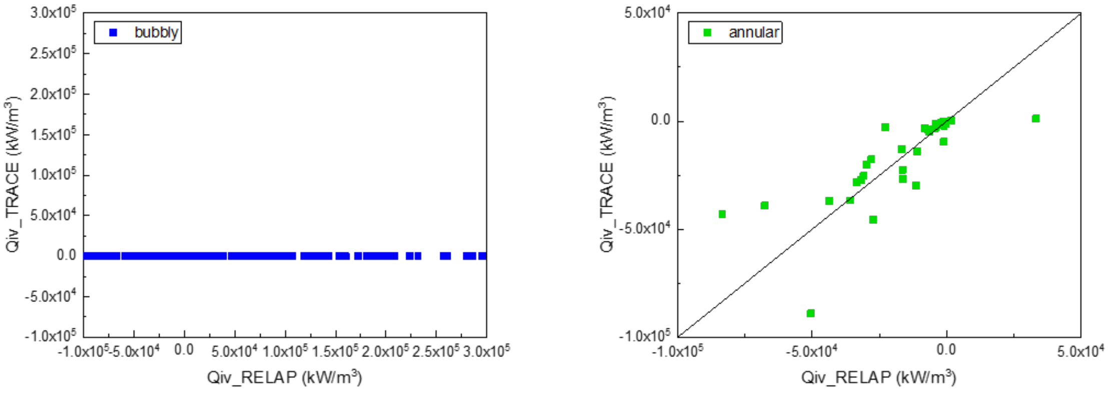

Figure 39 **Calculated Vapor-interface Volumetric Heat Transfer of TRACE and RELAP5 (a) in a Bubbly/Slug Flow Regime (b) in an Annular Flow Regime**

To confirm which factor is the most influential in the differences of interfacial heat transfer, equation (4.1) is revisited. Equation (4.1) shows that the amount of interfacial heat transfer is composed of the interfacial HTC and the interfacial area. Figure 40 shows the ratio of the interfacial HTC and the interfacial area calculated from TRACE and RELAP5. The ratio of the interfacial HTC has a difference up to the 1600 times for increasing Tvap – Tsat as shown in Figure 40(a). This is because TRACE and RELAP5 predict the vapor HTC differently in the bubbly flow regime. As explained in chapter 4.4 and 4.5, TRACE simply assigns a value of 10^3 at all times, but RELAP5 assigns 10^4 and includes the superheated vapor enhancement factor as shown in equation (4.64).

The interfacial area is also checked to be substantially different as shown in Figure 40(b). Both codes predict the interfacial area by the Sauter mean diameter value as defined in equation (4.12). Nevertheless, the interfacial areas calculated from the two codes are different due to the difference in the bubble diameter applied to the Sauter mean value. In both codes, the Laplace number multiplied by 2 is used, but RELAP5 has an upper limit as shown in equation (4.63). This upper limit is a function of the liquid superficial velocity and is drawn in Figure 41. When the liquid superficial velocity is larger than 2 m/s, the calculated bubble diameter is smaller than 10^{-4} and the bubble diameter is set to this value. Figure 40(c) represents the ratio of bubble diameters for the two codes. As the pressure becomes lower, bubble diameter of RELAP5 is 2.5% of TRACE value. As a result, interfacial areas of RELAP5 is 40 times larger than that of TRACE.

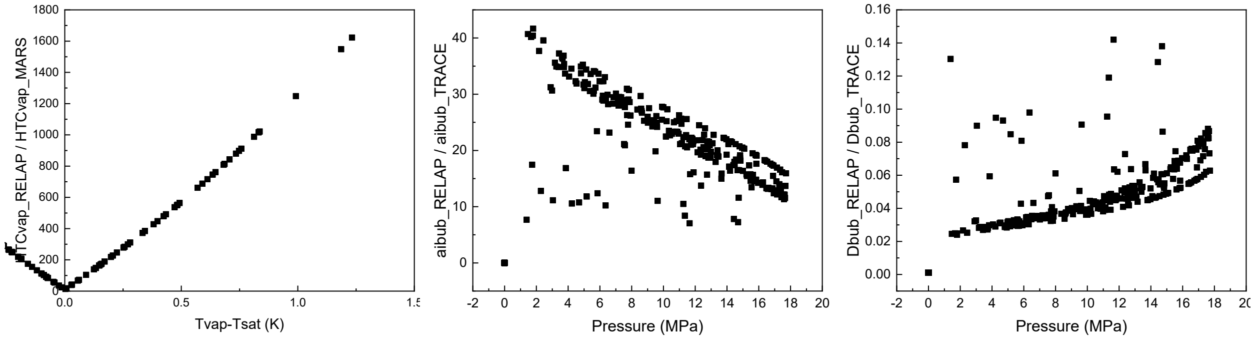

Figure 40 Separated Variables Affecting Vapor-interface Heat Transfer in a Bubbly Flow Regime (a) Heat Transfer Coefficient (b) Interfacial Area (c) Diameter of Bubble

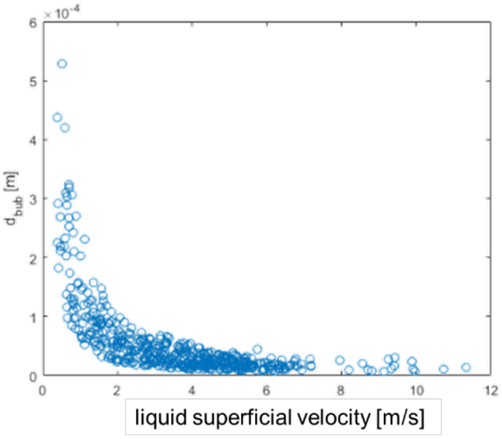

Figure 41 Bubble Diameter Calculated from Equation (4.63) in a Bubbly Flow Regime

5 WALL FRICTION MODELS

5.1 Background

The understanding of pressure drop due to wall friction under various fluid conditions is important for nuclear safety. While the single-phase friction is evaluated by the standard method such as the Darcy formula, two-phase friction is not as simple as single-phase friction. Generally, two-phase flow friction is greater than single-phase friction for the same mass flow rate due to the increased momentum transfer rate between phases. Lockhart-Martinelli [88] suggested a method to evaluate two-phase friction by multiplying the two-phase friction multiplier by the single phase friction pressure drop as shown in equation (5.1), namely, the Lockhart-Martinelli parameter. Many investigations of two-phase flow friction on the wall have been based on the use of the Lockhart-Martinelli parameter [89] and most of the thermal-hydraulic system analysis codes also adopt this method.

$$\left(\frac{dP}{dz}\right)_{2\phi} = \varphi_l^2\left(\frac{dP}{dz}\right)_l = \varphi_v^2\left(\frac{dP}{dz}\right)_v \tag{4.1}$$

5.2 Description of Wall Friction Modules

To solve the momentum conservation equation, information on the amount of friction at the wall is required, and the amount of friction between the wall and each phase is calculated in the wall friction module for TRACE and RELAP5. Because the wall friction mechanism depends on the shape of the fluid on the wall, both codes first have to determine the flow regime as described in the previous chapter of interfacial heat transfer models. Then, both codes evaluate friction on the wall using the correlation matching the selected flow regime. Regarding the implemented correlation, TRACE and RELAP5 use very different approaches to calculate the amount of friction on the wall. TRACE is based on the drag coefficient and considers only one non-zero wall drag coefficient in the equation, while RELAP5 calculates the total pressure drop using a two-phase friction multiplier and then distributes the total pressure drop to each phase. There is also a slight difference in the selection of the flow regime. In RELAP5, the same flow regime is selected as in the interfacial heat transfer models described in the previous chapter, but TRACE selects a new flow regime which is different from in the interfacial heat transfer models. In TRACE, the flow regime is determined by the void fraction. If the void fraction is less than 0.8, the bubbly-slug flow regime is selected, and in the case of a void fraction larger than 0.9, the annular-mist flow regime is selected. When the void fraction is between 0.8 and 0.9, the transition regime is selected, and the drag coefficient is an interpolated drag coefficient of the bubbly-slug flow and the annular-mist flow regimes.

5.3 Wall Friction Models and Correlations of TRACE

In TRACE, wall friction is evaluated on the basis of the drag coefficient. The wall drag coefficients of liquid and vapor have only one non-zero value. That is, in the bubbly/slug and the annular/mist flow regimes, all of the wall drag is applied to the liquid phase and the drag coefficient of the vapor phase is set to zero. For the friction factor in the drag coefficient, the correlation suggested by Churchill [90] is applied to all three regimes: laminar, transition, and turbulent, which are shown in equations (5.3) – (5.5), where the Reynolds number is defined as in equation (5.6) and p is phase p.

$$\left(\frac{dP}{dz}\right)_{2\phi} = C_{wl}\left|v_l\right|v_l + C_{wv}\left|v_v\right|v_v \tag{4.2}$$

$$f_w = 2\left[\left(\frac{8}{\mathrm{Re}}\right)^{12} + \frac{1}{(a+b)^{3/2}}\right]^{1/12} \tag{4.3}$$

$$a = \left\{2.457\ln\left[\frac{1}{\left(\frac{7}{\mathrm{Re}}\right)^{0.9} + 0.27\left(\frac{\varepsilon}{D_h}\right)}\right]\right\}^{16} \tag{4.4}$$

$$b = \left(\frac{3.753\times10^{4}}{\mathrm{Re}}\right)^{16} \tag{4.5}$$

$$\mathrm{Re}_p = \frac{\rho_p v_p D_h}{\mu_p} \tag{4.6}$$

For the pre-CHF regimes, the bubbly-slug and the annular-mist flow regimes, it is assumed that only the liquid phase has all of the wall drag as shown in equation (5.7), except for when the film thickness is too thin due to large entrainment in the annular-mist flow regime. The same expression for wall friction can also be derived and is shown in equation (5.8) in terms of the two-phase multiplier. By combining these equations, the wall drag coefficient is derived as equation (5.9). Models for the annular-mist flow regime is more straightforward than the bubbly-slug flow regime, so models for the annular-mist flow regime is explained first.

$$\left(\frac{dP}{dz}\right)_{2\phi} = C_{wl}\left|v_l\right|v_l \tag{4.7}$$

$$\left(\frac{dP}{dz}\right)_{2\phi} = \varphi_l^2\left(\frac{2f_{wl}\left|G_l\right|G_L}{D_h\rho_l}\right) \tag{4.8}$$

$$C_{wl} = \varphi_l^2\left(\frac{2f_{wl}\left(1-\alpha\right)^2\rho_l}{D_h}\right) \tag{4.9}$$

In the annular-mist flow regime, the annular flow theory [91, 92] is utilized to evaluate the two-phase multiplier as shown in equation (5.10), so the drag coefficient can be simplified as in equation (5.11), and this equation is modified by applying the entrainment factor as in equation (5.12). The entrainment fraction was mentioned in chapter 4 as in equations (4.39) and (4.45) for different sizes of hydraulic diameter. The friction factor for the annular film is evaluated by the power law of the laminar and turbulent values. The laminar friction factor is shown in equation (5.14) after modification is applied to reflect a thin film condition. The turbulent friction factor is obtained by Haaland's [93] explicit approximation to the Colebrook equation, which is described in equation (5.15). The transition to a single-phase gas flow is considered using the film thickness and the entrainment. In TRACE, if the film is smaller than a value of 25 microns, the film is considered to be breaking down into rivulets, so the fraction of the surface in contact with the liquid phase is estimated with equation (5.16) with the entrainment factor. If the wetted fraction is smaller than unity, the drag coefficient is described as equations (5.15) and (5.16), in which f_{wv} is calculated using Churchill's correlation.

$$\varphi_l^2 = \frac{1}{(1-\alpha)^2} \tag{4.10}$$

$$C_{wl} = f_{film}\frac{2\rho_l}{D_h} \tag{4.11}$$

$$C_{wl} = f_{film}(1-E_\infty)^2\frac{2\rho_l}{D_h} \tag{4.12}$$

$$f_{film} = \left[f_{lam}^{\ 3} + f_{turb}^{\ 3}\right]^{1/3} \tag{4.13}$$

$$f_{lam} = \begin{cases} {}^{16}\!/_{\mathrm{Re}_l} & \alpha \le 0.95 \\ {}^{16}\!/_{\mathrm{Re}_l} + {}^{8}\!/_{\mathrm{Re}_l}\min\left(1, \dfrac{\alpha - 0.95}{0.99-0.95}\right) & \alpha > 0.95 \end{cases} \tag{4.14}$$

$$f_{turb} = \frac{1}{\left[3.6\log_{10}\left(\dfrac{6.9}{\mathrm{Re}_l} + \left(\dfrac{\varepsilon/D_h}{3.7}\right)^{1.11}\right)\right]^2} \tag{4.15}$$

$$f_{wet} = (1-E_\infty)\frac{(1-\alpha)D_h}{4\left(25\times10^{-6}\right)} \tag{4.16}$$

$$C_{wl} = f_{wet}f_{film}(1-E_\infty)^2\frac{2\rho_l}{D_h} \tag{4.17}$$

$$C_{wv} = (1-f_{wet})f_{wv}\frac{2\rho_v}{D_h} \tag{4.18}$$

In the bubbly-slug flow regime, the same two-phase multiplier is applied as in the annular-mist flow regime, but the two-phase flow with nucleate boiling is more complicated so the correction factor is multiplied for enhancement due to wall nucleation as shown in equation (5.19). The enhancement factor due to wall nucleation is evaluated with Ferrell-Bylund's data [94] and the suggestion of Collier [50], which is show in equation (5.20). Collier also suggested utilizing Levy's model [95] to evaluate the bubble departure diameter from balances between surface tension and drag forces, where the wall shear stress is calculated from equation (5.22). In the transition regime, the interpolation between the bubbly/slug and the annular/mist flow regimes is conducted with respect to the void fraction, in which the wall drag coefficient is described in equations (5.23) – (5.25).

$$C_{wl} = f_{wl}\frac{2\rho_l}{D_h}\left(1 + C_{\mathrm{NB}}\right)^2 \tag{4.19}$$

$$C_{NB} = 155\left(\frac{d_B}{D_h}\right)\left[\alpha(1-\alpha)\right]^{0.62} \tag{4.20}$$

$$\frac{d_B}{D_h} = 0.015\left[\frac{\sigma}{\tau_w D_h}\right]^{1/2} \tag{4.21}$$

$$\tau_w = \frac{f_{wl}}{2}\rho_l v_l^2 \tag{4.22}$$

$$C_{wl} = wf \cdot C_{wl,bubbly-slug} + (1-wf)\cdot C_{wl,annular-mist} \tag{4.23}$$

$$C_{wv} = wf \cdot C_{wv,bubbly-slug} \tag{4.24}$$

$$wf = \left(\frac{0.9-\alpha}{0.9-0.8}\right) \tag{4.25}$$

5.4 Wall Friction Models and Correlations of RELAP5

In RELAP5, the total pressure drop is calculated and distributed to liquid and vapor phases based on an assumption that two-phase flows behave in a way similar to single-phase flows. The overall friction pressure drop is computed by the suggestion of Lockhart-Martinelli [88] as shown in equation (5.1). The Lockhart-Martinelli parameter is defined as a ratio of the phasic friction multiplier as shown in equation (5.26). The two-phase friction multiplier is expressed as equations (5.27) and (5.28) with the Lockhart-Martinelli parameter, where C is the correlation coefficient. To apply it for a broad range, this correlation coefficient is evaluated using heat transfer and fluid flow service (HTFS) – modified Baroczy correlation [96] instead of the Lockhart-Martinelli correlation, and equation (5.29) shows the correlation coefficient. If the HTFS correlation is combined with equation (5.1), the overall pressure drop can be derived as in equation (5.33), where f_l and f_v are friction factors of the liquid and vapor phases respectively calculated by the Zigrang-Sylvester [97] approximation to the Colebrook-White [98] correlation which is shown in equation (5.34) for a turbulent flow.

For partitioning the wall friction to each phase, Chisholm suggested the theoretical basis using the phasic momentum equations (5.35) and (5.36), where τ_l and τ_v are the liquid and vapor wall shear stresses, p_l and p_v are the liquid and vapor wetted perimeters, and S_{FI} is a stress gradient due to the interfacial friction. By rearranging equations (5.35) and (5.36), parameter Z is defined and liquid and vapor wall shear forces can be derived as equations (5.39) and (5.40). The parameter Z is expressed in equation (5.41) and λ_l and λ_v are the friction factor of each phase. These expressions are identical to f_l and f_v except that the hydraulic diameter in the Reynolds number for calculating λ_l and λ_v is the liquid and vapor hydraulic diameters as defined in equations (5.42) and (5.43) instead of the pipe hydraulic diameter. α_{lw} and α_{vw} are the liquid and vapor volume fractions on the wall and depend on the flow regime. The physical meaning is the ratio of the liquid and vapor perimeter to the pipe perimeter as shown in equations (5.44) and (5.45). The defined wall void fraction according to the flow regime is summarized in Table 7, where α_{BS} is the bubbly-slug regime boundary void fraction as in equation (4.3) and (4.4), $\alpha_{l,film}$ is the liquid film void fraction as in equation (4.88), α_{film} is the film void fraction as in equation (4.111) and α_{drop} is the droplet void fraction as in equation (4.120).

$$X^2 = \frac{\varphi_v^2}{\varphi_l^2} \tag{4.26}$$

$$\varphi_l^{\,2} = 1 + \frac{C}{X} + \frac{1}{X^2} \tag{4.27}$$

$$\varphi_v^{\,2} = X^2 + CX + 1 \tag{4.28}$$

$$C = \max\left(2, -2 f_1 T_1\right) \tag{4.29}$$

$$f_1 = 28 - 0.3\sqrt{G} \tag{4.30}$$

$$T_1 = \exp\left[-\frac{\left(\log_{10}\Lambda + 2.5\right)^2}{2.4 - G \times 10^{-4}}\right] \tag{4.31}$$

$$\Lambda = \frac{\rho_v}{\rho_l}\left(\frac{\mu_l}{\mu_v}\right)^{0.2} \tag{4.32}$$

$$\left(\frac{dP}{dx}\right)_{2\varphi} = \frac{1}{2D_h}\left\{f_l\rho_l\left[\left(1-\alpha\right)v_l\right]^2 + C\left[f_l\rho_l\left(\left(1-\alpha\right)v_l\right)^2 f_v\rho_v(\alpha v_v)^2\right]^{1/2} + f_v\rho_v(\alpha v_v)^2\right\} \tag{4.33}$$

$$\frac{1}{\sqrt{f}} = -2\log_{10}\left\{\frac{\varepsilon}{3.7D_h} + \frac{2.51}{\mathrm{Re}}\left[1.14 - 2\log_{10}\left(\frac{\varepsilon}{D_h} - \frac{21.25}{\mathrm{Re}^{0.9}}\right)\right]\right\} \tag{4.34}$$

$$\left(1-\alpha\right)A\left(\frac{dP}{dx}\right)_{2\phi} - \tau_l p_l + S_{FI} = 0 \tag{4.35}$$

$$\alpha A\left(\frac{dP}{dx}\right)_{2\phi} - \tau_v p_v - S_{FI} = 0 \tag{4.36}$$

$$Z^2 = \left(\frac{\tau_l p_l}{1-\alpha}\right)\Big/\left(\frac{\tau_v p_v}{\alpha}\right) = \frac{1 + S_R\left(\alpha/(1-\alpha)\right)}{1 - S_R} \tag{4.37}$$

$$S_R = \frac{S_{FI}}{\alpha A\left(\frac{dP}{dx}\right)_{2\phi}} \tag{4.38}$$

$$\tau_l p_l = \left(\frac{dP}{dx}\right)_l = \left(1-\alpha\right)\left(\frac{dP}{dx}\right)_{2\varphi}\left(\frac{Z^2}{\alpha + \left(1-\alpha\right)Z^2}\right) \tag{4.39}$$

$$\tau_v p_v = \left(\frac{dP}{dx}\right)_v = \alpha\left(\frac{dP}{dx}\right)_{2\varphi}\left(\frac{1}{\alpha + \left(1-\alpha\right)Z^2}\right) \tag{4.40}$$

$$Z^2 = \frac{\lambda_l\rho_l v_l^2\alpha_{lw} / \left(1-\alpha\right)}{\lambda_v\rho_v v_v^2\alpha_{vw} / \alpha} \tag{4.41}$$

$$D_{h,l} = \frac{4\left(1-\alpha\right)A}{p_l} \tag{4.42}$$

$$D_{h,v} = \frac{4\alpha A}{p_v} \tag{4.43}$$

$$\alpha_{lw} = {}^{p_l}\!/_{p} \tag{4.44}$$

$$\alpha_{vw} = {}^{p_v}\!/_{p} \tag{4.45}$$

Table 7 Void Fraction on the Wall for Different Flow Regimes

Flow Regime	Liquid void fraction on the wall (α_{lw})	Vapor void fraction on the wall (α_{vw})
Bubbly	$1-\alpha$	α
Slug	$1-\alpha_{BS}{}^{*}$	α_{BS}
Annular	$\alpha_{l,film}^{0.25}{}^{*}$	$1-\alpha_{l,film}^{0.25}$
Pre-CHF mist	$1-\alpha$	α
Inverted annular	$1-\sqrt{\alpha_{film}}\ {}^{*}$	$\sqrt{\alpha_{film}}$
Inverted slug	$\alpha_{drop}{}^{*}$	$1-\alpha_{drop}$
Mist	$1-\alpha$	α
Post-CHF mist	$1-\alpha$	α

5.5 Comparison Results

Figure 42 compares the wall friction of TRACE to the wall friction of RELAP5 when the same regime is selected for both codes. Figure 43 shows the wall friction when RELAP5 and TRACE each choose a different flow regime. Both codes predict similar magnitudes of wall friction in all tested flow regimes. When both codes select a bubbly flow regime, the wall friction values are fairly similar as the R-squared value becomes 0.9974 for the horizontal flow and 0.9975 for the vertical flow. Furthermore, when both codes choose an annular flow regime, both codes have similar wall friction values with an R-squared value of 0.9739 for the horizontal flow and 0.9739 for the vertical flow. Though RELAP5 predicts the post-CHF flow regime and TRACE chooses the pre-CHF flow regime, the wall friction values of RELAP5 are almost identical to those of TRACE with an R-squared value of 0.9556.

When both codes select the same flow regime, the most different case of wall friction values is in the slug flow regime. The R-squared value is 0.5289 for the horizontal flow and 0.7423 for the vertical flow. In Figure 44, the calculated wall friction in the slug regime is drawn according to the mass flux, and the difference in the wall friction between the two codes has a larger difference with a larger mass flux.

The most different case of wall friction values is when TRACE selects the transition flow regime but RELAP5 picks the annular flow regime. In this case, the R-squared value is 0.4945 for the horizontal flow and 0.5071 for the vertical flow. When the wall friction values of the transition flow regime in TRACE are calculated, the wall friction values are obtained by interpolating between the bubbly-slug and the annular flow regime wall friction values with respect to the void fraction as shown in equations (5.23) and (5.24). From this mechanism, Figure 43 is produced with respect to the void fraction as shown in Figure 45. From Figure 45, TRACE overestimates the wall friction values when the void fraction is near 0.8, and vice versa when the void fraction value is close to 0.9. This trend can be confirmed in Figure 42. TRACE overestimates the wall friction values very slightly in the bubbly-slug flow regime and underestimates them in the annular flow regime.

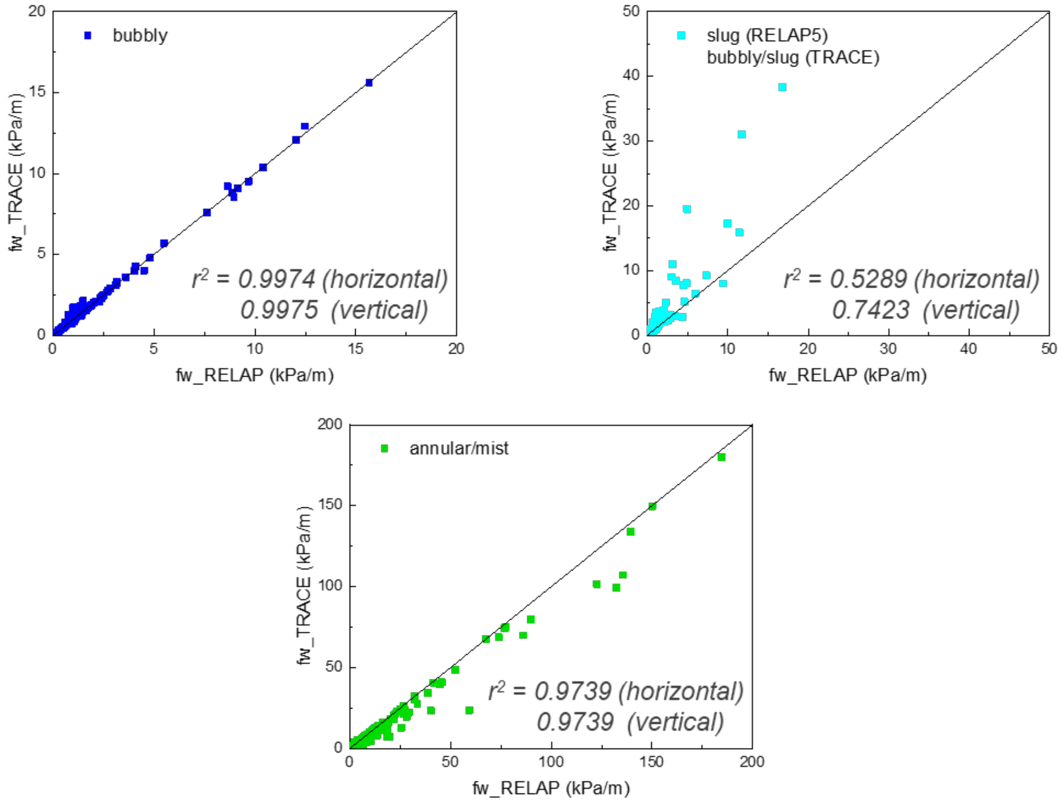

Figure 42 Calculated Wall Friction when TRACE and RELAP5 Select the Same Flow Regimes

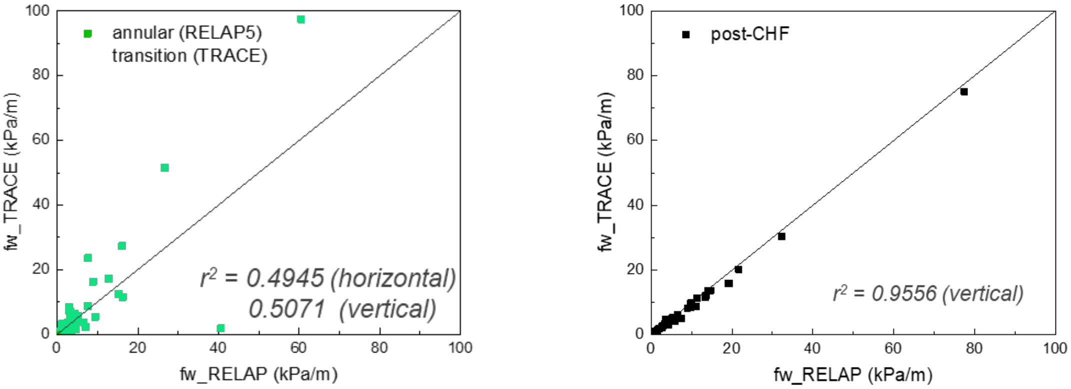

Figure 43 Calculated Wall Friction when TRACE and RELAP5 Select Different Flow Regimes

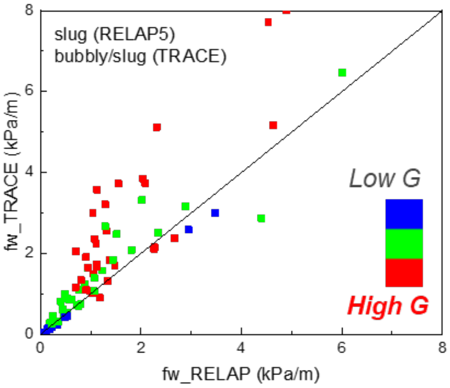

Figure 44 Calculated Wall Friction in the Slug Flow Regime according to the Mass Flux

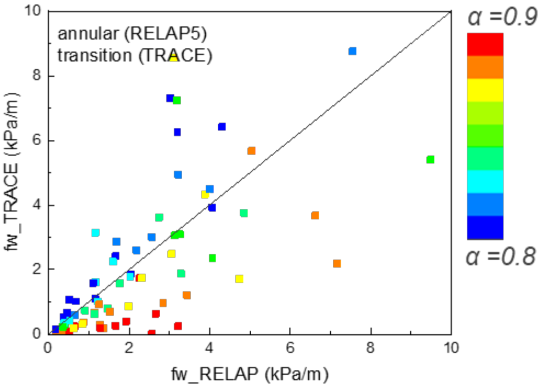

Figure 45 Calculated Wall Friction when TRACE Selects Transition and RELAP5 Selects Annular Flow Regimes

6 INTERFACIAL FRICTION MODELS

6.1 Background

Thermal-hydraulic system analysis codes mostly use a non-homogeneous non-equilibrium two-fluid model. Thus, liquid and vapor phases can have different velocities. It is well known that the vapor flow over the liquid-vapor interface can produce waves on the interface. The existence of waves at the interface makes the interfacial momentum transport different from the momentum transport at the tube wall. The equations of momentum for these two velocities are coupled by the interfacial drag force arising from shear forces between the phases. To evaluate the interfacial friction, there are two approaches: the drift flux method and the drag coefficient method. The drift flux model was developed by Wallis [91] as a model describing two-phase flows with an interest in the relative motion between each phase rather than in an individual flow in each phase. The drift flux method is utilized to improve the accuracy of the void fraction predictions and reduce void fraction oscillations under low pressure conditions. If the interfacial drag force is balanced by buoyancy, the drift flux correlation is used for the derivation of interfacial drag model as shown in equation (6.1), where v_r is the relative velocity. The interfacial drag coefficient is derived in equation (6.2) by equation (6.1). The basic equation of the drag coefficient method for the interfacial friction was suggested by Brauner-Maron [99], which is shown in equation (6.3). In equation (6.3), f_i is the interfacial friction factor, so the interfacial drag coefficient is defined as equation (6.4). The drift flux method is satisfactory for the flow in which the relative motion is determined by the interaction between bubbles and the surrounding liquid. The balance of drag force and buoyancy occurs in the low-velocity bubbly flow regime at a large vertical tube. On the other hand, the drag coefficient method can be applied to any flow, but it is often implemented for annular flows where the drift flux method is not appropriate.

$$\alpha(1-\alpha)g(\rho_l-\rho_v)=C_i v_r^2 \tag{5.1}$$

$$C_i=\frac{\alpha(1-\alpha)g(\rho_l-\rho_v)}{v_r^2} \tag{5.2}$$

$$\left(\frac{dP}{dz}\right)_i=f_i a_i\frac{\rho}{2}|v_r|v_r \tag{5.3}$$

$$C_i=f_i a_i\frac{\rho}{2} \tag{5.4}$$

6.2 Description of Interfacial Friction Modules

Both codes estimate interfacial friction by properly mixing the drift flux method and the drag coefficient method with respect to the flow regime. Similar to the interfacial heat transfer and wall friction modules, RELAP5 has the same selection logic for the flow regime, which is described in chapter 4, whereas TRACE does not divide the flow regime at all in the interfacial friction modules. In TRACE, the calculated interfacial friction coefficient varies by orders of magnitude between the bubbly-slug and annular-mist flow regimes, and this situation is illustrated in Figure 46 [13]. This may cause an oscillatory problem in the void fraction calculation. TRACE resolves this problem by applying a simple power law as shown in equation (6.5), and ultimately TRACE does not distinguish the flow regimes. Figure 46 shows an example of the transition region between bubbly-slug and annular-mist flow regimes. In RELAP5, the drift flux method is utilized only for vertical bubbly and slug flow regimes, and the drag coefficient method is applied for all the remaining regimes.

$$C_i = \sqrt{C_{i,BS}^{\;2} + C_{i,AM}^{\;2}} \tag{5.5}$$

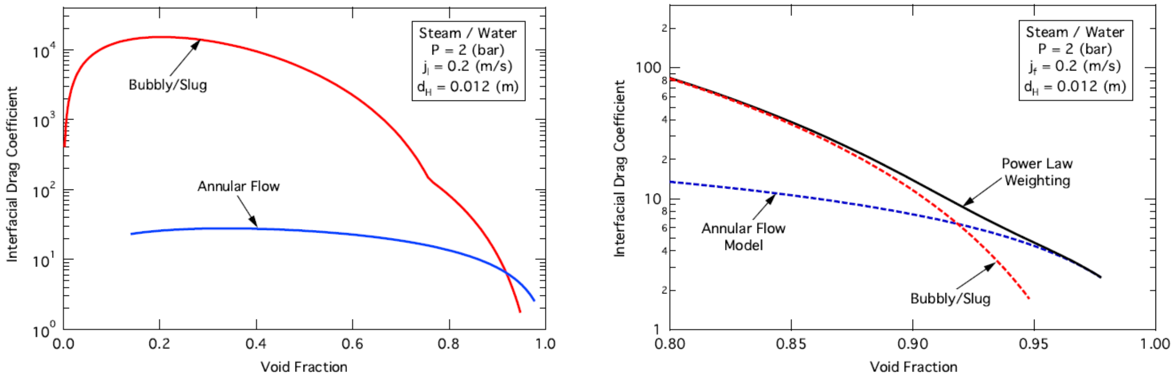

Figure 46 Comparison of the Interfacial Coefficient for the Bubbly-Slug and Annular-Mist Flow Regimes [13]

6.3 Interfacial Friction Models and Correlations of TRACE

In TRACE, the drag coefficient is evaluated by using equation (6.5). To estimate the bubbly-slug drag coefficient $C_{i,BS}$, the drift flux method is applied which is described in equation (6.2), where the relative velocity is a locally obtained value. To connect the drift flux model, equation (6.2) has to be translated to have a value averaged over the cross-sectional area. Ishii-Mishima [100] showed that area-averaged relative velocity can be approximated with equation (6.6), so the drag coefficient is rearranged as equation (6.7). The last term on the right-hand side of equation (6.7) is denoted as the profile slip factor P_s, which is derived as equation (6.8) as suggested by Ishii-Mishima [100]. C_0 is the distribution parameter and C_1 is the terminal velocity coefficient. In TRACE, a profile has an upper limit value of unity and a lower limit value of 0.05 for numerical reasons.

$$\langle v_r \rangle \approx \frac{\overline{v}_{gj}}{1-\langle \alpha \rangle} \tag{5.6}$$

$$C_i = \frac{\alpha\left(1-\alpha\right)^3 g\left(\rho_l-\rho_v\right)}{\overline{v}_{gj}^{\;2}} \times \frac{\langle v_r \rangle^2}{v_r^{\;2}} \tag{5.7}$$

$$P_s = \frac{\langle v_r \rangle^2}{v_r^{\;2}} = \frac{\left(C_1\overline{v}_v - C_0\overline{v}_l\right)^2}{v_r^{\;2}} \tag{5.8}$$

$$C_1 = \frac{1-C_0\langle \alpha \rangle}{1-\langle \alpha \rangle} \tag{5.9}$$

Since the characteristics of the bubble vary with the size of the bubbles, TRACE applies different correlations depending on the void fraction. TRACE includes two models for the churn-turbulent bubbly and slug flow regime or the Taylor cap bubbly flow regime, and allows for transition by a void fraction range of 10 percent. Zuber-Findlay argued that data can be better fit by the cap bubble model than by the dispersed flow model in several conditions, and this was also evaluated in TRACE. For the saturated flow, the void fraction is overestimated over the experimental data and indeed, even with a low void fraction, the cap bubble model provides a more reasonable prediction than the churn-turbulent flow model, whereas this problem was not found in the subcooled flow [101]. Thus, the transition point is evaluated by a function of the liquid sub-cooling as shown in equations (6.10) and (6.11). α_{BT} and α_{TS} are the bubbly – transition boundary and the transition – slug boundary. If the void fraction is smaller than the bubbly – transition flow regimes boundary, Ishii's correlation [102] is applied to define the drift flux velocity and the distribution parameter as defined in equations (6.12) and (6.13). For small diameter pipes, the drift flux velocity calculated from Ishii's correlation may exceed that for the slug flow regime, so the drift flux velocity of the bubbly flow regime has an upper limit which is evaluated from the model applied to the slug flow regime. For modeling the slug flow regime, in which the void fraction is larger than the transition-slug flow regimes boundary, Kataoka-Ishii's correlation [68] is utilized and it is shown in equation (6.15), where the drift velocity is evaluated from the non-dimensional drift velocity. Kataoka-Ishii recommended using the same distribution diameter applied to the bubbly flow regime, which is shown in equation (6.13). In the transition regime, the drift flux velocity is determined by interpolation between the bubbly and slug flow regimes.

$$\alpha_{BT} = 0.2\min\left(1, \frac{T_{sat} - T_l}{5}\right) \tag{5.10}$$

$$\alpha_{TS} = \alpha_{BT} + 0.1 \tag{5.11}$$

$$\bar{v}_{gj} = \sqrt{2}\left(\frac{\sigma g\left(\rho_l - \rho_v\right)}{\rho_l^2}\right)^{1/4} \tag{5.12}$$

$$C_0 = 1.2 - 0.2\sqrt{\frac{\rho_v}{\rho_l}} \tag{5.13}$$

$$\bar{v}_{gj}^{\,+} = 0.0019\left(\frac{D_h}{\sqrt{\sigma/g\left(\rho_l - \rho_v\right)}}\right)^{0.809}\left(\frac{\rho_l}{\rho_v}\right)^{0.157} \mathrm{N}_{\mu}^{\,-0.562} \tag{5.14}$$

$$\bar{v}_{gj} = \bar{v}_{gj}^{\,+}\left(\frac{\sigma g\left(\rho_l - \rho_v\right)}{\rho_l^2}\right)^{1/4} \tag{5.15}$$

To estimate the annular-mist flow regime drag coefficient $C_{i,AM}$, the drag coefficient method is applied which is described in equation (6.4) and the annular-mist flow regime is treated as a superposition of the interfacial drag on liquid film and the entrained droplets that are similar to the interfacial heat transfer models. This is shown in equation (6.16). The last term on the right-hand side of equation (6.16) is multiplied due to the overestimation of the wall drag. If the drag coefficient of the film and droplets are simply being added, the entrainment becomes significant and the drag between gas and liquid far exceeds the drag on the gas to film as shown in equation (6.17). Thus, equation (6.16) is obtained with an assumption of $v_v - v_{film} \approx v_v - v_l$. The drag coefficient of film and droplets is calculated with the friction factor, and the interfacial area densities are shown in (6.18) and (6.19) by substituting film or droplets in equation (6.4). For the drag coefficient of the film, the interfacial area is calculated as the same value in the interfacial heat transfer models, which is in equation (4.32). The interfacial friction factor is modeled by the correlation (6.20) of Wallis [103], but in the concurrent downward flow, the modified Asali's correlation [104] is also added because of the overestimation of the Wallis correlation. The original form of the Asali's correlation is equation (6.21), where f_s is the smooth tube friction factor calculated with correlation (5.3) of Churchill and the original form is an implicit formulation due to interfacial shear stress in the non-dimensional film thickness. By the definition of the interfacial shear stress, Asali's correlation is changed as equation (6.23) with coefficients defined in (6.24) and (6.25) and the film thickness is set to the same value in the interfacial heat transfer models as defined in equation (4.31).

$$C_{i,AM} = C_{i,film} + C_{i,drop} \frac{\left(v_v - v_d\right)^2}{\left(v_v - v_l\right)^2} \tag{5.16}$$

$$v_{film} << v_l < v_d \tag{5.17}$$

$$C_{i,film} = f_{i,film} a_{i,film} \frac{\rho_v}{2} \tag{5.18}$$

$$C_{i,drop} = f_{i,drop} a_{i,drop} \frac{\rho_v}{2} \tag{5.19}$$

$$f_{i,film} = 0.005\left(1 + 75\left(1 - \alpha_{film}\right)\right) \tag{5.20}$$

$$\frac{f_{i,film}}{f_s} = 1 + 0.45\,\mathrm{Re}_v^{-0.2}\left(\delta_v^+ - 5.9\right) \tag{5.21}$$

$$\delta_v^+ = \delta \frac{\sqrt{\tau_i / \rho_v}}{\nu_v} \tag{5.22}$$

$$f_{i,film} = \left[\frac{-b + \sqrt{b^2 - 4c}}{2}\right]^2 \tag{5.23}$$

$$b = -\frac{0.45 f_s \delta \left(v_v - v_l\right)}{\sqrt{2}\,\mathrm{Re}_v^{0.2}\,\nu_v} \tag{5.24}$$

$$c = f_s\left(-1 + 5.9\frac{0.45}{\mathrm{Re}_v^{0.2}}\right) \tag{5.25}$$

In the drag coefficient of droplets, the interfacial friction factor is taken from a correlation of Ishii-Chawla [105], which is given by equation (6.26). The Reynolds number of the droplets is defined as equation (6.27) and it uses the droplet velocity, the droplet diameter (4.46) used in the interfacial heat transfer model, and the mixture viscosity. The mixture viscosity is given by equation (6.28), where the void fraction of the droplets is set to equation (4.38) used in the interfacial heat transfer models. The relative velocity of the droplets is obtained from a correlation taken from Ishii [102]. For spherical droplets in the Newton regime, the relative velocity is described with equation (6.29), and equation (6.30) is used for larger distorted drops.

From the two equations (6.29) and (6.30), the relative velocity of droplets has an upper limit of $v_v - v_l$. The interfacial area in the drag coefficient of droplets is evaluated using the Sauter mean diameter as in equation (6.31) where α_{film} is the void fraction of film and $1-\alpha_{film}$ denotes the void fraction in the core. The void fraction of film is calculated from equation (6.32), and it is also used in the interfacial friction factor of film as in equation (6.20).

$$f_{i,drop} = \frac{24}{\mathrm{Re}_{drop}}\left(1+0.1\mathrm{Re}_{drop}{}^{0.75}\right) \tag{5.26}$$

$$\mathrm{Re}_{drop} = \frac{\rho_v \left|v_v - v_d\right| d_{drop}}{\mu_m} \tag{5.27}$$

$$\mu_m = \frac{\mu_v}{\left(1-\alpha_{drop}\right)^{2.5}} \tag{5.28}$$

$$v_v - v_d = 1.718\sqrt{d_{drop}\left(\frac{g\left(\rho_l - \rho_v\right)}{\rho_v}\right)}\left(1-\alpha_{drop}\right)^{1.5} \tag{5.29}$$

$$v_v - v_d = \sqrt{2}\left(\frac{\sigma g\left(\rho_l - \rho_v\right)}{\rho_v{}^2}\right)^{1/4}\left(1-\alpha_{drop}\right)^{1.5} \tag{5.30}$$

$$a_{i,drop} = \frac{3}{2}\frac{\left(1-\alpha_{film}\right)\alpha_{drop}}{d_{drop}} \tag{5.31}$$

$$\alpha_{film} = 1 - \frac{\alpha}{1-\alpha_{drop}} \tag{5.32}$$

6.4 Interfacial Friction Models and Correlations of RELAP5

The method for determining the interfacial friction in RELAP5 differs based on the flow regime and the flow direction. The drift flux method is utilized for the vertical bubbly and the slug flow regimes, and the drag coefficient method is applied for all remaining regimes. To apply the drift flux method in the vertical bubbly and slug flow regimes, equation (6.2) is implemented, which is similar to TRACE. However, in RELAP5, the relative velocity uses an averaged value not a local value as in equation (6.35). The drag coefficient is rearranged as equation (6.37). The drift flux velocity and the distribution parameter are calculated with the drift flux correlation from the literature based on Putney's work [106-110]. Table 8 summarizes which correlations are used for different geometry and flow conditions. A total of 4 drift flux correlations are used and these correlations are described in this chapter. For a large pipe or an intermediate pipe and a low flow rate, the correlation of Kataoka-Ishii or Zuber-Findlay for a bubbly flow regime is applied. The conditions for which correlations to apply depend on the superficial velocity. If the superficial velocity is larger than the value in equation (6.33), Kataoka-Ishii's correlation is utilized and if the superficial velocity is smaller than the value in equation (6.34), the Zuber-Findlay correlation is applied. If the superficial velocity has a value between the two conditions, the drift flux velocity is evaluated by the interpolation of correlations of Kataoka-Ishii and Zuber-Findlay for the bubbly flow regime.

$$j_g > 1.768\left(\frac{\sigma g\left(\rho_l - \rho_v\right)}{\rho_l^2}\right)^{1/4} \tag{5.33}$$

$$j_g < 0.5\left(\frac{\sigma g\left(\rho_l - \rho_v\right)}{\rho_l^2}\right)^{1/4} \tag{5.34}$$

Table 8 Drift Flux Correlation for a Vertical Bubbly Slug Flow Regime

Flow rate	Small pipes $D_h \leq 0.018$	Intermediate pipes $0.018 < D_h \leq 0.08$	Large pipes $0.08 < D_h < 10^6$	Very large pipes $D_h \geq 10^6$
High flow rate $\lvert G \rvert \geq 100$	EPRI	EPRI	Kataoka-Ishii (large j_g) Zuber-Findlay bubbly (small j_g)	EPRI
Medium flow rate $50 < \lvert G \rvert < 100$	Interpolation EPRI and Zuber-Findlay slug	Interpolation EPRI and Kataoka-Ishii or Zuber-Findlay bubbly	Kataoka-Ishii (large j_g) Zuber-Findlay bubbly (small j_g)	Interpolation EPRI and Gardner
Low flow rate or Countercurrent flow rate $\lvert G \rvert \leq 50$	Zuber-Findlay slug	Kataoka-Ishii (large j_g) Zuber-Findlay bubbly (small j_g)	Kataoka-Ishii (large j_g) Zuber-Findlay bubbly (small j_g)	Gardner

The correlation mentioned as EPRI is modeled by Chexal-Lellouche [111], and this correlation was modified to incorporate into RELAP5 [112]. The distribution parameter is evaluated with equation (6.38), where L is the Chexal-Lellouche fluid parameter as defined in equation (6.39). Other variables in the distribution parameter correlation are defined in equations (6.40) – (6.46). The Reynolds number is calculated based on the superficial velocity. The drift flux velocity is evaluated from equation (6.47), which is modified based on Ishii's correlation (6.12) with variables defined in equations (6.48) – (6.57). The parameter C_3 is dependent on the directions of liquid and vapor flows.

$$v_r = C_1 v_v - C_0 v_l \tag{5.35}$$

$$v_r = \frac{\overline{v}_{gj}}{\left(1-\alpha\right)} \tag{5.36}$$

$$C_i = \frac{\alpha\left(1-\alpha\right)^3 g\left(\rho_l - \rho_v\right)}{\overline{v}_{gj}^{\,2}} \tag{5.37}$$

$$C_0 = \frac{L}{K_0 + \left(1 - K_0\right)\alpha^r} \tag{5.38}$$

$$L = \frac{1 - \exp\left(-C_1\alpha\right)}{1 - \exp\left(-C_1\right)} \tag{5.39}$$

$$C_1 = \left|\frac{4P_{crit}{}^2}{P\left(P_{crit} - P\right)}\right| \tag{5.40}$$

$$K_0 = B_1 + \left(1 - B_1\right)\left(\frac{\rho_v}{\rho_l}\right)^{1/4} \tag{5.41}$$

$$B_1 = \min\left(0.8, A_1\right) \tag{5.42}$$

$$A_1 = \frac{1}{1 + \exp\left(-\frac{\mathrm{Re}}{60000}\right)} \tag{5.43}$$

$$\mathrm{Re} = \begin{cases} \mathrm{Re}_v & \mathrm{Re}_v > \mathrm{Re}_l \text{ or } \mathrm{Re}_v < 0 \\ \mathrm{Re}_l & \text{ortherwise} \end{cases} \tag{5.44}$$

$$\mathrm{Re}_p = \frac{\rho_p j_p D_h}{\mu_p} \tag{5.45}$$

$$r = \frac{1 + 1.57\left(\frac{\rho_v}{\rho_l}\right)}{1 - B_1} \tag{5.46}$$

$$\overline{v}_{gj} = 1.41\left(\frac{\sigma g\left(\rho_l - \rho_v\right)}{\rho_l^2}\right)^{1/4} C_2 C_3 C_4 C_9 \tag{5.47}$$

$$C_2 = \begin{cases} 1 & C_5 \geq 1 \\ \frac{1}{1 - \exp\left(-C_6\right)} & C_5 < 1 \end{cases} \tag{5.48}$$

$$C_5 = \left(150\left(\frac{\rho_v}{\rho_l}\right)\right)^{1/2} \tag{5.49}$$

$$C_6 = \frac{C_5}{1 - C_5} \tag{5.50}$$

$$C_4 = \begin{cases} 1 & C_7 \geq 1 \\ \frac{1}{1 - \exp\left(-C_8\right)} & C_7 < 1 \end{cases} \tag{5.51}$$

$$C_7 = \left(\frac{0.09144}{D_h}\right)^{0.6} \tag{5.52}$$

$$C_8 = \frac{C_7}{1 - C_7} \tag{5.53}$$

$$C_9 = \begin{cases} (1-\alpha)B_1 & \mathrm{Re}_v \geq 0 \\ \min\left(0.7, (1-\alpha)^{0.65}\right) & \mathrm{Re}_v < 0 \end{cases} \tag{5.54}$$

$$C_3 = \begin{cases} \max\left[0.5, 2\exp\left(-\frac{|\mathrm{Re}_l|}{60000}\right)\right] & j_l > 0 \text{ and } j_v > 0 \\ 2\left(\frac{C_{10}}{2}\right)^{B_2} & j_l < 0 \text{ and } j_v < 0 \\ 2\left(\frac{C_{10}}{2}\right)^{B_2} & j_l \cdot j_v < 0 \end{cases} \tag{5.55}$$

$$B_2 = \frac{1}{1 + 0.05\left|\frac{\mathrm{Re}_l}{35000}\right|^{0.4}} \tag{5.56}$$

$$C_{10} = 2\exp\left[\left(\frac{|\mathrm{Re}_l|}{350000}\right)^{0.4}\right] - 1.75|\mathrm{Re}_l|^{0.03}\exp\left[\frac{-|\mathrm{Re}_l|}{50000}\left(\frac{0.0381}{D_h}\right)^2\right] + \left(\frac{0.0381}{D_h}\right)^{0.25}|\mathrm{Re}_l|^{0.001} \tag{5.57}$$

The original form of Zuber-Findlay [14, 113] for the slug flow regime is shown in equations (6.58) and (6.59). The distribution parameter C_0 is modified as in (6.60) if the subcooled boiling occurs at the wall. By using the mass transfer defined in equation (4.112), that is, the distribution parameter C_0, the drift flux velocity $\overline{v}_{gj}$ is modified for large void fraction case to impose physical limits as shown in equations (6.61) and (6.62).

$$C_0 = 1.2 \tag{5.58}$$

$$\overline{v}_{gj} = 0.35\left(\frac{g(\rho_l - \rho_v)D_h}{\rho_l}\right)^{1/2} \tag{5.59}$$

$$C_0 = 1.2\left[1 - \exp(-18\alpha)\right] \text{ for } \Gamma_w > 0 \tag{5.60}$$

$$C_0 = \frac{(\alpha - 0.8) + 1.2 \cdot (1-\alpha)}{1 - 0.8} \tag{5.61}$$

$$\overline{v}_{gj} = \frac{1-\alpha}{1-0.8} \cdot 0.35\left(\frac{g(\rho_l - \rho_v)D_h}{\rho_l}\right)^{1/2} \tag{5.62}$$

In the case of using the correlation of Kataoka-Ishii or Zuber-Findlay for the bubbly flow regime, the distribution parameter is evaluated by the modified Rouhani correlation [84, 114] shown in equation (6.63), where v_{Tb} is the velocity of Taylor bubbles as in (6.66) and is evaluated using the drift flux velocity of Zuber-Findlay (6.59). Similar to using the correlation of Zuber-Findlay, the distribution parameter is modified using the mass transfer as defined in equation (4.112) and it is shown in equation (6.68) if the subcooled boiling occurs at the wall. The drift flux velocity calculated from the correlation of Kataoka-Ishii [68] is derived in equation (6.69) in a way similar to that in TRACE, but the conditions for the size of the diameter are added. D_h^* is the Bond number given by equation (6.71) and N_μ is the viscosity number defined as in equation (6.72). The drift flux velocity is determined by the correlation of Zuber-Findlay [14, 113] for the bubbly flow regime, and it is shown in equation (6.73). To impose physical limits at a high void fraction, equations (6.61)and (6.62) are implemented. The correlation of Gardner [115] is applied for a large pipe and it is described in equations (6.74) – (6.76).

$$C_0 = C_\infty - \left(C_\infty - 1\right)\left(\frac{\rho_v}{\rho_l}\right)^{0.5} \tag{5.63}$$

$$C_\infty = \min\left[1.2,\ 1.393 - 0.0155\log\left(\mathrm{Re}_l\right)\right] \tag{5.64}$$

$$C_\infty = 1 + v_{Tb}\left(C_\infty - 1\right) \quad \text{for } v_{Tb} < 1 \tag{5.65}$$

$$v_{Tb} = \frac{\rho_l\left|j_l\right| + \rho_v\left|j_v\right|}{\left(\left(1-\alpha\right)\rho_l + \alpha\rho_v\right)\overline{v}_{jg}} \tag{5.66}$$

$$C_\infty = C_\infty - \left(C_\infty - 1\right)\exp\left(-1000\alpha\right) \quad \text{for } \alpha < 0.016 \tag{5.67}$$

$$C_0 = C_0\left[1 - \exp\left(-18\alpha\right)\right] \quad \text{for } \Gamma_w > 0 \tag{5.68}$$

$$\overline{v}_{gj} = \overline{v}_{gj}^{\ +}\left(\frac{\sigma g\left(\rho_l - \rho_v\right)}{\rho_l^2}\right)^{1/4} \tag{5.69}$$

$$\overline{v}_{gj}^{\ +} = \begin{cases} 0.0019\left(D_h^*\right)^{0.809}\left(\dfrac{\rho_l}{\rho_v}\right)^{0.157}\mathrm{N}_\mu^{-0.562} & D_h^* \le 30 \\ 0.03\left(\dfrac{\rho_l}{\rho_v}\right)^{0.157}\mathrm{N}_\mu^{-0.562} & D_h^* > 30 \end{cases} \tag{5.70}$$

$$D_h^* = \frac{D_h}{\sqrt{\sigma/g\left(\rho_l - \rho_v\right)}} \tag{5.71}$$

$$\mathrm{N}_\mu = \frac{\mu_l}{\left(\rho_l\sigma\sqrt{\sigma/g\left(\rho_l - \rho_v\right)}\right)^{0.5}} \tag{5.72}$$

$$\overline{v}_{gj} = 1.41\left(\frac{\sigma g\left(\rho_l - \rho_v\right)}{\rho_l^2}\right)^{1/4} \tag{5.73}$$

$$C_0 = 1 \tag{5.74}$$

$$\overline{v}_{gj} = \overline{v}_{gj}^{\ +}\left(\frac{\sigma g\left(\rho_l - \rho_v\right)}{\rho_l^2}\right)^{1/4} \tag{5.75}$$

$$\overline{v}_{gi}^{+} = \left(\left(2.3409 - 0.2035\alpha_g \left[\frac{\rho_l^2 \sigma^{1.5}}{\rho_g^2 \mu_l^2 \sqrt{(\rho_l - \rho_g) g}} \right]^{3.2} \right) e^{-400\alpha^2} + 0.2035 \frac{\alpha}{(1-\alpha)^{1.5}} \left[\frac{\rho_l^2 \sigma^{1.5}}{\rho_g^2 \mu_l^2 \sqrt{(\rho_l - \rho_g) g}} \right]^{3.2} \right)^{0.5} \tag{5.76}$$

In horizontal bubbly and slug flow regimes, the drag coefficient method is used instead of the drift flux method. As shown in equation (6.4), the drag coefficient consists of the fluid density, interfacial area, and friction factor, but in RELAP5 an additional factor of 1/4 is included as shown in equation (6.77). It comes from the conversion of the projected area of spherical particles (i.e., πr^2) into the interfacial area (i.e., $4\pi r^2$). To evaluate the interfacial area, the dispersed bubbles or droplets can be assumed to be spherical particles with a size distribution of the Nukiyama-Tanasawa form according to Wallis [91] and Shapiro [116], and thus the interfacial area is obtained from equation (6.78). The Sauter mean diameter is obtained as in equation (6.80) by assuming that $d_{avg} = (1/3) d_{\max}$ and the definition of the Weber number is (6.79). The interfacial friction factor is evaluated by the correlation of Ishii-Chawla [105] used in TRACE for droplets in the annular flow regime.

$$C_i = f_i \frac{a_i}{4} \frac{\rho}{2} \tag{5.77}$$

$$a_i = \frac{3.6\alpha}{d_{avg}} \tag{5.78}$$

$$\mathrm{We} = \frac{d_{\max} \rho (v_v - v_l)^2}{\sigma} \tag{5.79}$$

$$d_{avg} = \frac{1}{3} d_{\max} = \frac{1}{3} \frac{\mathrm{We}\sigma}{\rho (v_v - v_l)^2} \tag{5.80}$$

$$f_i = \frac{24\left(1 + 0.1\mathrm{Re}^{0.75}\right)}{\mathrm{Re}} \tag{5.81}$$

In the bubbly flow regime, bubbles are assumed as spherical particles, so the correlations of Nukiyama-Tanasawa and Ishii-Chawla are utilized to evaluate the interfacial area and the friction factor with equations (6.78) and (6.81). The Weber number for the bubbly flow regime is set to 15 and the Reynolds number is calculated using the Weber number as shown in equation (6.84). The relative velocity has a lower limit as shown in equation (6.83), where diameter D' is set to 5 mm.

$$d_{avg} == \frac{1}{3} \frac{\mathrm{We}\sigma}{\rho_l \hat{v}_{fg}^{\,2}} \tag{5.82}$$

$$\hat{v}_{fg}^{\,2} = \max\left[(v_v - v_l)^2, \frac{\mathrm{We}\sigma}{\rho_l \min\left(D'\alpha^{1/3}, D_h\right)} \right] \tag{5.83}$$

$$\mathrm{Re} = \frac{1}{3} \frac{\mathrm{We}\sigma(1-\alpha)}{\mu_l \sqrt{\hat{v}_{fg}^{\,2}}} \tag{5.84}$$

In the slug flow regime, the interfacial friction is divided into friction from bubble droplets and Taylor bubbles, and this can be observed from equation (6.85). The interfacial friction by bubbles is calculated using the same correlations as the bubbly flow regime except that different void fractions and relative velocities are used for a smooth transition between bubbly and slug flow regimes. The void fraction of the bubble droplets can be obtained from an exponential function, and the diameter of the droplets is equal to the formula for the bubbly flow regime, but the relative velocity is modified by having an additional exponential function. The Reynolds number is evaluated with the modified relative velocity. For Taylor bubbles, the interfacial area is set to the ratio of the area to the volume derived in equation (6.92) with the definition of interfacial area. The interfacial friction factor is given by Ishii-Chawla [105] as shown in equation (6.93), where α_{Taylor} is defined as equation (6.94) and D' is the Taylor bubble diameter.

$$C_i = f_{i,drop} \frac{a_{i,drop}}{4} \frac{\rho}{2} + f_{i,Taylor} \frac{a_{i,Taylor}}{4} \frac{\rho}{2} \tag{5.85}$$

$$a_{i,drop} = \frac{3.6\alpha_{drop}}{d_{drop}} \left(1 - \alpha_{Taylor}\right) \tag{5.86}$$

$$\alpha_{drop} = \alpha_{BS} \exp\left[-8\left(\frac{\alpha - \alpha_{BS}}{\alpha_{SA} - \alpha_{BS}}\right)\right] \tag{5.87}$$

$$d_{drop} == \frac{1}{3} \frac{\mathrm{We}\sigma}{\rho_l \hat{v}_{fg}^{\ 2}} \tag{5.88}$$

$$\hat{v}_{fg}^{\ 2} = \max\left[\left(v_v - v_l\right)^2 \left(\exp\left[-8\left(\frac{\alpha - \alpha_{BS}}{\alpha_{SA} - \alpha_{BS}}\right)\right]\right)^4, \frac{\mathrm{We}\sigma}{\rho_l \min\left(D'\alpha^{1/3}, D_h\right)}\right] \tag{5.89}$$

$$f_{i,drop} = \frac{24\left(1 + 0.1\mathrm{Re}_{drop}^{\ 0.75}\right)}{\mathrm{Re}_{drop}} \tag{5.90}$$

$$\mathrm{Re}_{drop} = \frac{1}{3} \frac{\mathrm{We}\sigma\left(1 - \alpha_{drop}\right)}{\mu_l \sqrt{\hat{v}_{fg}^{\ 2}}} \tag{5.91}$$

$$a_{i,Taylor} = \frac{4\sqrt{\alpha_{Taylor}}}{dl} \alpha_{Taylor} \tag{5.92}$$

$$f_{i,Taylor} = 10.9 \frac{D'}{D_h} \left(1 - \alpha_{Taylor}\right)^3 \tag{5.93}$$

$$\alpha_{Taylor} = \frac{\alpha - \alpha_{drop}}{1 - \alpha_{drop}} \tag{5.94}$$

In the annular flow regime, sum of the liquid film and the entrained liquid droplets in the vapor core are considered as shown in equation (6.95). For the entrained liquid droplets, the same formulas for the bubbly flow regime are applied. The interfacial area is calculated from equation (6.96) with the defined void fraction for the droplets in equation (6.97). Here, the void fraction of the liquid film and the relative velocity are the same as in the interfacial heat transfer models shown in equations (4.88) and (4.102), respectively. The Weber number for the liquid droplets is set to 4.5 and the Reynolds number is calculated by equation (6.100). For the liquid film, the interfacial area is determined by equation (6.101) and the friction factor is based on Wallis' correlation [117] in the turbulent flow region and the factor is replaced with 0.02 rather than 0.005 [118].

$$C_i = f_{i,ann}\frac{a_{i,ann}}{4}\frac{\rho}{2} + f_{i,drop}\frac{a_{i,drop}}{4}\frac{\rho}{2} \tag{5.95}$$

$$a_{i,drop} = \frac{3.6\alpha_{l,drop}}{d_{drop}}\left(1-\alpha_{l,film}\right) \tag{5.96}$$

$$\alpha_{l,drop} = \max\left[\frac{\left(1-\alpha\right)-\alpha_{l,film}}{1-\alpha_{l,film}}, \alpha_{AM}\right] \tag{5.97}$$

$$d_{drop} == \frac{1}{3}\frac{\mathrm{We}\sigma}{\rho_v \hat{v}_{fg}^{\ 2}} \tag{5.98}$$

$$f_{i,drop} = \frac{24\left(1+0.1\mathrm{Re}_{drop}^{\ 0.75}\right)}{\mathrm{Re}_{drop}} \tag{5.99}$$

$$\mathrm{Re}_{drop} = \frac{1}{3}\frac{\mathrm{We}\sigma\alpha_{l,drop}^{\ 3}}{\mu_g\sqrt{\alpha_{l,drop}\hat{v}_{fg}^{\ 2}}} \tag{5.100}$$

$$a_{i,ann} = 6.1192775\frac{\sqrt{\alpha_{l,film}^{\ 0.25}}\sqrt{\left(1-\alpha_{l,film}\right)}}{D_h} \tag{5.101}$$

$$f_{i,ann} = \begin{cases} 64/\mathrm{Re}_v & \mathrm{Re}_v \le 500 \\ \left(\frac{1500-\mathrm{Re}_v}{1000}\right)64/\mathrm{Re}_v + \left(\frac{\mathrm{Re}_v-500}{1000}\right)0.02\left\{1+150\left[1-\left(1-\alpha\right)^{0.5}\right]\right\} & 500 < \mathrm{Re}_v < 1500 \\ 0.02\left\{1+150\left[1-\left(1-\alpha\right)^{0.5}\right]\right\} & \mathrm{Re}_v \ge 1500 \end{cases} \tag{5.102}$$

$$\mathrm{Re}_v = \frac{\rho_v\left(v_v - v_l\right)\sqrt{1-\alpha}D_h}{\mu_v} \tag{5.103}$$

In the pre-CHF mist flow regime, correlations of the dispersed droplets in the annular flow regime are used. However, in this regime, the liquid fraction of droplets and the modified relative velocity is replaced with the total liquid fraction in a cell and the relative velocity is modified as in equations (6.104) and (6.105).

$$\alpha_{l,drop} = 1-\alpha \tag{5.104}$$

$$\hat{v}_{fg}^{\ 2} = \max\left[\left(v_v - v_l\right)^2, \frac{\mathrm{We}\sigma}{\rho_v \min\left(D'\left(1-\alpha\right)^{1/3}, D_h\right)}\right] \tag{5.105}$$

6.5 Comparison Results

Figure 47 and Figure 48 show the interfacial friction values calculated from TRACE and RELAP5. For the assessment of the interfacial friction model of RELAP5 and TRACE, it should be evaluated for horizontal and vertical orientations of flow. In the horizontal flow, R-square values of bubbly, slug and annular flow regimes are -101.3, -978.4, and -2957.1, respectively.

This indicates that the two codes have substantially different interfacial friction values in all of the flow regimes. In the vertical flow, R-square values of bubbly, slug and annular flow regimes are -0.2558, -827.3, -3515.4, respectively. This also means that the two codes have a large discrepancy in the interfacial friction values in all of the flow regimes.

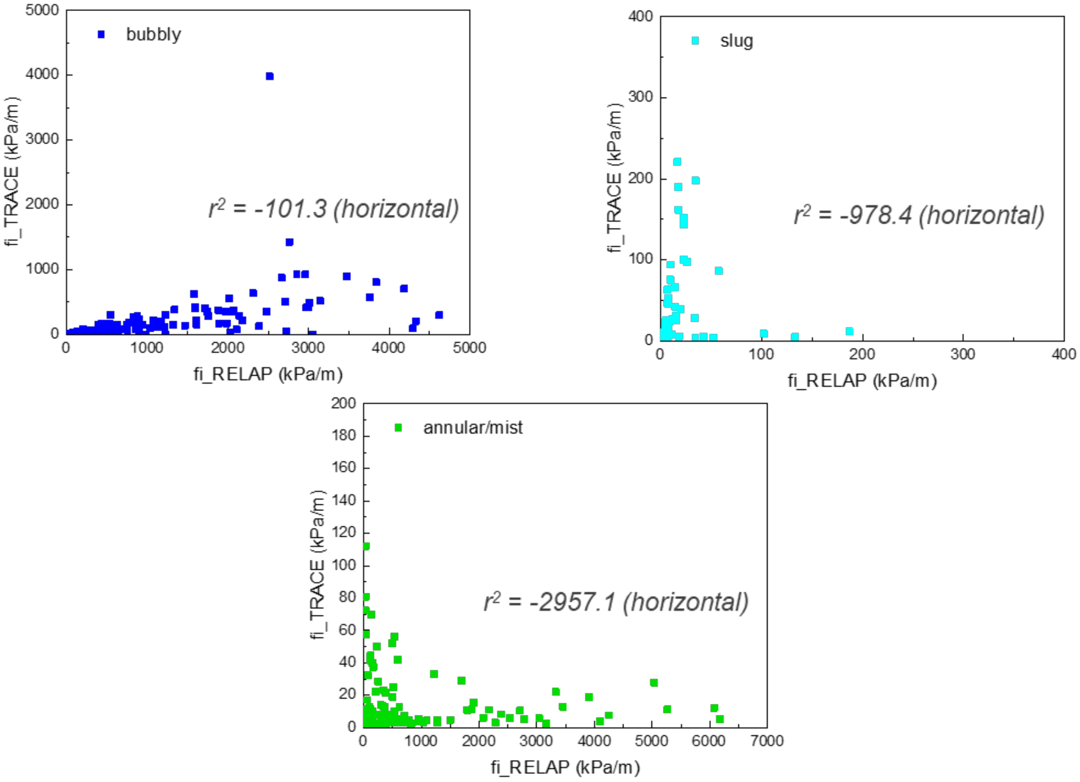

Figure 47 Calculated Interfacial Friction of TRACE and RELAP5 in a Horizontal Flow

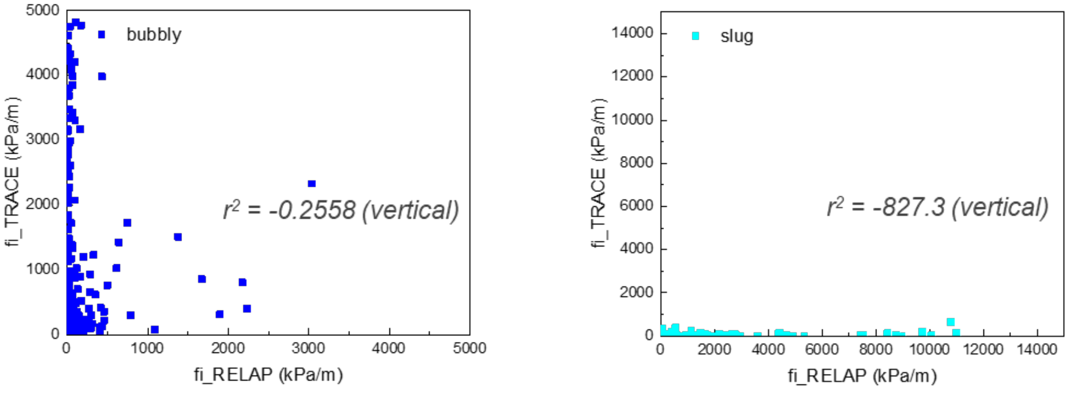

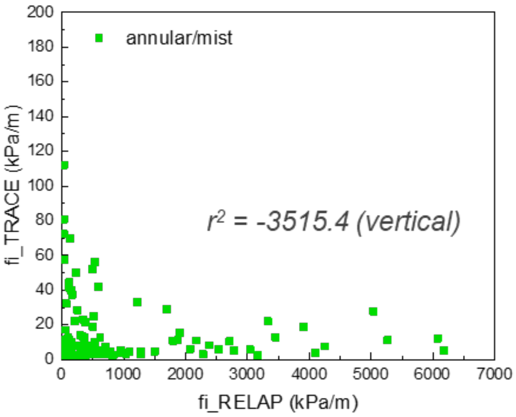

Figure 48 Calculated Interfacial Friction of TRACE and RELAP5 in a Vertical Flow

The regime in which the two codes show the largest deviation of interfacial friction values is the annular flow regime because the two codes calculate the interfacial area in different ways as shown in Figure 48. Figure 49 shows that RELAP5 overestimates the interfacial area over that of TRACE, which leads to a larger interfacial friction in RELAP5 than in TRACE.

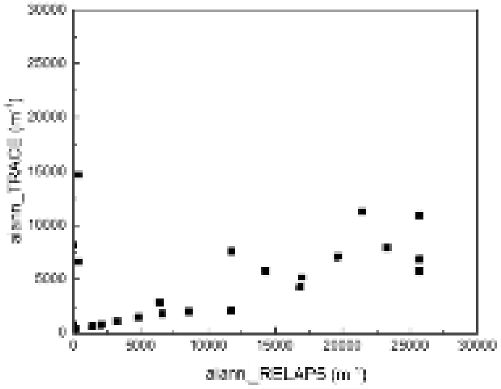

Figure 49 Interfacial Area of TRACE and RELAP5 in an Annular Flow Regime

7 SUMMARY AND CONCLUSIONS

System thermal hydraulic analysis codes such as TRACE or RELAP5 are often used for nuclear power plant simulation to evaluate the safety of the plants. In a system thermal hydraulic analysis code, fluid field equations are used to model two phase flow. System codes typically solve mass, momentum and energy equations for multiple phases. To solve field equations, constitutive relations are needed and these correlations are often dependent on the flow regime map. The major constitutive relation models in the codes are the wall heat transfer, wall and interfacial friction, interfacial heat and mass transfer. TRACE and RELAP5 are very different in the implemented thermal hydraulics models and correlations even though the field equations are almost identical. This report summarized the differences in the obtained results from the two codes by first examining the models and correlations for modeling two phase flow. To compare different constitutive models of each code, the constitutive relation modules were extracted and constructed in a separate computational environment. The platforms contained various constitutive relations: wall heat transfer, interfacial heat transfer, wall friction, and interfacial friction of TRACE and RELAP5. This was followed with the suggestion of a new evaluation method for comparing constitutive relation models. Qualitative and quantitative comparisons of the constitutive relation models of the TRACE and RELAP5 codes were conducted with computational platforms.

The comparison results of the constitutive relation models of the two codes led to the following conclusions.

- In the wall heat transfer models, different HT regimes are often selected and show substantial deviations. This is because the HT regime selection logics of TRACE and RELAP5 are different. TRACE includes models for determining the temperature of the ONB and MFB, but RELAP5 does not have this logic. In RELPA5, the temperature of ONB is set as a value of $T_{sat} – 0.001$ and heat fluxes calculated from transition and film boiling HT regimes are used as the MFB condition. Whether the two codes select the same HT regime or select another HT regime, the difference in heat fluxes calculated from the two codes is the largest when TRACE selects the transition boiling HT regime.
- In the interfacial heat transfer, RELAP5 includes a void generation term for evaluating the liquid interfacial heat transfer, but TRACE does not consider this term. This caused the major differences between the two codes. In vapor interfacial heat transfer, the order of the heat transfer calculated between the two codes was found to be significantly different in the bubbly flow regime, which is up to 1600 times for the vapor heat transfer coefficient and 40 times for the interfacial area.
- In the wall friction models, there was a fairly good agreement in all flow regimes, but when the void fraction was from 0.8 to 0.9, where TRACE selects the transition flow regime, wall friction values from two codes differ.
- In the interfacial friction models, the calculated friction values are very inconsistent in all flow regimes and the largest difference is observed in the annular flow regime due to the difference in the calculated interfacial area of the two codes.

8 REFERENCES

[1] D. Bestion, "System Code Models and Capabilities," 2008.

[2] F. Reventos, M. Perez, L. Batet, A. Guba, I. Tóth, and T. Mieusset, "BEMUSE Phase V Report Uncertainty and Sensitivity analysis of a LB-LOCA in ZION nuclear power plant," in NEA/CSNI/R (2009) 13, 2009.

[3] A. De Crecy, P. Bazin, H. Glaeser, T. Skorek, J. Joucla, and P. Probst, "BEMUSE Phase III Report Uncertainty and Sensitivity Analysis of the LOFT L2–5 Test," in NEA/CSNI/R (2007) 4, 2007.

[4] F. D'Auria, M. J. N. E. Lanfredini, and Design, "V&V&C in Nuclear Reactor Thermal-hydraulics," p. 110162, 2019.

[5] F. D’Auria and M. Lanfredini, "Moving From V&V to V&V&C in Nuclear Thermal-hydraulics," in 2018 26th International Conference on Nuclear Engineering, 2018: American Society of Mechanical Engineers Digital Collection.

[6] J. M. Kelly and W. Wang, "Two-Phase Wall Friction Model for the TRACE Computer Code," in Proc. of 13th Int. Conf. on Nucl. Eng., ICONE13, 2005.

[7] S. W. Bae, H. K. Cho, Y. J. Lee, H. C. Kim, Y. J. Jung, and K. Kim, "A Summary of Interfacial Heat Transfer Models and Correlations," 2007.

[8] G. A. Roth and F. Aydogan, "Theory and Implementation of Nuclear Safety System Codes – Part II: System Code Closure Relations, Validation, and Limitations," Progress in Nuclear Energy, vol. 76, pp. 55-72, 2014.

[9] U. NRC, "TRACE V5. 0 Assessment Manual – Main Report(Draft)," US Nuclear Regulatory Commission, 2005.

[10] V. Ransom, R. Wagner, and G. Johnsen, "RELAP5/MOD2 Code Manual, Volume 3: Developmental Assessment Problems," EGG-TFM-7952, 1987.

[11] M. KAERI IV, "Code Manual Volume IV: Developmental Assessment Report," KAERI/TR-30422009.

[12] V. H. Ransom, J. Trapp, and R. Wagner, "RELAP5/MOD3. 3 Code Manual Volume IV: Models and Correlations," Information Systems Laboratories, IR, Maryland Idaho Falls, Idaho (Ed.), 2001.

[13] "TRACE V5. 0 Theory Manual – Field Equations, Solution Methods and Physical Models," United States Nucl. Regul. Comm, ML120060218, 2008.

[14] N. Zuber and J. Findlay, "Average Volumetric Concentration in Two-phase Flow Systems," Journal of heat transfer, vol. 87, no. 4, pp. 453-468, 1965.

[15] C. E. Brennen, Cavitation and Bubble Dynamics. Cambridge University Press, 2013.

[16] M. D. McKay, R. J. Beckman, and W. J. Conover, "Comparison of Three Methods for Selecting Values of Input Variables in the Analysis of Output from a Computer Code," Technometrics, vol. 21, no. 2, pp. 239-245, 1979.

[17] N. E. Todreas and M. S. Kazimi, Nuclear Systems Volume I: Thermal Hydraulic Fundamentals. CRC Press, 2011.

[18] F. Dittus and L. Boelter, "Heat Transfer in Automobile Radiators of the Tubular Type," International Communications in Heat and Mass Transfer, vol. 12, no. 1, pp. 3-22, 1985.

[19] H. Hu, C. Xu, Y. Zhao, K. J. Ziegler, and J. Chung, "Boiling and Quenching Heat Transfer Advancement by Nanoscale Surface Modification," Scientific Reports, vol. 7, no. 1, p. 6117, 2017.

[20] N. Basu, G. R. Warrier, and V. K. Dhir, "Onset of Nucleate Boiling and Active Nucleation Site Density during Subcooled Flow Boiling," Journal of Heat Transfer, vol. 124, no. 4, pp. 717-728, 2002.

[21] J. Stewart and D. Groeneveld, "Low-quality and Subcooled Film Boiling of Water at Elevated Pressures," Nuclear Engineering and Design, vol. 67, no. 2, pp. 259-272, 1982.

[22] N. Lee, PWR FLECHT SEASET Unblocked Bundle, Forced and Gravity Reflood Task Data Evaluation and Analysis Report (no. 10). The Commission, 1982.

[23] T. Anklam, "ORNL Small-break LOCA Heat Transfer Test Series I: High-Pressure Reflood Analysis," Oak Ridge National Lab., TN (USA)1981.

[24] C. Hyman, T. Anklam, and M. White, "Experimental Investigations of Bundle Boiloff and Reflood under High-pressure Low Heat Flux Conditions," Oak Ridge National Lab.1982.

[25] D. Groeneveld, S. Cheng, and T. Doan, "1986 AECL-UO Critical Heat Flux Lookup Table," Heat Transfer Engineering, vol. 7, no. 1-2, pp. 46-62, 1986.

[26] J. R. Sellars, M. Tribus, and J. Klein, "Heat Transfer to Laminar Flow in a Round Tube or Flat Conduit: the Graetz Probem Extended," 1954.

[27] V. Gnielinski, "New Equations for Heat and Mass Transfer in Turbulent Pipe and Channel Flow," Int. Chem. Eng., vol. 16, no. 2, pp. 359-368, 1976.

[28] G. Filonenko, "Hydraulic Resistance in Pipes," Teploenergetika, vol. 1, pp. 40-44, 1954.

[29] W. Hufschmidt and E. Burck, "The Effect of Temperature-dependent Properties of Materials on Heat Transfer in the Turbulent Flow of Liquids in Tubes at High Heat Fluxes and Prandtl Numbers," Int. J. Heat Mass Transfer, vol. 11, pp. 1041-1968, 1968.

[30] J. C. Chen, "Correlation for Boiling Heat Transfer to Saturated Fluids in Convective Flow," Industrial & Engineering Chemistry Process Design and Development, vol. 5, no. 3, pp. 322-329, 1966.

[31] W. Rohsenow, "Heat Transfer, a Symposium," Engineering Research Institute, University of Michigan, Ann Arbor, Michigan, vol. 16, p. I7, 1952.

[32] W. Gambill, "Generalized Prediction of Burnout Heat Flux for Flowing, Subcooled, Wetting Liquids," in Chem. Eng. Prog., Symp. Ser, 1963, vol. 59, no. 41, pp. 71-87.

[33] K. Rezkallah and G. Sims, "An Examination of Correlations of Mean Heat-transfer Coefficients in Two-phase Two-component Flow in Vertical Tubes," in Heat transfer: Pittsburgh 1987, 1987.

[34] D. Gorenflo, E. Baumhögger, G. Herres, and S. Kotthoff, "Prediction Methods for Pool Boiling Heat Transfer: A State-of-The-Art Review," International Journal of Refrigeration, vol. 43, pp. 203-226, 2014.

[35] H. C. Hottel and W. McAdams, "Heat Transmissin," ed: McGraw-Hill, New York, 1954.

[36] W. H. McAdams, W. Kennel, C. Minden, R. Carl, P. Picornell, and J. Dew, "Heat Transfer at High Rates to Water With Surface Boiling," Industrial & Engineering Chemistry, vol. 41, no. 9, pp. 1945-1953, 1949.

[37] S. Levy, "Generalized Correlation of Boiling Heat Transfer," Journal of Heat Transfer, vol. 810, pp. 37-42, 1959.

[38] J. Holman, "Heat transfer, 1986," Mc Gran–Hill Book Company, Soythern Methodist University, 1986.

[39] T. A. Bjornard and P. Griffith, "PWR Blowdown Heat Transfer," in Thermal and Hydraulic Aspects of Nuclear Reactor Safety. Vol. I, 1977.

[40] K.-K. Fung, "Subcooled and Low Quality Film Boiling of Water in Vertical Flow at Atmospheric Pressure," Argonne National Lab.1981.

[41] D. Swinnerton, M. Hood, and K. Pearson, "Steady State Post-dryout Experiments at Low Quality and Medium Pressure," UKAEA Atomic Energy Establishment 1988.

[42] F. d. Cachard, "Development, Implementation and Assessment of Specific Closure Laws for Inverted-annular Film-boiling in a Two-fluid Model," Paul Scherrer Inst.(PSI)1994.

[43] N. Hammouda, D. Groeneveld, and S. Cheng, "Two-fluid Modelling of Inverted Annular Film Boiling," International Journal of Heat and Mass Transfer, vol. 40, no. 11, pp. 2655-2670, 1997.

[44] J. P. Hartnett and W. M. Rohsenow, "Handbook of Heat Transfer," Handbook of Heat Transfer, by Hartnett, JP; Rohsenow, Warren M. New York, McGraw-Hill [c1973], 1973.

[45] C. A. Sleicher and M. Rouse, "A Convenient Correlation for Heat Transfer to Constant and Variable Property Fluids in Turbulent Pipe Flow," International Journal of Heat and Mass Transfer, vol. 18, no. 5, pp. 677-683, 1975.

[46] A. Mills, "Experimental Investigation of Turbulent Heat Transfer in the Entrance Region of a Circular Conduit," Journal of Mechanical Engineering Science, vol. 4, no. 1, pp. 63-77, 1962.

[47] K. Sun, J. Gonzalez-Santalo, and C. Tien, "Calculations of Combined Radiation and Convection Heat Transfer in Rod Bundles under Emergency Cooling Conditions," Journal of Heat Transfer, vol. 98, no. 3, pp. 414-420, 1976.

[48] S. W. Churchill and H. H. Chu, "Correlating Equations for Laminar and Turbulent Free Convection from a Vertical Plate," International Journal of Heat and Mass Transfer, vol. 18, no. 11, pp. 1323-1329, 1975.

[49] H. Forster and N. Zuber, "Dynamics of Vapor Bubbles and Boiling Heat Transfer," AIChE Journal, vol. 1, no. 4, pp. 531-535, 1955.

[50] J. G. Collier and J. R. Thome, Convective Boiling and Condensation. Clarendon Press, 1994.

[51] J. C. Chen, R. Sundaram, and F. Ozkaynak, "A Phenomenological Correlation for Post-CHF Heat Transfer," Lehigh Univ., Bethlehem, Pa.(USA). Dept. of Mechanical Engineering and Mechanics1977.

[52] L. A. Bromley, "Heat Transfer in Stable Film Boiling," 1949.

[53] P. J. Berenson, "Film-boiling Heat Transfer from a Horizontal Surface," Journal of Heat Transfer, vol. 83, no. 3, pp. 351-356, 1961.

[54] B. P. Breen, "Effect of Diameter of Horizontal Tubes of Film Boiling," University of Illinois at Urbana-Champaign, 1961.

[55] Y. Sudo and Y. Murao, "Film Boiling Heat Transfer during Reflood Process," Japan Atomic Energy Research Inst.1976.

[56] B. J. Yun, B. U. Bae, W. M. Park, D. J. Euh, C. H. Song, and G. C. Park, "Experimental Investigation of Local Bubble Parameters of Subcooled Boiling Flow in an Annulus."

[57] A. Bennett, G. Hewitt, H. Kearsey, and R. Keeys, "Heat Transfer to Steam-Water Mixtures Flowing in Uniformly Heated Tubes in which the Critical Heat Flux Has Been Exceeded," Atomic Energy Research Establishment, Harwell, Eng.1968.

[58] 이상용, 김병주, and 김무환, "이상유동열전달," 대 영 사, 1993.

[59] W. Choe, L. Weinberg, and J. Weisman, "Observation and Correlation of Flow Pattern Transitions in Horizontal, Cocurrent Gas-Liquid Flow," in Two Phase Transport and Reactor Safety: Hemisphere Washington, 1978, pp. 1357-1375.

[60] Y. Taitel, D. Bornea, and A. Dukler, "Modelling Flow Pattern Transitions for Steady Upward Gas-Liquid Flow in Vertical Tubes," AIChE Journal, vol. 26, no. 3, pp. 345-354, 1980.

[61] D. Barnea, "Transition from Annular Flow and from Dispersed Bubble Flow—Unified Models for the Whole Range of Pipe Inclinations," International Journal of Multiphase Flow, vol. 12, no. 5, pp. 733-744, 1986.

[62] M. Kaichiro and M. Ishii, "Flow Regime Transition Criteria for Upward Two-phase Flow in Vertical Tubes," International Journal of Heat and Mass Transfer, vol. 27, no. 5, pp. 723-737, 1984.

[63] W. Ranz and W. R. Marshall, "Evaporation from Drops," Chem. Eng. Prog, vol. 48, no. 3, pp. 141-146, 1952.

[64] G. R. Warrier, N. Basu, and V. Dhir, Subcooled Boiling at Low Pressures: Annual Progress Report for USNRC Task Order. UCLA School of Engineering and Applied Science, 1999.

[65] G. B. Wallis, "The Terminal Speed of Single Drops or Bubbles in an Infinite Medium," International Journal of Multiphase Flow, vol. 1, no. 4, pp. 491-511, 1974.

[66] J. Richardson and W. Zaki, "Sedimentation and Fluidisation: Part I," Chemical Engineering Research and Design, vol. 75, pp. S82-S100, 1997.

[67] M. Ishii and K. Mishima, "Study of Two-fluid Model and Interfacial Area," Argonne National Lab., IL (USA)1980.

[68] K. Isao and I. Mamoru, "Drift Flux Model for Large Diameter Pipe and New Correlation for Pool Void Fraction," International Journal of Heat and Mass Transfer, vol. 30, no. 9, pp. 1927-1939, 1987.

[69] R. T. Lahey and F. Moody, "The Thermal Hydraulics of a Boiling Water Nuclear Reactor (Monograph Series on Nuclear Science and Technology)," 1977.

[70] S. Kuhn, V. Schrock, and P. Peterson, "Final Report on UC Berkeley Single Tube Condensation Studies," Dept. of Nuclear Eng., UCB-NE-4201, 1994.

[71] M. Ishii and K. Mishima, "Droplet Entrainment Correlation in Annular Two-phase Flow," International Journal of Heat and Mass Transfer, vol. 32, no. 10, pp. 1835-1846, 1989.

[72] I. Paleev and B. Filippovich, "Phenomena of Liquid Transfer in Two-phase Dispersed Annular Flow," International Journal of Heat and Mass Transfer, vol. 9, no. 10, pp. 1089-1093, 1966.

[73] I. Kataoka, M. Ishii, and K. Mishima, "Generation and Size Distribution of Droplet in Annular Two-Phase Flow," Journal of Fluids Engineering, vol. 105, no. 2, pp. 230-238, 1983.

[74] R. Kronig and J. Brink, "On the Theory of Extraction from Falling Droplets," Applied Scientific Research, vol. 2, no. 1, p. 142, 1951.

[75] G. Ryskin, "Heat or Mass Transfer from a Moving Drop—Some Approximate Relations for the Nusselt Number," International Communications in Heat and Mass Transfer, vol. 14, no. 6, pp. 741-749, 1987.

[76] S. Agrawal, G. Gregory, and G. Govier, "An Analysis of Horizontal Stratified Two Phase Flow in Pipes," The Canadian Journal of Chemical Engineering, vol. 51, no. 3, pp. 280-286, 1973.

[77] G. Brucker and E. Sparrow, "Direct Contact Condensation of Steam Bubbles in Water at High Pressure," International Journal of Heat and Mass Transfer, vol. 20, no. 4, pp. 371-381, 1977.

[78] H. Ünal, "Maximum Bubble Diameter, Maximum Bubble-growth Time and Bubble-growth Rate during the Subcooled Nucleate Flow Boiling of Water up to 17.7 MN/m2," International Journal of Heat and Mass Transfer, vol. 19, no. 6, pp. 643-649, 1976.

[79] R. Lahey, "A Mechanistic Subcooled Boiling Model," in Proceedings of the 6th International Heat Transfer Conference, 1978, vol. 1, pp. 293-297.

[80] T. Theofanous, "Modeling of Basic Condensation Processes," in The Water Reactor Safety Research Workshop on Condensation, 1979, pp. 24-25.

[81] M. Plesset and S. A. Zwick, "The Growth of Vapor Bubbles in Superheated Liquids," Journal of Applied Physics, vol. 25, no. 4, pp. 493-500, 1954.

[82] K. Lee and D. Ryley, "The Evaporation of Water Droplets in Superheated Steam," Journal of Heat Transfer, vol. 90, no. 4, pp. 445-451, 1968.

[83] M. Thurgood, "COBRA/TRAC-A Thermal-hydraulic Code for Transient Analysis of Nuclear Reactor Vessels and Primary Coolant Systems," Pacific Northwest Lab., Rept, pp. NUREG/CR-3046, 1983.

[84] W. L. Weaver, R. W. Shumway, G. L. Singer, and S. Z. Rouhani, "TRAC-BF1 Manual: Extensions to TRAC-BD1/MOD1," NUREG/CR^ t391, EGG-2417, August, 1986.

[85] G. Brown, "Heat Transmission by Condensation of Steam on a Spray of Water Drops," University of London (Imperial College of Science and Technology), 1948.

[86] M. Podowski, "Toward Next Generation Multiphase Models of Nuclear Thermal-hydraulics," in Eighth International Topical Meeting on Nuclear Reactor Thermal-hydraulics, 1997.

[87] P. Saha and N. Zuber, "Point of Net Vapor Generation and Vapor Void Fraction in Subcooled Boiling," in Heat Transfer, 1974. Vol. 4, 1974.

[88] R. Lockhart and R. Martinelli, "Proposed Correlation of Data for Isothermal Two-phase, Two-component Flow in Pipes," Chem. Eng. Prog, vol. 45, no. 1, pp. 39-48, 1949.

[89] M. Davis, "Wall Friction for Two-phase Bubbly Flow in Rough and Smooth Tubes," International Journal of Multiphase Flow, vol. 16, no. 5, pp. 921-927, 1990.

[90] S. W. Churchill, "Friction-factor Equation Spans All Fluid - Flow Regimes," Chemical Engineering, vol. 84, no. 24, pp. 91-92, 1977.

[91] G. B. Wallis, "One-dimensional Two-phase Flow," 1969.

[92] G. Hewitt, Annular Two-phase Flow. Elsevier, 2013.

[93] S. E. Haaland, "Simple and Explicit Formulas for the Friction Factor in Turbulent Pipe Flow," Journal of Fluids Engineering, vol. 105, no. 1, pp. 89-90, 1983.

[94] J. Ferrell, "A Study of Convection Boiling inside Channels," in MME, 1966, p. 42.

[95] S. Levy, "Forced Convection Subcooled Boiling — Prediction of Vapor Volumetric Fraction," International Journal of Heat and Mass Transfer, vol. 10, no. 7, pp. 951-965, 1967.

[96] K. T. Claxton, J. G. Collier, and J. Ward, HTFS Correlations for Two-phase Pressure Drop and Void Fraction in Tubes. Heat Transfer and Fluid Flow Service, 1972.

[97] D. Zigrang and N. Sylvester, "A Review of Explicit Friction Factor Equations," Journal of Energy Resources Technology, vol. 107, no. 2, pp. 280-283, 1985.

[98] C. F. Colebrook et al., "Correspondence. Turbulent Flow in Pipes, with Particular Reference to the Transition Region between the Smooth and Rough Pipe Laws. (Includes Plates)," Journal of the Institution of Civil Engineers, vol. 12, no. 8, pp. 393-422, 1939.

[99] N. Brauner and D. M. Maron, "Stability Analysis of Stratfied Liquid-Liquid Flow," International Journal of Multiphase Flow, vol. 18, no. 1, pp. 103-121, 1992.

[100] M. Ishii and K. Mishima, "Two-fluid Model and Hydrodynamic Constitutive Relations," Nuclear Engineering and Design, vol. 82, no. 2-3, pp. 107-126, 1984.

[101] P. Behringer, "Velocity of Rise of Steam Bubbles in Boiler Tubes," VDI Forschungsheft, vol. 365, p. B4, 1934.

[102] M. Ishii, "One-Dimensional Drift-flux Model and Constitutive Equations for Relative Motion between Phases in Various Two-phase Flow Regimes," Argonne National Lab., Ill.(USA)1977.

[103] G. B. Wallis, "Annular Two-Phase Flow — Part 1: A Simple Theory," Journal of Basic Engineering, vol. 92, no. 1, pp. 59-72, 1970.

[104] J. Asali, T. t. Hanratty, and P. Andreussi, "Interfacial Drag and Film Height for Vertical Annular Flow," AIChE Journal, vol. 31, no. 6, pp. 895-902, 1985.

[105] M. Ishii and T. Chawla, "Local Drag Laws in Dispersed Two-phase Flow," Nasa Sti/recon Technical Report N, vol. 80, 1979.

[106] J. Putney, "Proposals for Improving Interphase Drag Modelling for the Bubbly and Slug Regimes in RELAP5," Central Electricity Research Labs.1988.

[107] J. Putney, "Implementation of a New Bubbly-Slug Interphase Drag Model in RELAP5/MOD2," Central Electricity Research Labs.1988.

[108] J. Putney, "Equations for Calculating Interfacial Drag and Shear from Void Fraction Correlations," Central Electricity Research Labs.1988.

[109] J. Putney, "Development of a New Bubbly-Slug Interfacial Friction model for RELAP5," Nuclear Engineering and Design, vol. 131, no. 2, pp. 223-240, 1991.

[110] J. Putney, "Development of a New Bubbly-Slug Interfacial Friction Model for RELAP5-Final Report," CEGB Research Report ESTD/L/0075/R89, 1989.

[111] B. Chexal and G. Lellouche, "Full-range Drift-flux Correlation for Vertical Flows. Revision 1," Electric Power Research Inst.1986.

[112] B. Chexal, G. Lellouche, J. Horowitz, and J. Healzer, "A Void Fraction Correlation for Generalized Applications," Progress in Nuclear Energy, vol. 27, no. 4, pp. 255-295, 1992.

[113] N. Zuber, Steady State and Transient Void Fraction in Two Phase Flow Systems: Final Report for the Program of Two-phase Flow Investigation. Atomic Power Equipment Department, General Electric, 1967.

[114] S. Rouhani, "‘Modified Correlations for Void-fraction and Pressure Drop," AB Atomenergi Sweden, AE-RTV-841, pp. 1-10, 1969.

[115] D. Woodford and A. Scriven, "The Rise Velocity and Distribution of Vapour in a Liquid Pool during Depressurization," in International Conference on the Physical Modelling of Multi-Phase Flow, 1983, pp. 199-217.

[116] A. H. S. a. A. J. Erickson, "Transactions of ASME," vol. 79, p. 775, 1957.

[117] G. Wallis, "One-dimensional Two-phase Flow McGraw-Hill Book Company," New York, 1969.

[118] V. Ransom, "RELAP5/MOD1 Code Manual Volumes 1 and 2 (Draft)," NUREG/CR-1826, EGG-2070, Revision 11

NRC FORM 335
(12-2010)
NRCMD 3.7

U.S. NUCLEAR REGULATORY COMMISSION

BIBLIOGRAPHIC DATA SHEET

(See instructions on the reverse)

1. REPORT NUMBER
(Assigned by NRC, Add Vol., Supp., Rev., and Addendum Numbers, if any.)

NUREG/IA-0522

2. TITLE AND SUBTITLE

RELAP5 and TRACE Constitutive Relations Comparison

3. DATE REPORT PUBLISHED

MONTH	YEAR
January	**2021**

4. FIN OR GRANT NUMBER

5. AUTHOR(S)

S. Shin* and J. Lee*, A. Shin**, M. Cho**

6. TYPE OF REPORT

Technical

7. PERIOD COVERED (Inclusive Dates)

8. PERFORMING ORGANIZATION - NAME AND ADDRESS (If NRC, provide Division, Office or Region, U. S. Nuclear Regulatory Commission, and mailing address; if contractor, provide name and mailing address.)

Korea Advanced Institute of Science and Technology (KAIST) N7-1 4409 291 Daehak-ro. Yuseong-gu Daejeon 34141 Republic of Korea*
Korea Institute of Nuclear Safety, 62, Gwahak-ro, Yuseong-gu, Daejeon 34142, Republic of Korea**

9. SPONSORING ORGANIZATION - NAME AND ADDRESS (If NRC, type "Same as above", if contractor, provide NRC Division, Office or Region, U. S. Nuclear Regulatory Commission, and mailing address.)

Division of Systems Analysis
Office of the Nuclear Regulatory Research
U.S. Nuclear Regulatory Commission
Washington, D.C. 20555-0001

10. SUPPLEMENTARY NOTES

K. Tien, NRC Project Manager

11. ABSTRACT (200 words or less)

A system thermal hydraulic analysis code solves the fluid field equations to model two phase flow. System codes typically solve mass, momentum and energy equations of each phase numerically by approximating a one dimensional flow. The constitutive relation based on empiricism must be included for mathematical closure of the approximated governing equations. There is no available method to evaluate the constitutive relation models that include all regimes expected in applications of the system codes. This study proposes a new method for evaluating the constitutive relations by comparing between RELAP5 and TRACE to analyze the constitutive relation models of the two codes. RELAP5 and TRACE are very different in the implemented constitutive relation models even though the field equations are almost identical. To compare the different constitutive relations of the two codes, models and correlations of each code are studied and compared. Then constitutive relation modules are extracted in a separate computational environment. The developed platform is based on MATLAB and REFPROP, and it is proven to reproduce the same values of RELAP5 MOD3.3 patch5 and TRACE 5.0 patch5, respectively.

12. KEY WORDS/DESCRIPTORS (List words or phrases that will assist researchers in locating the report.)

Onset of Boiling (ONB)
Nucleate Boiling (NB)
Minimum Film Boiling (MFB)

13. AVAILABILITY STATEMENT

unlimited

14. SECURITY CLASSIFICATION

(This Page)
unclassified

(This Report)
unclassified

15. NUMBER OF PAGES

16. PRICE

Printed
on recycled
paper

Federal Recycling Program

UNITED STATES
NUCLEAR REGULATORY COMMISSION
WASHINGTON, DC 20555-0001

OFFICIAL BUSINESS

@NRCgov

NUREG/IA-0522

RELAP5 and TRACE Constitutive Relations Comparison

January 2021